Scaling and phase transitions in one-dimensional nonequilibrium driven systems

Meesoon Ha

A dissertation submitted in partial fulfillment of
the requirements for the degree of

Doctor of Philosophy

University of Washington

2003

Program Authorized to Offer Degree: Physics

ProQuest Information and Learning Company
300 North Zeeb Road
P.O. Box 1346
Ann Arbor, MI 48106-1346

In presenting this dissertation in partial fulfillment of the requirements for the Doctoral degree at the University of Washington, I agree that the Library shall make its copies freely available for inspection. I further agree that extensive copying of this dissertation is allowable only for scholarly purposes, consistent with "fair use" as prescribed in the U.S. Copyright Law. Requests for copying or reproduction of this dissertation may be referred to Bell and Howell Information and Learning, 300 North Zeeb Road, Ann Arbor, MI 48106-1346, to whom the author has granted "the right to reproduce and sell (a) copies of the manuscript in microform and/or (b) printed copies of the manuscript made from microform."

Signature 

Date May 29, 2003

University of Washington

Graduate School

This is to certify that I have examined this copy of a doctoral dissertation by

Meesoon Ha

and have found that it is complete and satisfactory in all respects,
and that any and all revisions required by the final
examining committee have been made.

Chair of Supervisory Committee:

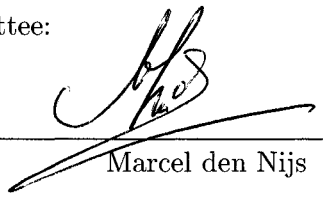

Marcel den Nijs

Reading Committee:

Marcel den Nijs

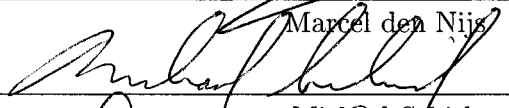

Michael Schick

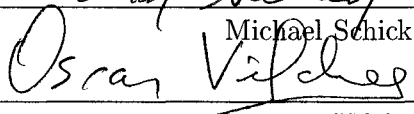

Oscar E. Vilches

Date: May 29 2003

University of Washington

Abstract

Scaling and phase transitions
in one-dimensional nonequilibrium driven systems

by Meesoon Ha

Chair of Supervisory Committee:

Professor Marcel den Nijs
Department of Physics

We investigate scaling and phase transitions in 1D driven lattice gas models, related to Kardar-Parisi-Zhang (KPZ) surface dynamics. The results of three studies are presented. In the first one, we generalize the asymmetric diffusion-reaction process $A + A \rightarrow A$ by adding a mass-conserving coalescence feature. This leads to novel scaling behavior, which we explain analytically and confirm numerically. In the second and third studies, we focus on the scaling properties of dynamic phase transitions in driven flow, like queues behind obstacles, in the context of the asymmetric simple exclusion process (ASEP). First, we collapse the entire queue onto a single special site, the so-called parking garage, where the road starts and terminates. This new variant of the ASEP exhibits a dynamic analogue of Bose condensation, in terms of macroscopic occupancy of the garage. Next, we consider the ASEP with open and periodic boundary conditions with a special bond, where particles can pass with reduced or enhanced probability. Below a critical reduced passage probability, a macroscopic queue emerges behind the slow bond. We establish numerically the existence of a queuing transition. Novel power-law shaped density profiles also emerge below and above the critical point. This project was triggered by our collaboration with an experimental group studying faceting in slow combustion of paper induced by a columnar defect. An exact mapping exists between the ASEP and KPZ type surface growth processes.

TABLE OF CONTENTS

LIST OF FIGURES

ACKNOWLEDGMENTS

First of all, I wish to express sincere appreciation to my advisor, Prof. Marcel den Nijs, for his valuable advice, nice assistance, and generous guidance through my graduate years. I would like to give my special thanks to Prof. Hyunggyu Park in Korea, who opened my eyes in statistical physics and helped me to go through some difficult time. Without him, it is impossible for me to finish this thesis. I would like to thank Prof. Michael Schick and Prof. Oscar E. Vilches for their critical reading of this thesis. I am also grateful to Prof. Jussi Timonen in Finland for his collaboration and helpful comments during my last project. I would like to thank my group mates, Chun-Chung Chen, Chen-Shan Chin, Douglas Davidson, Jae Dong Noh, Deok-Sun Lee, and Kyung Hyuk Kim for stimulating discussions and useful comments in the group meetings. I would like to thank my dear friend and classmate, Marina Hurska, for her friendship. I also thank to other Korean fellow graduate students, Ki-Young Choi, Sung Wu Rhee, Jae Yong Lee, Sukjin Yoon, and Chihak Ahn for their kindness and encouragement. Finally, I would like to thank my husband, Youngkyun Jung, and my family for their love, patience, and selfless support.

DEDICATION

This thesis is dedicated to my parents.

Chapter 1

INTRODUCTION

The field of nonequilibrium statistical mechanics continues to grow in scope and in depth. In this thesis, we explore driven diffusive processes of many particle systems. This has become one of the primary examples of nonequilibrium processes, in particular after the work by Katz, Lebowitz and Spohn [9, 10] to model superionic conductors. Systems driven by external fields reach a steady state with a non-vanishing current. These usually do not satisfy the detailed balance condition, familiar from thermal equilibrium, so that their properties are quite different from those of systems in equilibrium. For instance, several one-dimensional (1D) driven diffusive systems with local dynamics exhibit long range order and spontaneous symmetry breaking, which cannot occur in equilibrium when the interactions are short-ranged.

Simple models have been considered to gain analytical and numerical results to deepen our understanding of such problems. One of the major difficulties encountered is the lack of a well-defined Gibbs-like ensemble, compared to equilibrium phenomena, describing stationary states. In other words, there is currently no established systematic analytical procedure/formalism for predicting stationary state ensembles, even when the dynamics is only slightly perturbed from the familiar equilibrium one. In particular, perturbation expansions in small driving fields fail. Therefore, we rely mostly on numerical evidence and heuristic physical arguments. For a few special cases, exact and analytical results deepen our understanding and provide a guide to the more general behavior.

Most models of microscopic dynamics used in the statistical mechanics theory of nonequilibrium stochastic processes are just caricatures of the real experimental processes, but they enable one to provide qualitative and even quantitative information about the behaviors of

real microscopic systems as long as the model dynamics preserves the essential features of the real dynamics. The research presented in this thesis is formulated with this in mind.

We focus on 1D simple particle transport models and their scaling properties with or without dynamic phase transitions. In particular, 1D driven lattice gas models have been the focus of extensive research in terms of their underlying 1D Kardar-Parisi-Zhang (KPZ)-type surface growth dynamics. New scaling properties for a 1D fully asymmetric diffusion-reaction $A + A \rightarrow A$ process are discussed in Chapter 2 by an exact mapping onto the KPZ-type restricted ballistic deposition model. The scaling properties of dynamic phase transitions in driven flow, like queues (traffic jams) behind obstacles, are studied in Chapter 3, with the asymmetric simple exclusion process (ASEP) where the traffic jams are confined into a site defect, namely a parking garage. The 1D system is closed, like a road beginning and ending at the same garage. The ASEP is exactly mapped onto the KPZ-type body-centered-solid-on-solid model. In Chapter 4 we introduce another variant of the ASEP, with a bond defect at the middle of a 1D open system. We find novel power-law decays in density profiles and a defect-induced queuing transition.

This first chapter serves as a general introduction to this thesis. It reviews some of the major current results for driven interfaces and stochastic dynamics of interacting particle systems. Our attention will be limited to 1D KPZ-type surface growth and driven lattice gas models, related to the research presented in the following chapters.

1.1 Physics far from equilibrium

In this section we give a brief review of major current theoretical tools for studying nonequilibrium systems. Many phenomena in nature involve so many degrees of freedom that often only few of them can be taken into account in detail and the others are treated as *noise* with a certain postulated distribution. In order to study stationary and time-dependent properties in such simplified descriptions of complex behaviors, such as averages, fluctuations, correlations, and responses to external forces, we follow the traditional methods of statistical mechanics. We start at the "microscopic" level in terms of a *master equation* and try to solve this linear equation in order to find the steady-state probability distribution

and the asymptotic behavior of the approach to the steady state. However, this task is still insurmountable. That leads to further approximations and/or to numerical simulations, such as the *dynamic mean-field theory* and a "mesoscopic" continuum description in terms of coarse-grained *Langevin equations*. The latter approach forms the basis of many field theoretical analyses of dynamic critical phenomena; in these analyses it is crucial to make sure that both the microscopic lattice version and its mesoscopic continuum counterpart exhibit the same symmetries because the symmetries play a decisive role in determining the universality class and universal properties.

1.1.1 Master equation

In contrast to equilibrium systems where the stationary probability distribution over configuration space, $\exp(-\beta\mathcal{H})$, is the Gibbs' distribution with a well-defined global Hamiltonian $\mathcal{H}$, the steady-state distribution of nonequilibrium driven systems lacks a universal framework. It can be phrased in terms of an $\mathcal{H}$, but one which cannot be expressed solely in terms of the internal energies of the system.

The construction of a master equation involves the specification of how a given configuration $\mathcal{C}$ evolves into a new one, $\mathcal{C}'$. In other words, we have to specify a set of transition rates $W[\mathcal{C} \to \mathcal{C}']$. The time-dependent probability distribution $P(\mathcal{C}, t)$ is the master equation of motion

$$\frac{\partial}{\partial t}P(\mathcal{C}, t) = \sum_{\mathcal{C}'}\{W[\mathcal{C}' \to \mathcal{C}]P(\mathcal{C}', t) - W[\mathcal{C} \to \mathcal{C}']P(\mathcal{C}, t)\} \tag{1.1}$$

in continuous time or a similar balance equation in discrete time. The specific choice of W determines the model dynamics jointly with the boundary conditions. For equilibrium systems we know that the steady-state distribution $P^*(\mathcal{C}) = P(\mathcal{C}, t \to \infty)$ is the Gibbs' distribution, $P^*(\mathcal{C}) = P_{\rm eq}(\mathcal{C})$. To ensure that this state is reached, Monte Carlo type simulations of equilibrium studies conveniently impose the detailed balance condition,

$$\frac{W[\mathcal{C}' \to \mathcal{C}]}{W[\mathcal{C} \to \mathcal{C}']} = \frac{P_{\rm eq}(\mathcal{C})}{P_{\rm eq}(\mathcal{C}')} = \exp(-\beta\Delta\mathcal{H}), \tag{1.2}$$

as the ratio of two Boltzmann weights. Here $1/\beta = k_{\rm B}T$.

Most nonequilibrium processes have neither an explicit $\mathcal{H}$ nor obey a detailed balance. A particular example is when the process is driven, like the asymmetric exclusion process

discussed later in this thesis. Although the steady state is, in principle, completely specified by solving the linear equations, $\sum_{\mathcal{C}'}\{W[\mathcal{C}' \to \mathcal{C}]P^*(\mathcal{C}') - W[\mathcal{C} \to \mathcal{C}']P^*(\mathcal{C})\} = 0$, this is typically an unsurmountable task, with few exceptions.

1.1.2 Mean-field theory

As mentioned, it is quite difficult to figure out underlying physics for a given system directly from the microscopic model description and its master equation. That is why people study dynamic mean-field (MF) approaches to gain the first impression of the collective behaviors. The MF approaches can be quite successful, qualitatively yielding some rough outlines of the phase diagram, even for nonequilibrium cases; though they are naturally unable to predict critical singularities related to effects of infinite correlation lengths. Classic textbook examples of the dynamic MF theory are the Boltzmann equation and the BBGKY [1] hierarchy leading from Liouville's theorem to hydrodynamics (see [11] for a detailed discussion).

1.1.3 Langevin equation

At a "mesoscopic" hydrodynamic level we can describe dynamic stochastic processes by Langevin-type equations. This approach has been quite successful at the phenomenological level for studying the slowly-varying long wavelength properties of many-body systems. For the Ising model in equilibrium the corresponding mesoscopic picture is the Landau-Ginzburg-Wilson Hamiltonian [12]. In the same spirit, the mesoscopic dynamics for nonequilibrium driven systems has been introduced via a Langevin equation of motion for an appropriate mesoscopic field, e.g., local height $h(x,t)$ for a driven interface model or particle density $\rho(x,t)$ for a driven lattice gas model.

A coarse-grained version can be derived by some suitable averaging procedure from the master equation of microscopic variables, basically the MF approach. However, for most cases this route is not easy, so phenomenological equations are often just postulated based on symmetries and physical considerations, such as the proper choice of an order parameter and other slow variables. For example, if particle conservation exists in a given microscopic

[1] BBGKY stands for Bogoliubov-Born-Green-Kirkwood-Yvon.

model, all equations of motion for the density field must obey the continuity equation, $\partial_t \rho = -\vec{\nabla} \cdot \vec{J}$. For studying critical dynamics near equilibrium, the standard form for the systematic current is defined as

$$\vec{J} = -\mathcal{D}\vec{\nabla}\mu, \tag{1.3}$$

with a transport coefficient $\mathcal{D}$ and the chemical potential $\mu = \delta\mathcal{H}/\delta\rho$. Then, a typical 1D Langevin equation of motion, in terms of the current and a noise, takes the form

$$\partial_t \rho = \partial \left\{ \mathcal{D}\partial \frac{\delta \mathcal{H}}{\delta \rho} + \eta \right\}, \tag{1.4}$$

where η denotes a random noise type Langevin force, typically with $\langle \eta(x,t) \rangle = 0$ and $\langle \eta(x,t)\eta(x',t') \rangle = N\delta(x-x')\delta(t-t')$. When the dynamics leads to thermal equilibrium, the noise amplitude relates to the temperature, via the fluctuation-dissipation theorem [13] as $N = 2\mathcal{D}k_B T$.

In the presence of a driving field the above Hamiltonian description typically fails and the additional current, say $\vec{j}_d$, is included in an ad-hoc fashion to the Langevin equation. The simplest form of $\vec{j}_d$ is postulated based on the symmetries and typically proportional to a specific field. Depending on which region we are interested in, we may neglect higher order terms in the driving field. Often we can justify neglecting such higher order terms in the sense of the renormalization group (RG) theory.

1.1.4 Overview: Far-from-equilibrium critical phenomena and phase transitions

Critical phenomena have captivated statistical physicists for many decades (see e.g., Ref. [14] and the Domb & Green (1972-76) and Domb & Lebowitz (1977-present) series). Much theoretical progress has resulted from the parallel application of various approaches, including exact solutions, MF theories, computer simulations, series expansions, and RG methods applied to simple lattice models and their continuum analogues. Such approaches lead to the structure of the phase diagram for many systems, the identification of universality classes, and their scaling behavior [12, 15, 16].

Nonequilibrium phenomena are overwhelmingly more abundant in nature than equilibrium ones, with many examples in biology, chemistry and physics [6, 17, 18, 19]. Their

simplest aspect, *a nonequilibrium steady state*, involves a constant flux of matter, energy, or some other quantity. As the control parameters, e.g., temperature, potential gradients, or reactant feed rates are varied, a steady state may become unstable and be replaced by another. Such nonequilibrium instabilities represent *nonequilibrium phase transitions* [6, 17, 18, 19, 20, 21].

In the next two sections, we explore far-from-equilibrium critical phenomena and phase transitions through the example of fluctuations of driven interfaces and stochastic dynamics of driven lattice gases.

1.2 Fluctuations of driven interfaces

There are lots of interesting interface dynamics in nature and in physical experiments: evolving coast lines and mountain shapes in geography [22], fluid flow in disordered media [23, 24], propagation of flame fronts in forest fires [25] or slow combustion of paper [1, 26], flux lines in a type II superconductor with impurities [2], the growth of thin films by molecular beam epitaxy [27], the actual surface morphology in sputter erosion [3, 4], cluster boundaries of bacterial colonies [28, 29], and suspension-aggregation interfaces for colloidal sedimentation [30]. Figures 1.1, 1.2 and 1.3 illustrate some of these recent experimental observations.

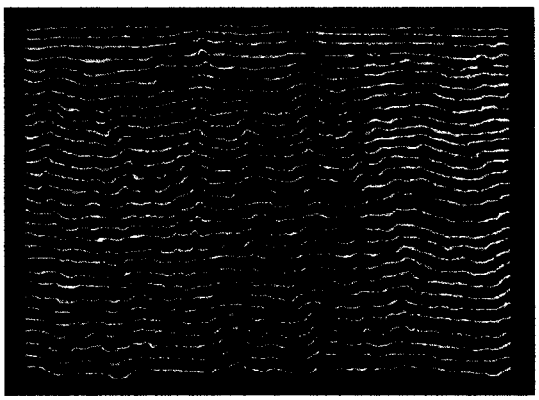

Figure 1.1: (color) Series of typical digitized fronts in the slow-combustion experiment. Burning fronts were taken from top to bottom. The time step between successive fronts is 10 s, and the width of the digitized area is 310 mm, from [1].

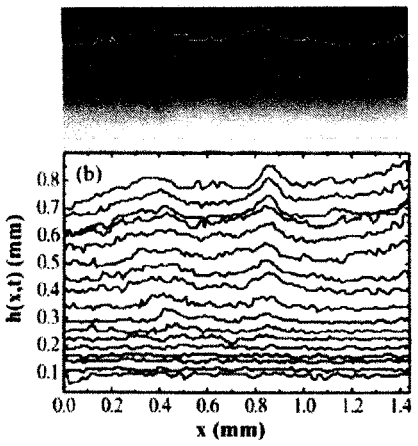

Figure 1.2: (a) (color) Magneto-optical image taken at 11 mT after zero field cooling to 4.2 K of a 80 nm thick $YBa_2Cu_3O_{7-x}$ film on $NdGaO_3$, from [2]. High (low) vortex density is represented with yellow (blue). The image shows only the part used for analysis (1.44 mm in the total length of the sample 8.1 mm) and the wiggly white line indicates the flux front. (b) Flux fronts observed in sample No. 2. The applied external field is increased by 1 mT between subsequent fronts from bottom (1 mT) to top (17 mT).

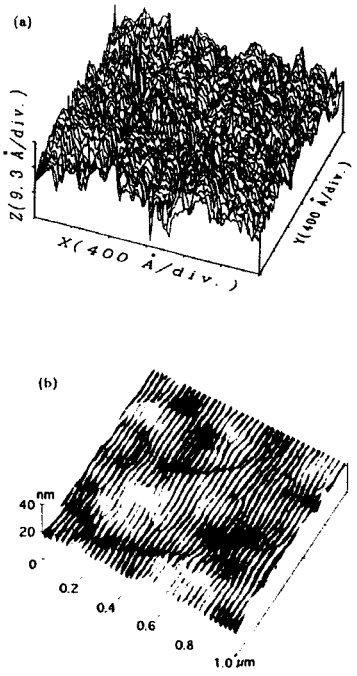

Figure 1.3: (a) Scanning Tunneling Microscopic topography of a graphite surface after bombarding with a constant flux at room temperature, where the sample size is 2400Å × 2400Å and the vertical size 18.6Å, from [3]. (b) Atomic Force Microscopic image of a Xe-bombarded SiO_2 film, where the periodic ripple structure is shown, from [4].

The morphology of interfaces depends on *the length of scale of observation.* In addition, it has been observed that many interfaces are intermediate between fractal and non-fractal objects. This is called *self-affine.* If objects are fractal, they appear exactly the same on different observation scales. If they are non-fractal, they may look totally different on different scales. Self-affine objects are not scale invariant under isotropic rescalings of all lengths when we use the same scale factor in all directions, but their morphologies are invariant under an anisotropic scaling of the horizontal and vertical directions, respectively. This anisotropic scaling allows a classification and better understanding of some properties of kinetic roughening of interfaces. (See Fig. 1.4.)

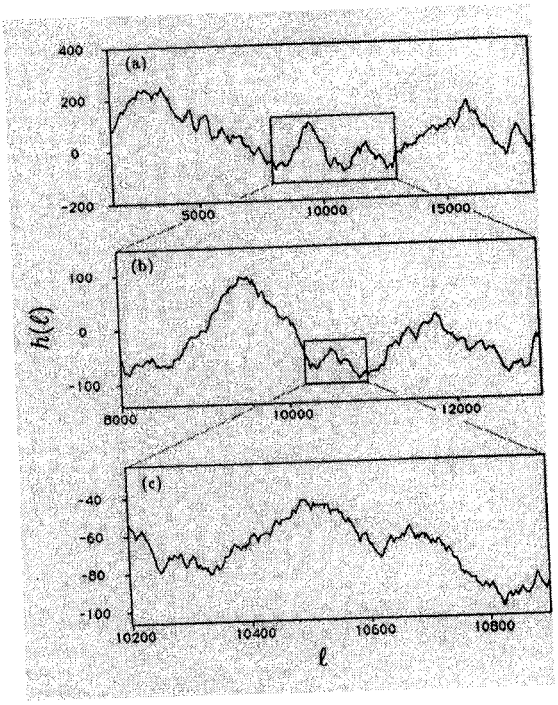

Figure 1.4: Rescaling a self-affine function. If we correctly select the two unequal magnification factors, M_ℓ and M_h, by which the ℓ and h directions are re-scaled, the enlarged portions have the same statistical properties as the original, from [5].

1.2.1 Lattice models and major physical quantities

In this subsection we focus on lattice models. The growth models of interest are defined by local environments and a few general concepts, e.g., whether the process is reversible or irreversible, flux or reaction-limited, or parallel or sequential-updated in time. For the flux-limited case, the rate of growth is limited by the supply of new particles. Most deposition processes are flux-limited. In contrast, for the reaction-limited case, the availability of growth sites is the limiting factor. The latter case appears quite naturally in the context of biological applications, e.g., the so-called Eden-type models, first formulated by Eden in 1956 as minimal description of biological morphologies [31]. Solid-on-solid (SOS)-type models with local growth restrictions also belong to the reaction-limited case. Sequential updating means the process occurs at randomly chosen update sites one by one and the unit of the time increment is the inverse of the lattice size, so it is often referred to as

continuous-time updating. In contrast, parallel updating is intrinsically discrete in time. All of the growth sites are simultaneously updated in a single time step.

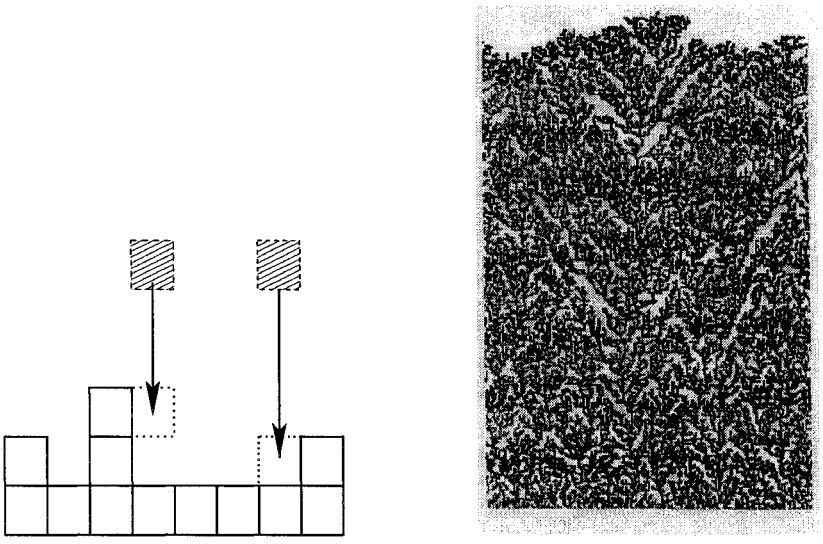

(a) (b)

Figure 1.5: (a) The BD model with the nearest-neighbor sticking rule, illustrating two sticking possibilities for the newly-deposited particles. The case shown here is $L = 8$. (b) A BD cluster obtained by depositing 35,000 particles on a substrate of $L = 200$. The shading reflects the arrival time of the particles. After the deposition of each set of 2500 particles, the shading changed, from [6].

The roughness of interface growth can be illustrated in terms of a simple lattice model, namely *ballistic deposition* (BD), introduced by Family and Vicsek [32]. The dynamic rule of the BD model on a 1D lattice is shown in Fig 1.5(a). A particle is released from a randomly chosen position above the surface, say site i, follows a straight vertical trajectory until it reaches the surface, and then deposits following the rule $h(i, t+1) \rightarrow \max[h(i-1, t), h(i, t)+1, h(i+1, t)]$. The deposited particles form a cluster or an aggregate with a unique self-affine geometry as shown in Fig. 1.5(b). This BD interface can be quantitatively described in terms of the mean height, the surface width, and the height-height correlation function.

(i) The *mean height* of the surface, $\bar{h}$, is defined by

$$\bar{h}(t) \equiv \frac{1}{L}\sum_{i=1}^{L} h(i,t), \tag{1.5}$$

where $h(i,t)$ is the height of column i at time t and L is the lattice size. If the deposition rate is constant, the mean height increases linearly with time, $\bar{h}(t) \sim t$.

(ii) The *surface width*, $w(L,t)$, which characterizes the roughness of the surface, is defined by the root-mean-square fluctuation in the height,

$$w(L,t) \equiv \sqrt{\frac{1}{L}\sum_{i=1}^{L}[h(i,t) - \bar{h}(t)]^2}. \tag{1.6}$$

Typically, the simulation starts from a horizontally flat configuration, i.e. $w = 0$. As deposition proceeds, w gradually increases to describe how the surface becomes rough, compared to its initial configuration. In the long time limit, surface roughness saturates. A typical plot of w has two regions separated by a "crossover (saturation)" time t_s, at which the surface crosses over from the time-dependent behavior of w to its size-dependent (time-independent) behavior. Initially, $w(L,t) \sim t^{\beta}$ for $t \ll t_s$, where β is the growth exponent characterizing the time-dependent dynamics of the roughening process. Then, w reaches its saturation value, w_s, at $t = t_s$ for a given system size. As L increases, $w_s(L) \sim L^{\chi}$ for $t \gg t_s$, where χ is the roughness exponent. It characterizes the roughness of the steady state. The saturation time depends on the system size as $t_s \sim L^z$, where z is called the *dynamic exponent.*

Fig. 1.6 shows how to obtain the scaling exponents χ, β and z. They are generally not independent. Rescaling w and t with their scaling forms L^{χ} and L^z, respectively, we obtain a simple dynamic scaling relation [32],

$$w(L,t) \sim L^{\chi} f(t/L^z), \tag{1.7}$$

where $f(u)$ is a *scaling function* in terms of $u \equiv t/L^z$. The general form of $f(u)$ can be read off from Fig. 1.6. For $u \ll 1$, $f(u) \sim u^{\beta}$ and for $u \gg 1$, $f(u) \to$ constant. The validity of the dynamic scaling relation can be tested by replotting numerical and/or analytical data.

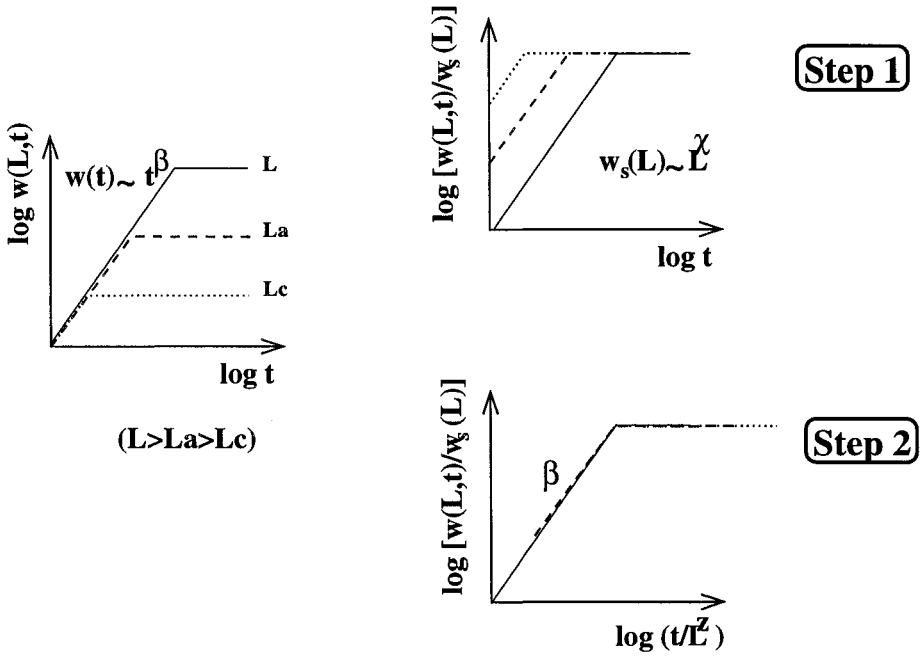

Figure 1.6: Schematic illustration of the steps involved in rescaling the time-dependent roughness in a log-log scale. The left figure shows the variation of the width with time for three different system sizes.

In some experiments, the power spectrum of the surface can be measured. The structure factor,

$$S(k,t) \equiv \langle h(k,t)h(-k,t)\rangle, \tag{1.8}$$

is the Fourier transformation of the width, where $h(k,t) \equiv \frac{1}{\sqrt{L}}\sum_x [h(x,t) - \bar{h}]\exp(ikx)$, which scales as

$$S(k,t) = k^{-1-2\chi} g(tk^z). \tag{1.9}$$

The scaling function behaves as $g(u) \sim u^{(2\chi+1)/z}$ for $u \ll 1$ and $g(u) \to$ constant for $u \gg 1$. The structure factor provides an alternative way to determine the scaling exponents.

(iii) The *width*, $w_L(\ell,t)$, at length scale ℓ and the *height-height correlation function*, $C_L(\ell,\tau)$, are defined by

$$w_L^2(\ell,t) \equiv \overline{\langle [h(x,t) - h_\ell(x,t)]^2\rangle} \tag{1.10}$$

and

$$C_L(\ell,\tau) \equiv \overline{\langle [h(x+\ell,t+\tau) - h(x,t)]^2\rangle} \tag{1.11}$$

where $h_\ell(x,t)$ is the average height in a local window of length ℓ in the surface. The brackets $\langle ... \rangle$ denote ensemble averages. The bar means a spatial average over x in w_L, while it means both spatial and temporal averages in C_L. Numerical results for theses quantities are very useful in cases when we do not have any prior information on the growth dynamics.

The fact that both t_s and w_s increase with the system size implies that saturation phenomena constitute a *finite size effect.* In other words, an infinite system does not saturate at all. "Information" spreads through the surface. The typical distance over which the heights know about each other, i.e., the characteristic distance over which they are correlated, is called the *correlation length* and denoted by $\xi_{||}$. The correlation length grows with time as $\xi_{||} \sim t^{1/z}$, but cannot grow infinitely for a finite system because it is limited by the size of the system, L. Once $\xi_{||}$ reaches L, the entire surface becomes correlated and w saturates. Therefore, at saturation, $\xi_{||} \sim L \sim t^{1/z}$. One may consider another correlation length $\xi_\perp$ to characterize the fluctuations in the growth direction, but this is already captured in the surface width $w(L,t)$. The scaling forms for $w_L(\ell,t)$ and $C_L(\ell,\tau)$,

$$w_L^2(\ell,t) = b^{2\chi} w_L^2(b^{-1}\ell, b^{-z}t), \tag{1.12}$$

and

$$C_L(\ell,\tau) = b^{2\chi} C_L(b^{-1}\ell, b^{-z}\tau), \tag{1.13}$$

reflect the spreading of information with the scaling factor b. For $\ell \ll \xi_{||}$, $w_L^2(\ell,t) \sim C(\ell,0) \sim \ell^{2\chi}$. The local width reaches its saturation value at $\ell = \xi_{||}(t)$, $w_L(\xi_{||},t) = \xi_\perp(t)$. For the process of BD, $\chi = \frac{1}{2}$ and $z = \frac{3}{2}$ [6, 32].

1.2.2 Continuum equations and universality classes

Langevin equations for interface growth have the generic form

$$\frac{\partial h(x,t)}{\partial t} = G(h,x,t) + \eta(x,t), \tag{1.14}$$

where the surface is characterized by a single-valued height field $h(x,t)$ and $G(h,x,t)$ is a general function that depends on the surface height, position, time and symmetry consideration. The random noise $\eta(x,t)$ has $\langle \eta(x,t) \rangle = 0$ and $\langle \eta(x,t)\eta(x',t') \rangle = 2D\delta(x-x')\delta(t-t')$.

To determine the generic form of $G(h,x,t)$, we make a list of the symmetries of the process at the microscopic level and consider all terms that can be formed from combinations of powers of $(\nabla^n h)$. Then, one by one, we eliminate the terms that violate at least one of the symmetries listed: invariance under translation in time, translational invariance along the growth direction or in the direction perpendicular to the growth direction, rotation and inversion symmetry about the growth direction, up/down symmetry for h, and so on.

Since we are interested in constructing a mesoscopic description, we focus on the *long-time, long-distance* behavior of functions that characterize the surface. In this *hydrodynamic limit* higher order derivatives should be less relevant compared to the lowest order derivatives, which can be confirmed by using either scaling arguments or more sophisticated methods available from the RG treatment. For example, in rescaling the self-affine interface with the roughness exponent χ by a scaling factor b in the x direction, $x \to x' \equiv bx$, the height must be rescaled as well as $h \to h' \equiv b^{\chi} h$ in order to obtain an interface with similar geometrical properties. Similarly, $\nabla^2 h \to \nabla^2 h' \equiv b^{\chi-2}\nabla^2 h$, $\nabla^4 h \to \nabla^4 h' \equiv b^{\chi-4}\nabla^4 h$, and so on. This implies that in the hydrodynamic limit ($b \to \infty$), the term $\nabla^4 h$ is less relevant than the term $\nabla^2 h$, so that the former can be neglected, assuming that the operator algebra does not contain other fundamental operators beside h and its gradients. A similar argument can be used to show other cases, e.g., $(\nabla^2 h)(\nabla h)^2$ is the most relevant of the possible $(\nabla^{2m} h)(\nabla h)^{2k}$ terms, but is irrelevant compared to $\nabla^2 h$. However, the nonlinear term $(\nabla h)^2$ is relevant.

Fluctuations of driven interfaces are generally categorized by three universality classes.

(A) Random growth

The simplest of the growth models is *random deposition* (RD), where a particle falls vertically from a randomly chosen column over the surface until it reaches the surface at the chosen column and is deposited just above the surface.

$$\frac{\partial h(x,t)}{\partial t} = F + \eta(x,t), \tag{1.15}$$

with $\langle \eta(x,t) \rangle = 0$ and $\langle \eta(x,t)\eta(x',t') \rangle = 2D\delta(x-x')\delta(t-t')$. F is a constant representing the flux of particles, and $\eta(x,t)$ reflects the random, so-called *Gaussian* fluctuations in the

deposition process. The statistical properties of this RD can be obtained by the exact integration of (1.15) and are quite trivial since the process lacks correlation along the x direction. Thus, the RD shows $\beta = \frac{1}{2}$ ($w \sim t^{\beta}$ for $t \ll L^z$, see Eq. (1.7) for details), i.e.,

$$\langle h(x,t) \rangle = Ft \quad \text{and} \quad w^2(t) = 2Dt. \tag{1.16}$$

Since there are no correlations between the columns, w does not saturate and the roughness χ is not defined, i.e., the morphology of the RD surface is not self-affine.

(B) Edwards-Wilkinson Growth

The simplest form of $G(h,x,t)$ that takes into account the local surface profile is the *Edwards-Wilkinson* (EW) equation [33, 34],

$$\frac{\partial h(x,t)}{\partial t} = \nu \nabla^2 h + F + \eta(x,t), \tag{1.17}$$

where ν is sometimes called a 'surface tension' since the $\nu\nabla^2 h$ term tends to smooth the surface. Equation (1.17) is linear in h, so it can be solved through Fourier transformation into momentum space. The uniform motion generated by the growth rate (particle flux) F term does not affect the scaling properties of the interface. It can be transformed away by viewing the process from coordinates moving with velocity F, i.e. by performing the change of variables $h \to h + Ft$. Thus, $F = 0$ is normally taken without any loss of generality. In momentum space all modes decouple and the parameters are not modified under the renormalization transformation. With $x' \to b^{-1}x$, $h' \to b^{-\chi}h$, $t' \to b^{-z}t$, and $\eta' \to b^{(d+z)/2}\eta$, the rescaled EW equation is

$$\frac{\partial h'}{\partial t'} = \nu b^{z-2} \nabla^2 h' + b^{z-\chi-(d+z)/2} \eta', \tag{1.18}$$

where d is the spatial dimension. To ensure scale invariance, each term on the right-hand side of (1.18) must be independent of b which implies $\chi = (z-d)/2$ and $z = 2$. For $d = 2$, EW interface fluctuations are logarithmic in both time and system size. The EW equation describes an equilibrium surface.

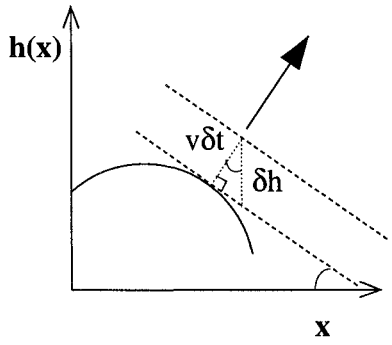

Figure 1.7: The origin of the nonlinear term in the KPZ equation: Growth occurs along the local normal v by Eq. (1.19).

(C) Kardar-Parisi-Zhang Growth

The generic form of $G(h, x, t)$ relevant for surface growth was introduced by Kardar, Parisi, and Zhang [35]. They added the nonlinear term $(\nabla h)^2$ to the EW equation. This model is capable of explaining the values of the exponents obtained in many microscopic nonequilibrium interface models, including the BD model.

$$\frac{\partial h(x,t)}{\partial t} = \nu \nabla^2 h + \frac{\lambda}{2}(\nabla h)^2 + \eta(x,t). \tag{1.19}$$

In the case of a continuum interface that has some systematic bias inherent in uniform translation, elementary geometric considerations reveal the bias to be proportional to the local slope of the segment. In order to compensate the local bias of the uniform translation mechanism, it is easy to see that an extra term should be added to the EW equation. Since the 'locally' normal propagation to the surface (see Fig. 1.7) must be projected on the forwarded axis to represent the effective advance, the growth rate must depend on the KPZ nonlinear term $(\nabla h)^2$:

$$\delta h = \sqrt{(v\delta t)^2 + (v\delta t \nabla h)^2} = v\delta t\sqrt{1 + (\nabla h)^2} \approx v\delta t[1 + \frac{1}{2}(\nabla h)^2 + ...], \tag{1.20}$$

when $|\nabla h| \ll 1$. This indicates that the nonlinear term $(\nabla h)^2$ must be present in the growth equation.

In contrast to the EW equation, the KPZ equation lacks up-down symmetry for h. An

interface governed by the KPZ equation has nonzero velocity even in the absence of an external driving force, with $v = \frac{\lambda}{2}\int_0^L d^dx\langle(\nabla h)^2\rangle \neq 0$ (unless $h(x,t) =$ constant). The contribution from the Laplacian term $\nu\nabla^2 h$ vanishes for periodic boundary conditions.

1.2.3 Burgers Equation and Galilean Invariance

By a change of variables, $\mathbf{v} = -\nabla h$, the KPZ equation can be reinterpreted as the noisy Burgers equation [36] for a vorticity-free ($\nabla \times \mathbf{v} = 0$) velocity field. The Burgers equation has been a paradigm of turbulence studies (but with different noise correlations),

$$\frac{\partial \mathbf{v}}{\partial t} + \lambda(\mathbf{v}\cdot\nabla)\mathbf{v} = \nu\nabla^2\mathbf{v} - \nabla\eta(x,t). \tag{1.21}$$

Here $\mathbf{v}(x,t)$ is the velocity of the fluid, ν is the viscosity, and $\nabla\eta(x,t)$ is a random force. The left-hand side of Eq. (1.21) represents the total derivative $\frac{\mathrm{d}v}{\mathrm{d}t}$ for $\lambda = 1$ and λ remains unchanged after any rescaling. The invariance of λ under renormalization is called Galilean invariance. This symmetry physically means the fact that when we tilt the mathematical coordinate system slightly by an infinitesimal angle ϵ, our dynamic equation should remain invariant because the physics remain the same before and after any operation. The following coordinate transformation,

$$h \to h + \epsilon x, \quad x \to x + \lambda\epsilon t, \tag{1.22}$$

leaves both Eqs. (1.19) and (1.21) invariant. As a result of this local symmetry, the KPZ equation is Galilean invariant, which implies that $\chi + z = 2$.

1.2.4 Fokker-Planck equation for the KPZ equation

The value of the remaining independent scaling exponent for $d = 1$ can be found by describing the time evolution of the probability $P[h,t]$ at height h at time t by means of a Fokker-Planck equation [37] and the fluctuation-dissipation theorem [13]. The Fokker-Planck equation is derived as an approximation to the master equation, where two assumptions are made: (i) only small jumps between configurations occur, e.g., $|h' - h| < \Delta$ is only allowed for growth, and (ii) the solution $P[h,t]$ varies slowly in h. The corresponding Fokker-Planck equation of the generic Langevin equation for the time evolution of the

fluctuation heights, e.g., Eq. (1.14), is as follows:

$$\frac{\partial P}{\partial t} = -\sum_{i=1}^{L} \frac{\partial}{\partial h_i}[G(h_i)P] + D\sum_{i=1}^{L} \frac{\partial^2 P}{\partial h_i^2}. \tag{1.23}$$

When the discrete variables $h_i(t)$ are replaced by $h(x,t)$ in the 1D KPZ equation, functional notation is necessary. Thus, the corresponding Fokker-Planck equation is

$$\frac{\partial P}{\partial t} = -\int dx \frac{\delta}{\delta h}\left[\left(\nu\partial_x^2 h + \frac{\lambda}{2}(\partial_x h)^2\right)P\right] + D\int dx \frac{\delta^2 P}{\delta h^2}, \tag{1.24}$$

which admits a stationary solution, $P = \exp\left(-\int_0^L dx[\frac{\nu}{2D}(\partial_x h)^2]\right)$. See [38, 39] for details [2]. This means that there are no correlations between local slopes at different locations. The sum of such local slopes generates the interface which is exactly characterized by Brownian motion. As a consequence, the 1D KPZ interface has $\chi = 1/2$. From Galilean invariance, $z = 2 - \chi = 3/2$. For $d > 1$ with nonzero λ, the 1D solution is no longer valid [40].

1.2.5 RG approach in the KPZ equation and its results

Forster *et al.* [41] applied the RG technique to dynamical systems, in particular to the Burgers equation with a Gaussian noise. Later, their RG results of the noisy Burgers equation were translated into the KPZ representation [35, 42].

After the KPZ equation is transformed to momentum space, it is approached perturbatively from the known solution of the linear problem at $\lambda = 0$. First, we integrate out the fast modes from the growth equation. Second, we remove the difference between the integrated system and the original one by rescaling $k \to kb$, i.e., rescaling the lattice $a_0 \to a_0/b$ to obtain the original lattice spacing a_0. Then we obtain the flow equations describing the change in the parameters under the RG transformation up to order λ^2,

$$\frac{\mathrm{d}\nu}{\mathrm{d}l} = \nu\left[z - 2 + K_d g^2 \frac{2-d}{4d}\right], \frac{\mathrm{d}D}{\mathrm{d}l} = D\left[z - d - 2\chi + K_d\frac{g^2}{4}\right], \frac{\mathrm{d}\lambda}{\mathrm{d}l} = \lambda\left[\chi + z - 2\right], \tag{1.25}$$

which can be collapsed into one single equation as

$$\frac{\mathrm{d}g}{\mathrm{d}l} = \frac{2-d}{2}g + K_d\frac{2d-3}{4d}g^3, \tag{1.26}$$

[2] The λ-dependent contribution is proportial to $\frac{\lambda}{2}\int dx(\partial_x h)^2\partial_x^2 h$, which is identically zero and this is readily seen by an integration by parts. With the definition $\delta h(x)/\delta h(x') = \delta(x - x')$, one can verify that the above solution satisfies Eq. (1.24).

where the coupling constant $g^2 \equiv \lambda^2 D/\nu^3$; $K_d \equiv S_d/(2\pi)^d$ and S_d the surface area of the d-dimensional unit sphere. Setting $\mathrm{d}g/\mathrm{d}l = 0$, we obtain two fixed points, $g_1^* = 0$ and $g_2^* = \sqrt{\frac{2d(d-2)}{K_d(2d-3)}}$.

As shown in Fig. 1.8, for $d = 1$, there is an attractive nonzero fixed point g_2^*, while the $g_2^*(d)$ fixed point for $d > 2$ is repulsive, separating two distinct scaling regimes: one is dominated by the EW (linear theory) fixed point and the other is governed by an unknown (strong coupling) fixed point. In the regime where g flows to infinity, the exponents cannot be obtained analytically. For $d = 2$, the flow of g indicates that the coupling constant g is marginally relevant and grows under rescaling. There is no fixed point at a nonzero g. The fixed point is determined by a strong-coupling behavior which is not accessible by perturbation theory. The existence of a KPZ upper critical dimension, d_u, has been heavily argued in the recent literature. However, no evidence for d_u has been found in numerical simulations up to $d = 5$ [43].

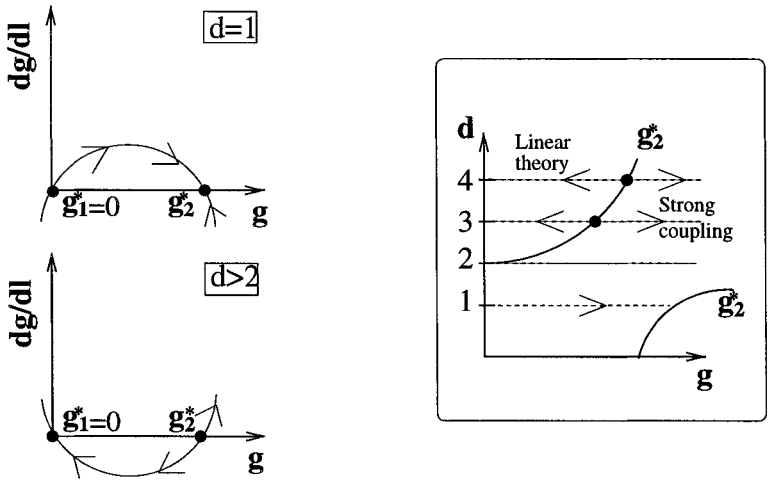

Figure 1.8: The RG flow of the coupling constant g and its phase diagram.

1.2.6 Other processes related to KPZ growth

The numerically-obtained exponents for the BD model are in remarkable agreement with the scaling exponents of the KPZ equation. This tells us that both the KPZ equation

and the BD model indeed belong to the same universality class. Moreover, it has been observed that many other nonlinear growth models belong to the KPZ universality class. Among lots of KPZ-type growth models, we review two solid-on-solid (SOS) type models. They allow neither overhangs nor holes, and limit the height difference between neighboring sites to eliminate large slopes. These models not only minimize the effect of corrections-to-scaling in the BD model, but also provide theoretical connections to other systems via exact mapping onto stochastic spin/particle dynamics.

The first model is the restricted SOS model introduced by Kim and Kosterlitz (KK). It permitted the first systematic investigation of growth exponents for higher dimensions [44]. The KK growth randomly selects a site on a d-dimensional interface, and increases the height of the interface by one, provided that at every stage of growth the restricted SOS condition $\Delta h = 0, \pm 1$ is fulfilled between the selected site and its neighboring sites, as shown in Fig. 1.9(a). The KK growth model simulations showed that it exhibits very good scaling properties, without noticeable intrinsic width or corrections-to-scaling. Moreover, the 1D KK growth can be mapped to stochastic spin-1 dynamics since the possibility of three type Δh values is analogous to the z-component of spin-1 variables [6, 45, 46].

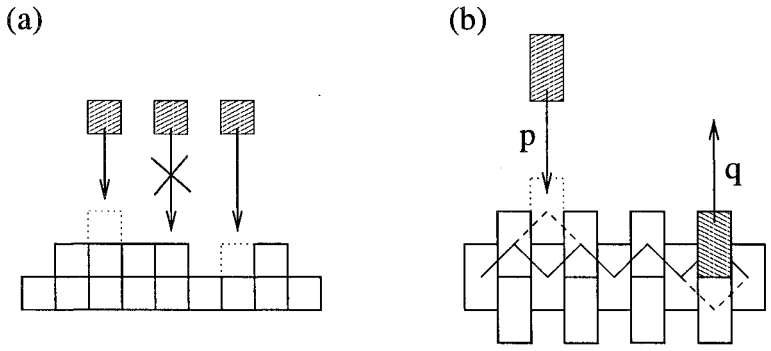

Figure 1.9: (a) KK model and (b) BCSOS model in $d = 1$.

The second model is the body-centered SOS (BCSOS) model studied by Meakin *et al.* [47], Plischke *et al.* [48], and Neergaard and den Nijs [49]. As illustrated in Fig. 1.9(b), either 1×2 shaped particle deposition occurs with probability p at each local minimum, resulting in $h_i \rightarrow h_i + 2$, or evaporation occurs at local maxima with probability q, resulting

in $h_i \rightarrow h_i - 2$. Initially, the interface has a grooved shape, with $h(2i) = 0$ and $h(2i+1) = 2$, where $i = 0, ..., L/2$. The fact that we always choose only the local minima (maxima) to grow (desorb) guarantees that at any stage of the growth process the height difference between two neighboring sites must be exactly unity. Due to this condition, the BCSOS model is sometimes referred to a "single step" model.

By mapping the BCSOS model to a kinetic Ising model, we can describe the interface properties in terms of a set of Ising spin variables $\{s\} = \{s_1, s_2, ..., s_L\}$, where $s_i = \Delta h \equiv h(i) - h(i-1) = \pm 1$. The spin variables located between the original lattice sites represent up (+1) steps and down (-1) steps of the interface. Growth can occur if two spins $(s_i s_{i+1})$ have a $(\downarrow\uparrow)$ configuration with probability p, so that $(\downarrow\uparrow) \rightarrow (\uparrow\downarrow)$. Similarly, evaporation occurs with probability q at a configuration $(\uparrow\downarrow)$, resulting in the transition $(\uparrow\downarrow) \rightarrow (\downarrow\uparrow)$. This can be also interpreted as a lattice gas model if a down step is replaced by a hard core particle and a up step with a hole. In the lattice gas model, we initially have $L/2$ particles at every other lattice site. Figure 1.10 illustrates such mappings:

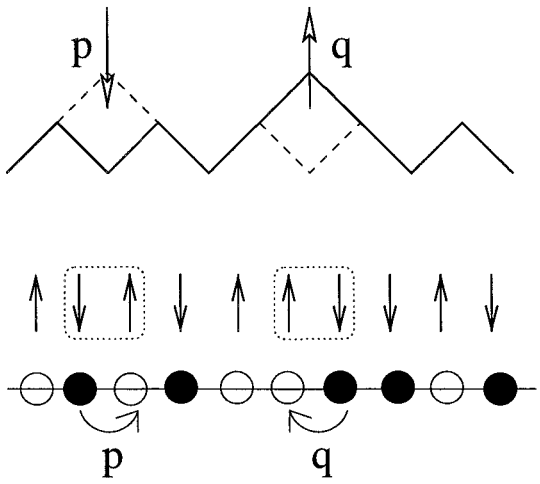

Figure 1.10: Schematic representation of the BCSOS model with the equivalent spin-$\frac{1}{2}$ and lattice gas representations. When $p \neq q$, this lattice gas representation is called the asymmetric simple exclusion process.

The coefficient of the nonlinear term in the KPZ equation, λ, is proportional to $-(p-q)$. At $p = q$, the nonlinear term vanishes and the model is described by the EW equation. The

growth-dominant case ($p > q$) has $\lambda < 0$, so the local velocity decreases with the local slope. A simple argument from spin dynamics can provide the roughness exponent as well. In equilibrium, all configurations are equally probable, so neighboring spins are uncorrelated, $\langle s_i s_j \rangle = \delta_{ij}$. These properties are reminiscent of a Brownian (random) motion. Hence, the roughness exponent of the interface, χ, is 1/2, which coincides with the predictions of both the EW and KPZ equations. Note that the height of the interface at site i can be written with spin variables, $h_i = \sum_{k=1}^{i} s_k + h_1$. The 1D BCSOS model can be mapped onto the famous, exactly soluble, 2D equilibrium models: the so-called XXZ spin-$\frac{1}{2}$ quantum chain model, a quantum six-vertex model [50, 51], and a crystal faceting model [52].

1.2.7 Directed polymer and KPZ equation

The mapping from the KPZ equation itself to the Burgers equation leads to a further connection to *directed polymer problems*, based on the so-called Hopf-Cole transformation [53, 54] of the nonlinear Burgers equation into a linear one. Defining $Z \equiv \exp(-\lambda h/2\nu)$, the KPZ equation becomes

$$\frac{\partial}{\partial t} Z(x,t) = \left[\nu \nabla^2 - \frac{\lambda}{2\nu} \eta(x,t) \right] Z(x,t), \tag{1.27}$$

which is Schrödinger-like, with a random potential of $\eta(x,t)$. Using the Feynman path integral formation of quantum mechanics [55], an interpretation of Z emerges as the partition function for a directed polymer in a disordered medium [56]. For $d = 1$, we may regard the polymer as an interface, so that the anomalous scaling behavior of interfaces in this type of growth processes can be translated into anomalous roughening in the presence of quenched bulk disorder. For a review of the latter, see [57].

1.3 Stochastic dynamics of driven lattice gases

Another class of examples for nonequilibrium random processes includes driven lattice gases [58, 59] and reaction-diffusion mechanisms [60, 61]. In particular, the former is directly related to the KPZ type surface growth, in terms of the symmetric or asymmetric simple exclusion process.

1.3.1 Motion of single polymer chains: Symmetric Exclusion Process

The first example is the motion of a single polymer chain in a random environment of other polymers. Edwards [62] introduced the concept of the confining tube and de Gennes [63] the concept of reptation for this kind of motion, deriving from the topological constraints of the entanglement.

Figure 1.11 illustrates the motion of an entangled polymer in the confining tube and the mapping to a lattice gas model after discretizing a DNA into L consecutive unit segments of the mean pore size δ. Segments connecting two consecutive pores of the surrounding network correspond to particles (filled circles) and segments fully contained in a pore correspond to holes (open circles). Diffusion within the tube amounts to particle-hole exchange. The motion of the end segments in and out of the tube correspond to annihilation and creation of a particle, respectively. This lattice gas description is known in the probabilistic literature as the symmetric simple exclusion process (SSEP) [64].

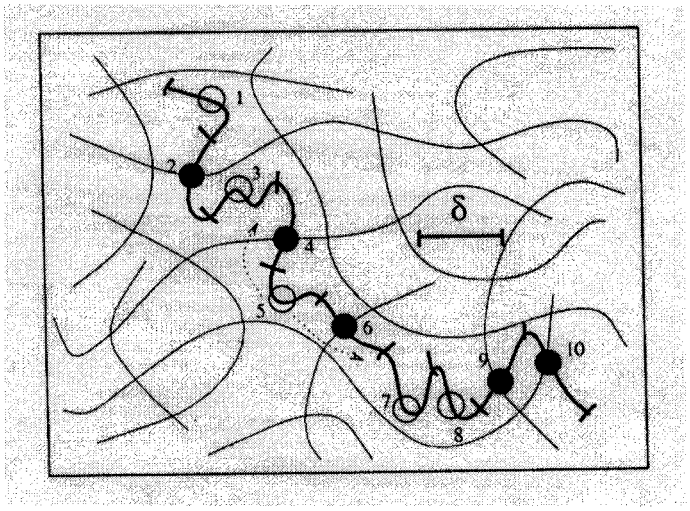

Figure 1.11: Polymer segments of $L = 10$ with a size of the mean entanglement distance δ move diffusively to neighboring pores, from [7].

To account for the additional degree of freedom at the boundary, annihilation and creation of particles has to be allowed with suitable chosen rates at the left and right boundaries, which lets us obtain the SSEP with open boundaries where the lattice gas is in contact with

reservoirs of some fixed density. It is known that the generator appearing in the master equation for this process is the quantum Hamiltonian for a Heisenberg ferromagnet [65]. Recently, the motion of a single entangled polymer has been directly monitored by fluorescence microscopy [66, 67].

1.3.2 Protein synthesis: Asymmetric Exclusion Process

Next, we show how protein synthesis can be modeled by an ASEP model. Protein synthesis is a rather complex process involving a complicated interplay of many different agents. The kinetics of biopolymerization on nucleic acid templates was studied with a lattice gas model by MacDonald and his coworkers [68, 69].

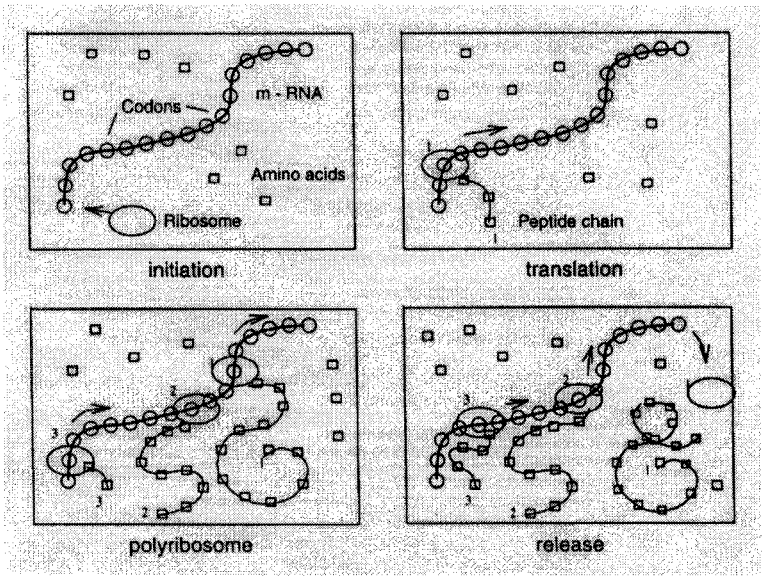

Figure 1.12: Kinetics of biopolymerization on a messenger-RNA (m-RNA) template. Ribosomes attach to the beginning of an m-RNA chain and read the genetic information which is encoded in triplets of base pairs, called codons, by moving along the m-RNA. When a ribosome has reached the end of the m-RNA, the polymer is fully synthesized and the ribosome is released, from [7].

Fig. 1.12 shows the mechanism that MacDonald *et al.* wanted to describe in their model, with few restrictions for the motion of ribosomes, e.g., neighboring ribosomes sitting at the same time on the m-RNA cannot simultaneously read the same information. More

importantly, they cannot pass each other. So if a ribosome is currently located at one particular base pair and temporarily does not proceed further, then an oncoming ribosome from behind will stop until the first eventually moves on.

Therefore, the m-RNA can be represented by a 1D lattice of L sites (the numbers of base pairs) and the ribosome as a particle covering $\mathcal{R}$ neighboring sites which moves randomly by one lattice site with a constant rate p from site 1 until it reaches site L of the lattice. There is no long-range interaction between particles, except for hard-core repulsion (no overlap of ribosomes). Particles at the beginning of the chain are added with rate αp (initiation) and at the end of the chain are removed with rate βp (release). In the idealized case $\mathcal{R} = 1$, this model becomes the well-known ASEP (equivalent to the BCSOS model of the KPZ-type surface growth) with open boundary conditions. It is known that its generator is related to the anisotropic Heisenberg quantum chain [70, 71, 72].

It has been observed that the 1D exclusion process, symmetric or asymmetric, and some of their variants serves as a model not only for the biological systems, but also for fast ionic conductors [10], interface growth [47, 48], diffusion in thin channels [73], spin relaxation dynamics [74], or even real traffic flow [3] (see [76, 77] for traffic models).

1.3.3 Reaction-diffusion mechanisms: $A + A \to A$ and $A + A \to \emptyset$

As the final application, we introduce the modeling of the reaction-diffusion mechanism by lattice gases. An experimentally relevant class of physical reactions rather than chemical ones comprises diffusion-limited annihilation processes, $A + A \to A$ and $A + A \to \emptyset$ [60]. Such processes were used to describe the dynamics of laser-induced excitons on polymers and similar systems, where the excitons hops along a polymer chain, symbolically represented by $A\emptyset \rightleftharpoons \emptyset A$. They may decay spontaneously after some typical lifetime, represented by $A \to \emptyset$, but can also annihilate either in pairs $AA \to \emptyset\emptyset$ or undergo fusion (coalescence) $AA \to A\emptyset, \emptyset A$. In exciton annihilation on TMMC chains ($(CH_3)_4NMnCl_3$), such a situation can be observed experimentally, where excitons of Mn^{2+} ion are initially created by laser excitations

[3] The ASEP has a stationary current-density relation with a single maximum of the current at some intermediate density as is known from the flow diagram of real freeway traffic [75] and exhibits shocks, an important feature of real traffic.

and then the excitons move along the widely separated $MnCl_3$ chains and coalescence when they meet, leading to the emission of light. See [78, 79] for the detailed reviews of these experiments.

To capture the essential physics of 1D diffusion-limited annihilation, a minimal lattice gas model is considered with the symmetric simple exclusion process augmented by a pair annihilation reaction. If a particle attempts to move on an occupied lattice site, then the move is rejected but both particles annihilate. A detailed discussion for the asymmetric case of the latter will be given in Chapter 2.

1.3.4 Overview for relevant studies of 1D driven lattice gases

For stochastic dynamics of interacting particle systems, the symmetric/asymmetric simple exclusion model is one of the conceptually simplest lattice gas models, with only a hard-core on-site interaction between particles. In the presence of some external driving field, this model develops a rather complex behavior. Under the action of the external field, the motion of particles is driven. In this nonequilibrium situation (even in the stationary state), a finite particle current can be maintained.

The asymmetric simple exclusion process (ASEP) is the simplest process for driven lattice gas with a hard core exclusion interaction. The steady state of driven flow depends strongly on the boundary conditions, in contrast to equilibrium systems. The coupling of the 1D driven system to external reservoirs of constant density leads to various kind of phase transitions with divergent spatial length scales [80, 81, 82] and temporal ones [83]. Since this model was first introduced by MacDonald and Pipkin in 1968 [68], it has been exactly solved with various boundary conditions and various updated methods of simulations. It can be interpreted as a lattice realization of the noisy Burgers equation, so that it contains the relevant features of the KPZ growth (see Fig. 1.10). The existence of nonlinearity allows for the formation of shocks that may be seen as a gas of solitons [84]. Based on its many applications, rich dynamical behavior, and an abundance of interesting exact results, the ASEP has achieved a paradigmatic status for nonequilibrium systems. It has also been studied by various nonrigorous macroscopic hydrodynamic theories/approaches [85, 86, 87,

88]. Its boundary-induced phase transitions lead to an extremal principle [89, 90] with open boundary conditions for the steady-state selection of driven diffusive systems.

1.3.5 Dynamics of the ASEP and Different Updates

Before we review in detail the earlier works for the ASEP, we define its dynamics and different updates clearly. Consider a chain of length L. Each site i $(1 \leq i \leq L)$ is either occupied by a particle or a hole (no particle). If the system is periodic, *hopping* is only the basic mechanism by definition. Provided that particle hopping is driven to the right with probability p $(\frac{1}{2} < p \leq 1)$, a particle at site i can move to site $i+1$ with probability p if the target site is empty. Without loss of generality, we assume that there is no hopping allowed to the left, so that nothing happens in the remaining cases [4]. If the system is open with two reservoirs, two more mechanisms, *injection* and *removal*, should be considered since particles/holes at boundaries can be injected and/or removed. Figure 1.13 illustrates the definition of the totally ASEP with open boundary conditions.

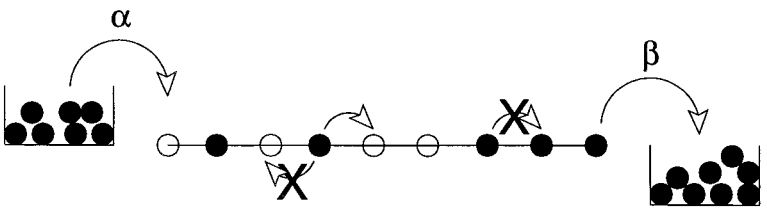

Figure 1.13: The 1D Totally ASEP with OBC.

In general, we categorize the dynamics of the ASEP into two main update rules, *random-sequential updating* and *parallel updating*, based on whether the update is continuous (random-sequential) or discrete (parallel) in time.

- *Random-sequential updating* is the realization of the usual master equation in continuous time. Choose a site at random. Each particle at site i $(1 \leq i \leq L-1)$ has a

[4] Particle hopping in the ASEP can be allowed to both directions with left hopping probability $q = 1 - p$, just like the mapping of the BCSOS model (see Fig. 1.10). However, the general consideration only makes the analytical treatment of the model more difficult than before, without changing its basic features. Thus, most models set $q = 0$.

probability pdt of hopping to the right if the target site is empty. A particle can be added at site $i = 1$ with probability αdt if site 1 is empty, while a particle at site $i = L$ can be removed with probability βdt. Since p simply rescales time, one can set $p = 1$ for the most efficient computer simulations.

- *Parallel updating* is applied simultaneously to all sites of the whole chain in discrete time. However, the whole system can also be sublattice-parallel updated or particle/site ordered-sequential updated. The former allows all possible hopping at all odd sites after those at all even sites and then increases one unit time. The latter starts at the left boundary and ends at the right boundary in one time step, i.e., one sweep through the lattice.

1.3.6 Exact results for the ASEP with translational invariance

For periodic boundary conditions, the ASEP can be exactly solved by Bethe ansatz in the quantum mechanical Hamiltonian interpretation, $\mathcal{H}$, of the time evolution generator. Its ground state and first excited state were computed in the thermodynamic limit [70, 71, 72]. Because of the fact that this $\mathcal{H}$ commutes with the transfer matrix of the six-vertex model [91, 92, 93] when the vertex weights of the latter satisfy certain conditions, the stochastic dynamics of the 1D ASEP maps onto the 2D equilibrium statistical mechanics of the six-vertex model. Dhar [70] and later Gwa and Spohn [71] rewrote the ASEP with translation invariance as a 1D probabilistic cellular automaton described by a spin configuration $\{s_n(t)\}$ updated to a new configuration $\{s_n(t+dt)\}$, where $s_n = \pm 1$ (+1 for particle and -1 for hole), $n = 1, ..., L$, and dt is a short time interval.

Two neighboring spins exchange their positions with probability $p = \frac{1}{2}[1 + Bs_n(t)]dt$, or remain stationary with probability $(1 - p)$. Given the dynamic updating rule, it is straightforward to obtain the master equation for the time evolution of the probability distribution $P(t, \{s_n\})$. Each spin configuration $\{s_n\}$ is denoted by a basis vector $|s\rangle$, so that $P(t, \{s_n\})$ translates into a state vector $|P\rangle = \sum_s P(t, s)|s\rangle$ and the generator $\mathcal{H}$ of the master equation is defined as the normalized transition probability $\langle s|\exp(-\mathcal{H}t)|s'\rangle$ at time t. With the usual Pauli matrices $\sigma_n \equiv (\sigma_n^x, \sigma_n^y, \sigma_n^z)$ at site n, satisfying $[\sigma_n^x, \sigma_l^y] = 2i\delta_{nl}\sigma_n^z$

and cyclic permutations,

$$\mathcal{H} = -\frac{1}{4}\sum_{n=1}^{L}[\sigma_n \cdot \sigma_{n+1} - 1 + iB(\sigma_n^x \sigma_{n+1}^y - \sigma_k^y \sigma_{n+1}^x)] \tag{1.28}$$

which reduce to the ferromagnetic Heisenberg chain if $B = 0$.

In the steady state, time-dependent correlations are expressed by the dynamic structure factor,

$$S(k,t) = \sum_{n=1}^{L} \exp(ikn)[\langle 0|\sigma_0^z \exp(-\mathcal{H}t)\sigma_n^z|0\rangle - \langle 0|\sigma_0^z|0\rangle] \tag{1.29}$$

where the limit of $L \to \infty$ with a fixed number of up-spins, M $(0 \leq M \leq L)$, is understood. For long times, the decay of $S(k,t)$ is controlled by the energy gap between the group state and the first excited state. The real part of the gap is expected to scale as $\Delta E \propto L^{-z}$ because the energy gap represents the inverse of the characteristic time in the ASEP and KPZ-type growth. After some detailed calculations, Gwa and Spohn obtained $\Delta E \simeq cL^{-3/2}$ where c is a constant [71, 72]. Their exact result of $z = 3/2$ is in agreement with Galilean invariance for the 1D noisy Burgers equations mentioned in the previous section.

For ordinary diffusion ($B = 0$, i.e., no nonlinearity), the Heisenberg chain exhibits a gap scaling as L^{-2} [94], corresponding to $z = 2$ of the EW class. The symmetric case ($B = 0$) has been exploited for the arrow-arrow correlation functions [95, 96]. The analysis was also subsequently extended to the partially asymmetric case with arbitrary particle number M by Kim [97]. For finite density, $z = 3/2$, but for finite particle number, $\Delta E \sim \sqrt{M}L^{-2}$. This $z = 2$ for finite M is in agreement with an earlier result by Henkel and Schütz [98].

The motion of a tagged particle in the ASEP with translational invariance is another interesting time-dependent problem. Key quantities are the average drift velocity of the particle, as well as the dynamic scaling of the root-mean-square displacement around the average drift. Not surprisingly, it has been found that the results sensitively depend on the order of the limits $L \to \infty$ and $t \to \infty$.

Let $\langle x(t)\rangle$ denote the average displacement of the tagged particle at time t with $\langle x(0)\rangle$=0. Then $\sigma(t) \equiv \langle [x(t) - \langle x(t)\rangle]^2\rangle$ represents the variance of the fluctuations around the average distance traveled and the diffusion constant D is written as $D \equiv \lim_{t\to\infty} \sigma(t)/2t$ by an Einstein relation, provided that the limit exists. Now we explore how the order of the limits affect the results of $\delta(t)$:

- The limit $L \to \infty$ is taken before $t \to \infty$ at fixed particle density ρ.

  If all averages are performed over the stochastic dynamics of the particles and over the random initial distribution of the untagged particles, the motion of a tagged particle is diffusive, $\langle x(t) \rangle \simeq vt$, and $\delta(t) \simeq Dt$, where the drift velocity $v = B(1-\rho)$ and $D = \frac{v}{2}$ [99, 100]. For $B = 0$ (symmetric case), $\sigma(t) \propto t^{1/2}$ [101]. In contrast, $\sigma(t) \propto t^{2/3}$ in the long-time limit with the same initial condition [102, 103]. This implies that the motion of a single tagged particle differs from that of density patterns. However, the overall center of mass drifts with $v_{\rm cm} = B(1-2\rho)$, and the variance of its fluctuations around the average drift scale as $t^{4/3}$, irrespective of the choice of the initial configuration. Similarly, the variance of the center of mass position of a density perturbation spreads as $t^{2/3}$ for both average procedures. Further details and related results can be found in the literature: [103] for a discussion of the stochastic motion of mass points, [104] for the connection between tag diffusion and interface growth, and [105] for two-tag correlation functions.

- The limit $t \to \infty$ is taken at finite L, no dependency of initial conditions.

  Derrida *et al.* [106] expressed the weight of configurations as products of non-commuting matrices. In their study, the totally ASEP ($B = 1$) is considered with M untagged particles distributed randomly and a single tagged one placed at the origin. They found that $\langle x(t) \rangle \simeq vt$ with $v = \frac{(L-M-1)}{(L-1)} \approx (1-\rho)$ in the limit $L \to \infty$ at fixed $\rho \equiv M/L$, and that the exact expression of D allows for the discussion of two limits. For the first limit, $L \to \infty$ at finite M, the process does not approach the collisionless limit. Rather, collisions are highly correlated in time. As a result, D depends on the exact number of particles in the system ($D \simeq 4^M (M!)^2/(2M+1)!$). For the second limit, $L \to \infty$ at finite ρ (a physically more relevant situation), $D \simeq \sqrt{\pi}(1-\rho)^{3/2}(4\rho L)^{-1/2}$ to leading order in L, so that $\delta(t) \propto t/\sqrt{L}$ [106]. For a substrate of L, the roughness can only increase to $O(L)$, i.e., $\delta(t_s) \propto L$, so that $t_s \propto L^{1/z}$ with $z = 3/2$ (1D KPZ dynamic exponent).

1.3.7 Relevant studies and results for the ASEP without translational invariance

There are two major ways to break translational invariance in the ASEP, with interesting results. One is to consider open boundary conditions in which particles are added at one end and removed at the other end [80, 81, 82, 83, 107]. The other is to retain periodic boundary conditions, but to introduce a defect into the system by modifying the transition rates locally [8, 108, 109, 110, 111]. By properly chosen injection/removal rates or defect strength, nonequilbrium phase transitions occur between profiles of different shapes and average densities [80, 81, 83, 98, 107, 110, 111]. These situations make shock fronts develop. Such shock profiles and their fluctuations have been widely investigated via numerical simulations [8, 109] and exact solutions(for some restricted cases) [106, 108, 112].

Phase diagram and phase transitions for the ASEP with open boundary conditions

In the choice of open boundary conditions for the ASEP, particles enter the system at the left end (at site $i = 0$) with probability α and leave it at the right end (at site $i = L$) with probability β. Within the bulk, particles hop to the right only, which is the simplest case ($B = 1;\ p = 1$) (see Fig. 1.13). The steady state for this case can be exactly found, either in form of a recursion relation relating the steady state of an $(L-1)$-site system to that of an L-site system [81, 107] or by rewriting the configurational weights as products of noncommuting matrices, the so-called matrix product ansatz [82]. Exact results for the density profile and stationary equal-time correlations were first obtained for $\alpha = \beta = 1$ [107, 113] and then generalized to all α, β [81, 82].

An intriguing feature of the ASEP with open boundary conditions is the emergence of boundary-induced phase transitions. Krug first observed it by the MF theory [80]. In his study, the boundary densities of the ASEP were set to ρ_o at the left end and to zero at the right end of the system (equivalent to $\alpha > 0, \beta = 1$). In the steady state, the system selects its density profile in such a way as to maximize the current flowing through it, so that the current-density relation $j = j(\rho)$ typically has a maximum at some ρ^* (specifically, $\rho^* = 1/2$ for the ASEP). Then, the sum of a systematic current $j(\rho)$ and an excess current generated by the boundary conditions, i.e., the total current J, would adjust

itself to $J = \max_{\rho\in[0,\rho_o]} j(\rho)$ in the thermodynamic limit. This induces a phase transition controlled by ρ_o. If $\rho_o > \rho^*$, the bulk density becomes the same as ρ^* and the density profile shows an algebraic decay to zero at the right boundary. Otherwise ($\rho_o < \rho^*$), the profile approaches a plateau at density ρ_o exponentially over a correlation length that diverges as $\rho_o \to \rho^*$.

Derrida *et al.* explored the general case of various α and β, first by a MF analysis [107] and then by an exact solution of the steady state [82]. See also the subsequent paper by Schütz and Domany [81] for details. The behavior of the exact density profile $\langle n_x \rangle$ allows for the identification of two regimes in the large L limit: a "boundary-dominated" regime characterized by $L \to \infty$ at fixed x followed by $x \to \infty$, and a "bulk-dominated" regime where $L, x \to \infty$ and $|L - x| \gg 1$, i.e. $x \equiv Lf$ with $0 \leq f \leq 1$ in the scaling limit. The exact solution of the steady state confirms that the MF theory already yields correctly three distinct phases and the exact locations of the phase boundaries. See Fig. 1.14, e.g., the line of $\beta = 1$ is what Krug studied. The steady-state exact solution offered two key insights. Firstly, the slope $t_L(x) \equiv n_x - n_{x-1}$ of the density profile factorizes into two functions, $t_L(x) \propto F_x(\alpha) F_{L-x}(\beta)$, up to an amplitude. Secondly, two characteristic length scales, $\xi_\alpha^{-1} = -\log[4\alpha(1-\alpha)]$ and $\xi_\beta^{-1} = -\log[4\beta(1-\beta)]$, are identified to determine the behavior of the function F. The latter indicates the possibility of phase transitions (nonanalytic changes in the x-dependence of the density profile) at the two lines, $\alpha = 1/2$ at any β and $\beta = 1/2$ at any α.

Consequently, the high-density phase subdivides into two regions, phase $\mathrm{A_I}$ for $\beta < \alpha < 1/2$ and $\mathrm{A_{II}}$ for $\beta < 1/2$, $\alpha > 1/2$, respectively. By particle-hole symmetry, a similar statement holds for the low-density phase into $\mathrm{B_I}$ and $\mathrm{B_{II}}$, respectively. Thus, this new distinction in the high/low-density phase is obtained by considering how the bulk density is approached from the edges of the chain. Asymptotically, the slope of the profile can be written as $t_L(x) \sim x^\nu \exp(-x/\xi)$, with a proper characteristic length ξ and a decay exponent ν of the density profile, based on the exact solutions. Phase $\mathrm{A_I}$ has $\xi^{-1} \equiv \xi_\alpha^{-1} - \xi_\beta^{-1}$ and $\nu = 0$, where the profile approaches the bulk density exponentially with a length scale ξ. As $\alpha \to 1/2$, ξ_α diverges and ν changes to $1/2$, and then, in phase $\mathrm{A_{II}}$, $\xi = \xi_\beta$ and $\nu = 3/2$. Similar results hold for phases $\mathrm{B_I}$ and $\mathrm{B_{II}}$ as the roles of α and β are exchanged

and x is replaced by $L - x$. In the maximal current phase where both ξ_α and ξ_β diverge, $t_L(x) \sim x^\nu (1 - x/L)^\nu$ with $\nu = 3/2$, i.e., the density profile shows a pure power-law decay as $x^{-1/2}$ towards the bulk value $1/2$. Along the coexistence line, none of length scales diverges, but ξ^{-1} vanishes by accident since $\xi_\alpha = \xi_\beta$, where the density profile is linear with positive slope $(1 - 2\alpha)/L$. Note that the linear profile on the coexistence line $\alpha = \beta < 1/2$ results from a superposition of states where a shock between a low density (α, left) and a high density ($1 - \beta$, right) is present at an arbitrary position.

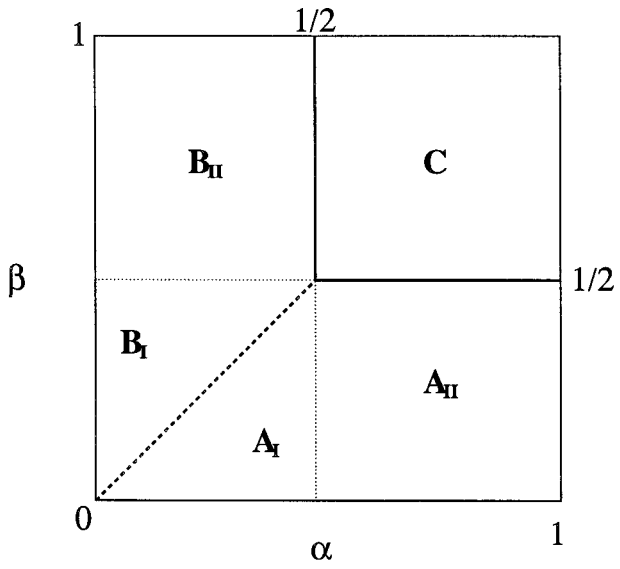

Figure 1.14: Exact phase diagram of the ASEP with open boundary conditions: For $\beta \leq 1/2$ and $\beta < \alpha$, a high density phase (A_I and A_{II}, say A) exists with current $\beta(1 - \beta)$ and the bulk density $1 - \beta$ (almost everywhere except for near the left boundary), and for $\alpha \leq 1/2$ and $\alpha < \beta$, a low density phase (B_I and B_{II}, say B) exists with current $\alpha(1 - \alpha)$ and the bulk density α where the boundary layer is located near the right edge. Phases A and B are separately by a coexistence (first-order phase transition) line $\alpha = \beta < 1/2$. In the third phase C for $\alpha, \beta \geq 1/2$ (namely a maximal current phase), the bulk density reaches $1/2$ (except in both boundary layers), so that the current takes its maximal value $1/4$.

Given that the steady state is exactly known, all higher equal-time correlation functions can also be exactly computed. Derrida and Evans [113] obtained the two-point function explicitly, and conjectured the form of three- and four-point correlation functions, based on the structure of the one-point (the density profile) and the two-point functions. Their results

and conjectures are in excellent agreement with numerical checks. Long range correlation functions induced by boundary conditions persist in the bulk. In particular, the two-point function provides information about the fluctuations in the total number of particles (mass), $M = \sum_{i=1}^{L} n_i$, because $\langle M^2 \rangle = L/2 + 2\sum_{i>j}\langle n_i n_j \rangle$. The variance of the total mass, $\langle M^2 \rangle - \langle M \rangle^2$, approaches the value $L/8$ for $L \to \infty$, in contrast to $L/4$ if correlations were ignored.

For a wider perspective, we mention the reinterpretation of the ASEP with open boundary conditions as the KPZ-type BCSOS model. In the interface dynamics, the parameters α and β describe inhomogeneities in the deposition process at the boundaries of the system [8, 110, 113, 114, 115]. The surface height $h(x)$ at distance from the left edge is obtained from the occupation number n_i, i.e., $h(x) = \sum_{i=1}^{x}(1 - 2n_i)$. In the case of $\alpha = \beta > 1/2$, the boundaries are, on average, at the same height, while the bulk is lower than them. The results for the density profile translate into $\langle h(x) \rangle \propto \sqrt{x}$ at the boundary, which is in agreement with [115](see also [114]), and $\langle h(Lf) \rangle \propto [Lf(1-f)]^{1/2}$ in the bulk, where $f \equiv x/L$.

Results for the ASEP in presence of local inhomogeneity

Finally, we review earlier studies for the microscopic nature of shocks in the ASEP without translational invariance. Since this subject is also covered in Chapter 3 and Chapter 4, we here focus on the most relevant issues.

Based on considerable analytic studies [112, 116, 117, 118, 119, 120, 121] and numerical studies [8, 122, 123], it has been established that shocks are microscopically sharp and stable, extending only over a few lattice spacings. The microscopic shock location performs a random walk around its average position if randomness in the initial configurations is allowed [116, 118]. Otherwise, the shock fluctuations are reduced to $t^{1/3}$ from $t^{1/2}$ [102, 103]. These results generically appear, in the sense that they also apply to a variety of other 1D stochastic lattice models with sequential or parallel dynamics, even if ferromagnetic or anti ferromagnetic interactions are included [124]. In the ASEP with translational invariance, the microscopic shock profile was determined exactly, following from the exact solutions by Derrida *et al.* [112, 121] for the steady state of a system of first and second class particles

on a ring, with two given densities ρ_1 and ρ_2, respectively. This steady state does not allow for inhomogeneities in the density distribution of first class particles, so the observation of a shock is unexpected. However, we can see that if such a uniform system is viewed from a specific (tagged) second class particle, the *tagged* second class particle sees exactly the same shock profile as a single second class particle in a system where the density approaches the limiting value $\rho_+ \equiv \rho_1 + \rho_2$ and $\rho_- \equiv \rho_1$ at $\pm\infty$, respectively [119]. The exact shock profile approaches $\rho_\pm$ exponentially. This implies that the shock is sharp over a characteristic length which diverges as $(\rho_+ - \rho_-)^{-2}$ as $\rho_+ \to \rho_-$.

Another interesting feature of such shock fronts is the finite-size scaling (FSS) of their fluctuations. Janowsky and Lebowitz [8] introduced a blockage into the ASEP on a ring of L sites, where the hopping probability r is reduced, $0 < r < p$, compared to $p = 1$ for other parts. Based on their numerical study and MF analysis, for a fixed overall density ρ_o and $r \leq (1 - |2\rho_o - 1|)/(1 + |2\rho_o - 1|)$, the system shows a segregated phase of two regions, separated by a sharply defined shock front. The asymptotic densities on either side, ρ_{high} and $\rho_{\text{low}} = 1 - \rho_{\text{high}}$, depend only upon r. The FSS results show that the fluctuations of the shock position scale as $L^{1/2}$ in the generic case and as $L^{1/3}$ in the half-filled system, i.e., $\rho_o = 1/2$. Based on their intuitive argument where they tried to claim the $t^{1/2}$ versus $t^{1/3}$ behavior of shocks in the infinite system, the former behavior is caused by the random motion of particles and holes across the blockage, while the latter is due to the dynamical randomness of motion in the bulk since the random motion is canceled as the shock front is located exactly (on average) at the middle of the system. But neither exact solutions nor any rigorous arguments for 1/3 have been found. A qualitatively similar diagram was found by Schütz [83], but in his model, the motion of particles was fully deterministic because he used a sublattice-parallel dynamics which updates even and odd lattice sites separately. The phase diagrams for deterministic and stochastic models are different even though both phase diagrams consist of the same three distinct phases. Not surprisingly, there are no FSS fluctuations of the shock position observed in the half-filled deterministic model.

Janowsky and Lebowitz also tried to estimate analytically the average steady-state current $J_{L\to\infty}(r, a = \alpha = \beta)$ by extrapolating exact results for a finite open system [108]. They found that $J_{L\to\infty}(r, a)$ is an increasing function of r for a given value of a and that

the half-filled system current, $J_\infty(r, \frac{1}{2})$, seems to approach the limiting value 1/4 already around $r \simeq 0.8$ (see [125] for a detailed discussion). However, it is not clear enough to determine the existence of the critical blockage strength $r_c(< 1)$ because their calculation for J_∞ exhibits an essential singularity at $r = 1$. Up to now, neither any rigorous proofs nor any strong reliable arguments for this issue have been found. Similar transitions in a 1D SOS-type inhomogeneous growth model were observed numerically by Kandel and Mukamel [110], in which they mostly focused on the parallel update version of the model and mentioned that its sequential one shows similar results.

Earlier studies of the ASEP tells us that 1D nonequilibrium driven systems with short-ranged interactions can exhibit boundary/defect-induced dynamic phase transitions, in contrast to 1D equilibrium cases. So it is really meaningful for us to investigate them in terms of universal scaling properties in this thesis. In particular, we explore a puzzling problem in the ASEP: scaling properties of the queue length before/after the shock front (traffic jams), or the existence of a continuous transition at $r_c < 1$ in the half-filled system. A new way to study the fluctuations of traffic jams is discussed in Chapter 3, and the puzzling problem in the half-filled system is resolved in Chapter 4, which was motivated by the most recent experimental result: faceting in slow combustion of paper with a columnar defect, which has been observed by Timonen's group [126]. This group also reported that kinetic roughening in slow combustion of paper belongs to the KPZ university class [1].

Chapter 2

PARTICLE DYNAMICS IN A MASS-CONSERVING COALESCENCE PROCESS

We consider a fully asymmetric one-dimensional diffusion model with mass-conserving coalescence. Particles of unit mass enter at one edge of the chain and coalesce while performing a biased random walk towards the other edge where they exit. The conserved particle mass acts as a passive scalar in the reaction process $A + A \to A$, and allows an exact mapping to a restricted ballistic surface deposition model for which exact results exist. In particular, the mass-mass correlation function is exactly known. These results complement earlier exact results for the $A + A \to A$ process without mass. We introduce a comprehensive scaling theory for this process. The exact analytical and numerical results confirm its validity.

This chapter has been published separately in M. Ha, H. Park, and M. den Nijs [127].

2.1 Introduction

Diffusion-limited chemical processes are at the focus of recent research. These are dynamic systems where the chemical reaction time scales are short compared to those controlling spatial fluctuations in concentration. The latter dominate the kinetics, in particular in low dimensions. Such processes display dynamic scale invariance with scaling properties that are robust, tend to be universal, and not sensitive to many details of the actual dynamics at the microscopic level. Simplified models are therefore able to catch the essence of the process. Moreover, some of these models are accessible to exact solutions in one dimension.

An example of these is the one-species coalescence process, $A+A \to A$ [128, 129, 130, 131, 132, 133, 134, 135, 136, 137, 138, 139, 140, 141, 142]. Exact results for this process were obtained recently using the so-called inter-particle distribution function (IPDF) method,

also known as the method of empty intervals [143, 144]. This includes several versions of the model, with and without external input of particles and in the presence or absence of a diffusion bias along the chain [145, 146]. Coagulation processes with a localized input like this have been studied analytically earlier [145] in context of potential applications, such as the mass distribution of stars [147] or cluster distributions in chemical reactions [148, 149].

In this chapter, we address the fully asymmetric diffusion version where particles enter at one edge of the chain, and coalesce when they meet each other, while performing a driven random walk towards the other edge [146]. We enhance this model by assigning a mass to each particle, which is preserved during each merging event [145]. Our motivation for this generalization of the model is that it allows the derivation of exact results for its physical quantities through an exact mapping of our model onto a growth model (namely the restricted ballistic deposition model [150]) describing inhomogeneously growing surfaces.

2.2 Model

Consider a linear chain with L sites. Particles of unit mass enter at the left boundary $x = 1$, diffuse to the right and coalesce when they meet, and ultimately exit at the right boundary $x = L$. The diffusion of the particles along the chain is totally biased. Choose a site x at random. If occupied, the particle at this site moves to the next site $x \to x + 1$ with probability 1. If site $x + 1$ is already occupied, the two particles merge,

$$m_x(t+1) = 0 \quad \text{and} \quad m_{x+1}(t+1) = m_{x+1}(t) + m_x(t) \tag{2.1}$$

with m the total mass of each particle. Total mass is conserved during coalescence. Site $x = 1$ is the input boundary. If chosen as an update site, it is immediately refilled by the reservoir $m_1(t+1) = 1$ and $m_2(t+1) = m_2(t) + m_1(t)$ At the opposite edge, $x = L$, the particles simply fall off the chain, $m_L(t+1) = 0$, back into the reservoir.

The mass rides like a passive scalar on top of the particles. It has no effect on the transition probabilities. In the subspace of the occupation numbers, $c_x = 0, 1$ (for empty or occupied site), the process is the fully asymmetric process $A + A \to A$. The mass is a useful parameter. It allows an exact mapping onto an exactly soluble restricted ballistic surface deposition (RBD) model [150]. Consider a one dimensional interface, as shown in Fig. 2.1.

The RBD model is restricted in the sense that the steps can only be downward. Up-steps are forbidden. The down-step size can take any value, $m_x = 0, 1, 2, \cdots$. During each time step, one of the columns at $x + \frac{1}{2}$ is chosen at random, m_x particles are deposited onto it such that the entire step fills up and the step at $x + 1$ grows to $m_{x+1} + m_x$. Exact results for this RBD model have been obtained earlier using a generating function approach [150]. We can reinterpret those exact results in framework of the asymmetric $A + A \rightarrow A$ reaction process.

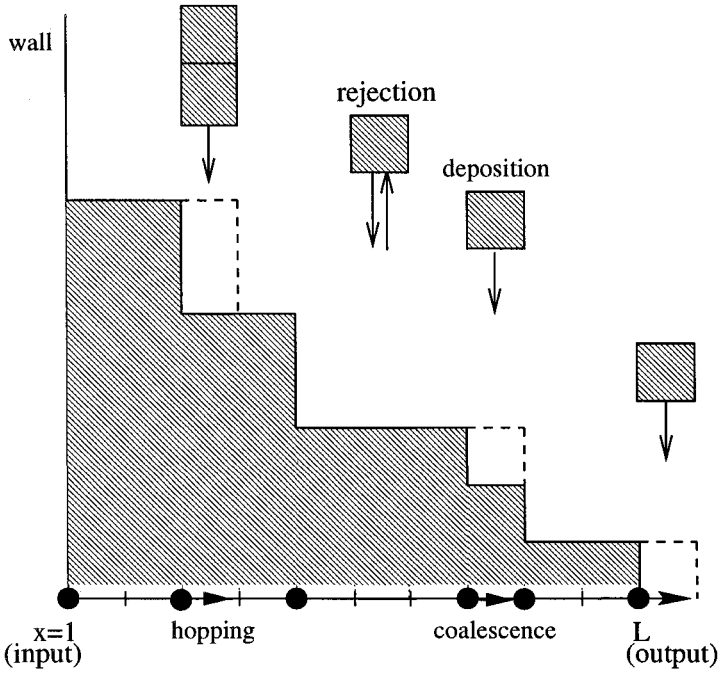

Figure 2.1: Surface representation of the $A + A \rightarrow A$ process. The step heights along the stairway represent the mass of the particles. Each deposition process fills-up the entire step, such that the adjacent step has a new height equal to the sum of the two.

2.3 Numerical and exact results

Starting from the master equation, closed form recursive equations of motion are obtained for the mass distribution along the chain $M(x,t) = \langle m_x(t) \rangle$ and also (as discussed later) the two-point mass correlations. $M(x,t)$ obeys the relation

$$M(x,t+1) = (1-\frac{1}{L})M(x,t) + \frac{1}{L}M(x-1,t) \tag{2.2}$$

with boundary condition $M(1,t) = 1$ (see Eqs. (8)-(15) in Ref. [150] for details). This implies that in the stationary state the mass distribution is uniform, $M(x) = 1$, and there is a direct link between particle concentration $C(x) = \langle c_x \rangle$ and the average mass carried by each particle, $\tilde{M}(x)$. They are exactly related as $\tilde{M}(x) = M(x)/C(x)$ where $\tilde{M}(x)$ measures the average mass over occupied sites only. Particle coalescence creates increasingly heavier particles in the chain towards the right. At the same time they become more sparsely spaced, because on average the mass remains constant along the chain.

In the alternate RBD surface representation, this means that although the step heights increase along the surface from left to right, the steps occur at correspondingly larger intervals, such that the stationary state average slope of the staircase remains constant. This dynamic process has a peculiar hierarchical structure. Consider the path of one unit of mass. It performs a biased random walk, but completely uncorrelated from all other masses. Similarly, two specific mass units perform completely independent random walks, until the moment they meet. From there on they move randomly but as a bound pair. Again, all other particles play no role. This hierarchical property suggests the following scaling theory. Consider a specific unit of mass. It moves to the right with average velocity $v = 1$. The standard deviation in its position is proportional to the square root of the time and distance traveled, i.e. $\Delta r \sim x^{\frac{1}{2}}$. While diffusing to the right this particle merges with other masses. The total amount of mass it sweeps up is expected then to be of order Δr, i.e., that the average mass of occupied sites scales as $\tilde{M}(x) \sim x^{\frac{1}{2}}$. The amount of swept-up mass does not depend on the particle concentration $C(x)$, because although the merging events become less frequent, they increase in size. However, this increasing lumpiness will show in increasing statistical fluctuations along the chain in Monte Carlo simulations.

Next, we predict that the above random walk exponents are exact. This presumes the absence of intricate correlations between the particles. The hierarchical structure of the equations of motion, and the diffusion equation structure of recursion relations in both exact solution methods suggest this prediction. In the following we demonstrate the validity

of this scaling theory from both numerical and analytical exact results.

Hinrichsen *et al.* [146] obtained the exact stationary state particle concentration. It scales as

$$C(x) = \sqrt{\frac{1}{\pi x}}[1 + \frac{3}{8x}] + O(x^{-5/2}). \tag{2.3}$$

This agrees with our scaling theory, because of the exact relation $\tilde{M}(x) = M(x)/C(x)$. The scaling argument predicts that $\tilde{M}(x)$ grows as $x^{\frac{1}{2}}$, while Eq. (2.2) implies that $M(x) = 1$.

Figure 2.2 illustrates the above numerically. It shows the time evolution of the particle density at various values of x starting from the uniform initial state where every site is occupied by one unit of mass particle. We averaged over 10 independent Monte Carlo runs. Initially the curves coincide, until the time when particles from the input edge reach that specific site. As expected this crossover time scales linearly with x, i.e., with the uniform average particle velocity along the chain. The slope of the initial curve is $C(x,t) \sim t^{-\frac{1}{2}}$, and the stationary state plateau values scale as $C(x) \sim x^{-\frac{1}{2}}$, both in accordance with the scaling theory. Notice also that the statistical fluctuations increase with the distance from the source x.

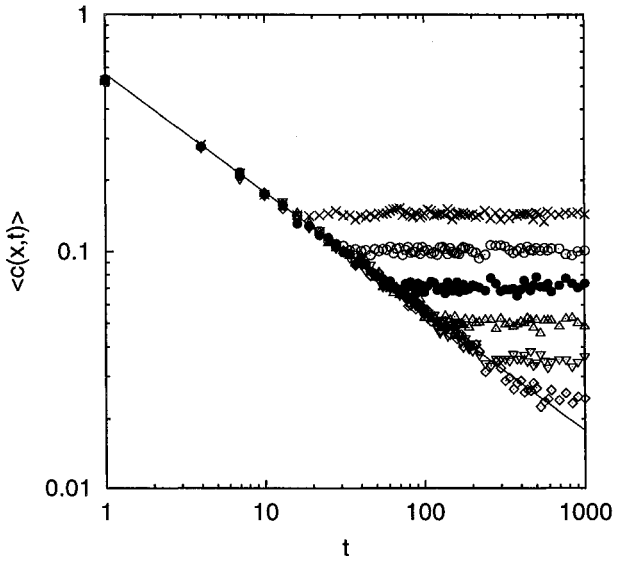

Figure 2.2: The time dependent particle concentration $\langle c(x)\rangle$ as function of time at various values of the distance from the source, $x = 16(\times), 32(\circ), 64(\bullet), 128(\triangle), 256(\triangledown)$, and $512(\diamond)$ at chain length $L = 512$. The slope of the drawn line is -1/2.

The mass auto-correlation function, $w_m^2 = \langle m_x^2 \rangle - \langle m_x \rangle^2$ measures these fluctuations, and is a special case of the two-point correlator discussed below for which we have an exact solution from the mapping to the RBD model. At large x the fluctuations grow as $w_m(x) \simeq \sqrt{x}$, in accordance with our random-walk based scaling theory. We checked numerically the fluctuations in the particle density. Figure 2.3 shows that they decay as $w_p \simeq A/\sqrt{x}$, again consistent with the scaling theory.

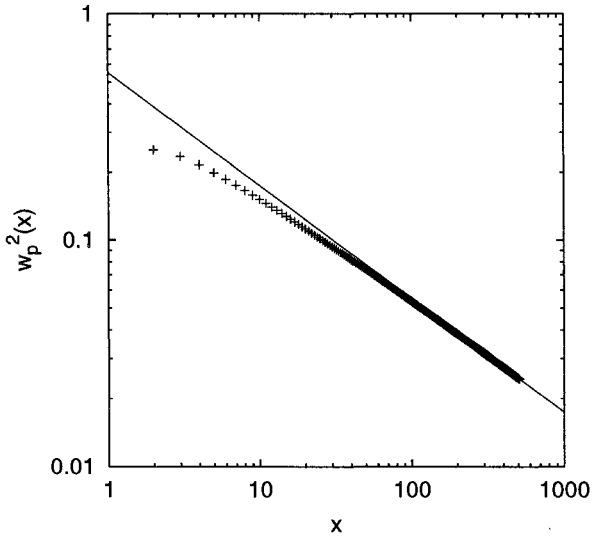

Figure 2.3: Fluctuations in the particle concentration from the auto-correlation functions $w_p^2(x) = \langle c^2(x) \rangle - \langle c(x) \rangle^2$ at chain length $L = 512$. The slope of the drawn line is -1/2.

Consider the particle-particle correlation function, $g_p(x,r) = \langle c_x c_{x+r} \rangle - \langle c_x \rangle \langle c_{x+r} \rangle$ and the mass-mass correlation function, $g_m(x,r) = \langle m_x m_{x+r} \rangle - \langle m_x \rangle \langle m_{x+r} \rangle$. As far as we know, no exact results are available for $g_p(x,r)$, from the method of empty intervals, although it seems within reach. On the other hand, the two-point mass correlator $G_m(x,y,t) = \langle m_x(t) m_y(t) \rangle$ was shown in [150] to obey in the stationary steady state the recursion relations

$$\begin{aligned} G_m(1,x) &= G_m(1,x-1), \\ G_m(x,x) &= 2G_m(x-1,x) + G_m(x-1,x-1), \\ G_m(x-1,x) &= \frac{1}{2} G_m(x-2,x), \\ G_m(x,y) &= \frac{1}{2}[G_m(x-1,y) + G_m(x,y-1)], \end{aligned} \tag{2.4}$$

where $|x-y| \geq 2$. This set of coupled equations can be solved exactly,

$$\begin{aligned} G_m(1,x) &= 1, \\ G_m(x,x) &= 1 + 4(x-1)Z_{2(x-1)}(0), \\ G_m(x-1,x) &= Z_{2(x-2)}(0), \\ G_m(x,y) &= \sum_{n=0}^{r-1} Z_{2(y-2)}(n) = 1 - \sum_{n=r}^{y-2} Z_{2(y-2)}(n), \end{aligned} \tag{2.5}$$

with $r \equiv (y-x) > 0$, and

$$Z_{2p}(n) = \frac{(2p-n)!}{p!(p-n)!}(\frac{1}{2})^{2p-n}, \tag{2.6}$$

which is related to the probability that a random walker returns to its starting point exactly n times up to $2p$ steps, see [150] for details.

We expect the following scaling form for both g_m and g_p in the stationary state:

$$g_\alpha(x,r) = b^{-2\mathrm{x}_\alpha} g_\alpha(b^{-1}x, b^{-1/2}r), \tag{2.7}$$

with b an arbitrary scale factor. The distance x from the source plays the role of time in our diffusion-coalescence type scaling argument. Therefore x should scale with respect to the correlator distance r as $r \sim \sqrt{x}$. The other exponents, x_p and x_m, follow by power-counting. They must be the dimensions of the particle and mass concentrations, $C(x)$ and $M(x)$, which are equal to $\mathrm{x}_p = \frac{1}{2}$ and $\mathrm{x}_m = 0$ according to the previous discussion. We perform numerical simulations for g_p, and exact enumerations of the exact formula for g_m. Figures 2.4 and 2.5 show the scaling functions f_p and f_m, defined as

$$\begin{aligned} g_p &= x^{-1} f_p(r/\sqrt{x}), \\ g_m &= f_m(r/\sqrt{x}), \end{aligned} \tag{2.8}$$

The data collapses perfectly and thus confirms the validity of the scaling relations, eq.(2.7).

Both scaling functions vanish at large $R = r/\sqrt{x}$, as they should. At small R they are both linear in the scaling variable. It is easy to evaluate the exact recursion relations for G_m in the limit of large x and fixed small r. This yields $f_m(R) \simeq -1 + \frac{1}{\sqrt{\pi}}R$. The particle correlator scaling function is also linear at small R. We find numerically that

$$f_p(R) \simeq -a + bR \tag{2.9}$$

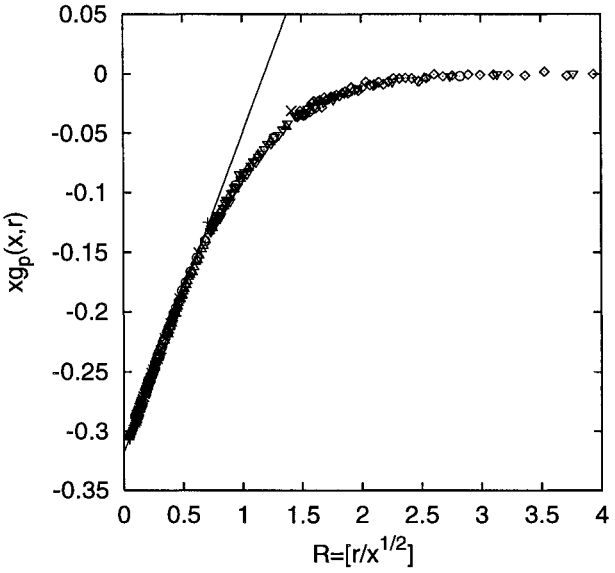

Figure 2.4: The scaling function for the particle-particle correlator g_p, from 10 independent Monte Carlo runs each averaged over 10^6 time steps at chain length $L = 512$ for various distances from the source, $r = 1(+), 2(\times), 4(\circ), 8(\triangle), 16(\triangledown)$, and $32(\diamond)$. The drawn line is obtained from Eq. (2.9).

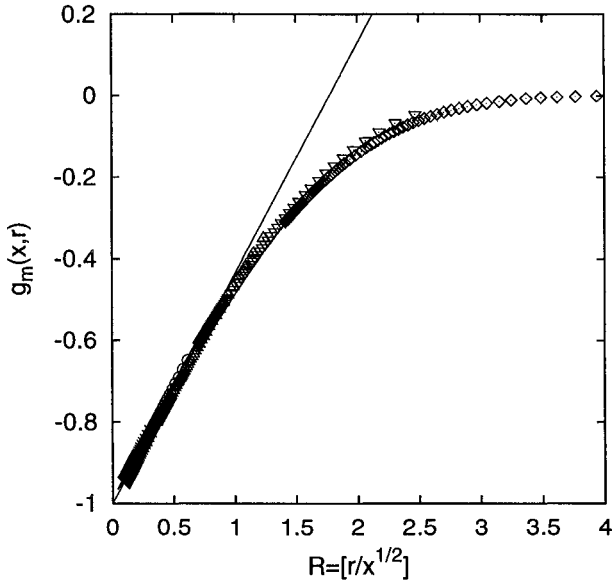

Figure 2.5: The scaling function of the mass-mass correlator g_m, from enumeration of the exact recurrence relations, at chain length $L = 512$ for various distances from the source, $r = 2(\times), 4(\circ), 8(\triangle), 16(\triangledown)$, and $32(\diamond)$. The drawn line is the tangent at small R, see between Eqs. (2.8) and (2.9).

with $a = 0.318(1)$ and $b = 0.268(6)$ and we suspect that the overall factor $a = 1/\pi$.

The above numerical and exact results are all in full agreement with the simple scaling picture where we treat the particles as performing free independent biased random walks before they merge. None of the scaling exponents differ from their diffusion values. The final verification for the validity of this intuitive explanation is the shape of the stationary state mass distribution function, $p(m, x)$, i.e., the probability to find a particle of mass m at a site $x \gg 1$. Our scaling theory presumes that this distribution behaves in the same manner as the probability for a specific tagged particle to reach site x with mass m. Each tagged particle follows an independent biased random walk and its mass grows proportional to the spatial fluctuations about its average path.

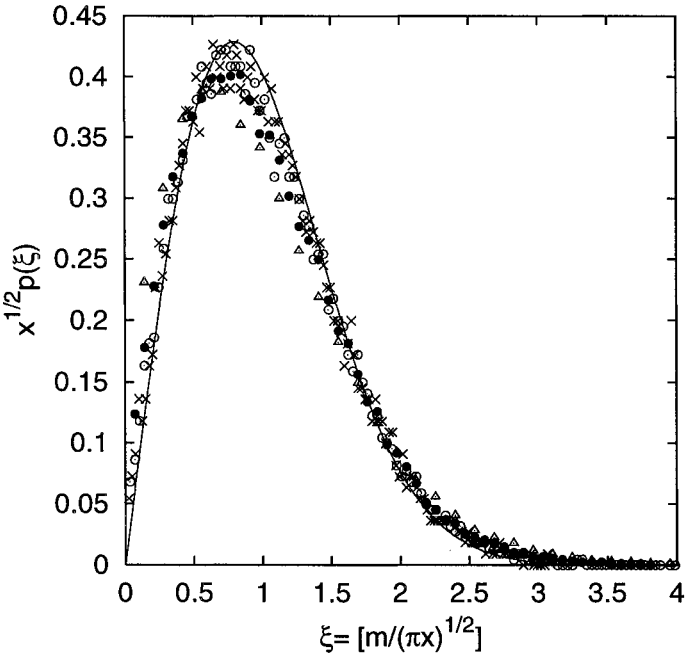

Figure 2.6: Numerical Monte Carlo scaling plot of the stationary state distribution $p(m, x)$, the probability to find a particle of mass m at site x, for various $x = 16(\times), 64(\circ), 256(\bullet)$, and $512(\triangle)$. We plot $\sqrt{x}p(x, m)$ versus $\xi = m/\sqrt{\pi x}$, the Gaussian form of Eq. (2.10).

Figure 2.6 shows numerical results for $p(m, x)$ at system size L=512 for various values of x=16, 64, 256, and 512. It is obtained from 10 independent runs, each 10^6 Monte Carlo steps long. The data is plotted in terms of $\sqrt{x}p(m, x)$ versus the scaling variable $\xi = m/\sqrt{\pi x}$

and collapses well onto a Gaussian with a linear prefactor,

$$p(m,x) = A\,\frac{m}{x}\,\exp(-Bm^2/x). \tag{2.10}$$

The parameters A and B are predetermined by the normalization condition and the scaling of the particle density (see Eq. (2.3))

$$\begin{aligned} \sum_{m=0}^{\infty} p(m,x) &= 1, \\ \tilde{M}(x) = \sum_{m=0}^{\infty} mp(m,x) &= 1/C(x), \end{aligned} \tag{2.11}$$

which yields $A = \frac{1}{2}$ and $B = \frac{1}{4}$. The drawn curve in Fig. 2.6 corresponds to this Gaussian with the above values of A and B. Equation (2.10) is the simplest Gaussian form consistent with the requirement that $p(m,x)$ vanishes in the limit $m \to 0$. According to our intuitive picture, $p(m,x)$ is related to the probability that a biased random walker with drift velocity $v_d = \frac{1}{2}$, makes an excursion of size m from its average path before reaching site x, irrespective of (i.e., averaged over all) the starting times at site $x = 1$.

2.4 Summary and conclusion

In this chapter, we presented new exact results for the $A+A \to A$-type coalescence process by introducing mass to the particles, and exploring the exact mapping to a surface deposition model, the so-called RBD type surface growth model. In addition, we propose a scaling theory based on the assumption we can treat the particles as performing free independent biased random walks before they merge. All scaling exponents should then take naive diffusion values. The above numerical and exact results are all in full agreement with this random walk type scaling. It appears therefore that the scaling properties of $A + A \to A$ dynamics are now fully understood, and actually, in the final analysis, are predictable from random walk considerations only.

Chapter 3

MACROSCOPIC CAR CONDENSATION IN A PARKING GARAGE

An asymmetric exclusion type process, where cars move forward along a closed road that starts and terminates at a parking garage, displays dynamic phase transitions into two types of condensate phases where the garage becomes macroscopically occupied. The total car density ρ_o and the exit probability α from the garage are the two control parameters. At the transition, the number of parked cars N_p diverges in both cases, with the length of the road N_s, as $N_p \sim N_s^{y_p}$ with $y_p = 1/2$. Towards the transition, the number of parked cars vanishes as $N_p \sim \epsilon^\beta$ with $\beta = 1$, $\epsilon = |\alpha - \alpha^*|$ or $\epsilon = |\rho_o^* - \rho_o|$, being the distance from the transition. The transition into the normal phase represents also the onset of transmission of information through the garage. This gives rise to unusual parked car autocorrelations and car density profiles near the garage, which depend strongly on the group velocity of the fluctuations along the road.

This chapter has been published separately in M. Ha and M. den Nijs [151].

3.1 Introduction

The scaling properties of nonequilibrium-type phase transitions are a topic of intensive current research [6, 60, 152, 153]. From the theoretical side, focus has been mostly on model calculations using stochastic dynamics with simple local rules and local interactions. These models serve as prototypes for various physical processes, such as surface catalysis [154, 155, 156], population growth [157, 158], surface growth [6, 47, 48, 150, 159], electronic transport in wires [160, 161, 162, 163], traffic flow [164, 165, 166], and avalanches in granular materials[167, 168, 169]. The simplicity of the models is justifiable when, as we expect, the scale invariant collective fluctuations at large length scales are universal and insensitive to most microscopic details.

Queuing phenomena, like traffic jams behind slow moving trucks on single-lane highways,

are common to many nonequilibrium processes. One of the interesting phenomena in such systems is the transition from a finite queue to an infinitely long one, i.e., the transition from a queue that does not scale with the road length N_s to one whose length is proportional to N_s. Such transitions can be induced by changing the total density of cars in the system or by varying the probability rate at which cars pass the truck [8].

A simplification of the above is first to replace the slow moving truck by a stationary object, and then to ignore the excluded volume effects in the queue by allowing the cars behind this stationary impurity to pile on top of each other. This bare-bone version of the phenomenon can then be rephrased in terms of the parking garage model introduced in this chapter: an asymmetric simple exclusion process (ASEP) on a road starting and terminating at a garage with an infinite parking capacity. The control parameters are the total number of cars, N_c, in the system (which compared to the road length N_s, defines a total car density $\rho_o = N_c/N_s$) and the probability α with which cars exit the garage (compared to the hopping probability along the road, set equal to one). The infinitely long queue is represented by a macroscopic occupation of the garage. The density of parked cars, $\rho_p = N_p/N_s$, is nonzero when the number of cars at the garage N_p is proportional to N_s.

The analogy with equilibrium Bose condensation is obvious as well as the basic question, i.e., whether the scaling properties of such queuing transitions are universal. For example, how sensitive are the exponents β and x_p in

$$\rho_p \sim |\alpha - \alpha_c|^{\beta} \quad \text{for} \quad \alpha < \alpha_c \tag{3.1}$$

and

$$\rho_p \sim N_s^{-x_\rho} \quad \text{at} \quad \alpha_c \tag{3.2}$$

to the details of the queuing dynamics, particularly to the simplifications we made. As a start, we need to establish and understand the scaling properties of the simplest model in as much detail as possible. The scaling properties of the parked car condensation transitions presented here are indeed already surprisingly rich. After this, we will be well positioned to restore the omitted queuing details one-by-one, and establish how robust those scaling properties are.

This chapter is organized as follows. The parking garage model is introduced in Sec. 3.2, and the phase diagram is presented in Sec. 3.3. In Sec. 3.4, we explore the relation to Kardar-Parisi-Zhang (KPZ) type surface growth. The group velocity is introduced in Sec. 3.5, and its important role in setting the density profile in the various phases is reviewed in Sec. 3.6. In Sec. 3.7, we do the same for the density-density correlations. Sections 3.8 and 3.9 form the core of this paper. We present our numerical Monte Carlo analysis for the parked car density at the condensate-normal phase transitions in Sec. 3.8, together with explanations of these results. Next, we do the same for the parked car fluctuations in various phases and at the phase boundaries in Sec. 3.9. Finally, in Sec. 3.10, we summarize our results.

3.2 Parking Garage Model

Consider a one-dimensional road of N_s sites with periodic boundary conditions. Each site on this road, $1 \leq x \leq N_s - 1$, is either empty or occupied by only one car, $n_x = 0, 1$. The parking garage at site N_s has no occupation upper limit, $N_p \equiv n_{N_s} = 0, 1, 2, 3, ...$ The total number of cars (N_c) in the systems is conserved. From the perspective of other physical processes, the cars can be reinterpreted just as well as, e.g., molecules (driven down a circular tube), kinks in steps on crystal surfaces, electrons driven around a wire by an electric field, or domain walls in magnetic spin chains.

The stochastic update rule, from time t to $t+1$ is sequential. One of the sites, $1 \leq x \leq N_s$, is selected at random with uniform probability $p(x) = 1/N_s$. If that site is part of the road, $1 \leq x \leq N_s - 2$, and occupied, the car moves forward to over one unit, presuming site $x + 1$ is empty; otherwise nothing happens. If the selected site is the one just in front of the garage, $N_s - 1$, and is occupied, then that car moves with certainty into the garage, irrespective of the occupation level of the garage. If the chosen site is the garage, $x = N_s$, the probability for a car to jump out of it onto site $x = 1$ is equal to α, independent of the number of cars in the garage, provided that the garage has at least one car and site $x = 1$ is empty. This exit probability from the garage is smaller than the hopping probability on the road, $0 \leq \alpha \leq 1$.

The above process has two control parameters: the total density of cars ρ_o and the

probability α with which cars can escape from the garage. We define the following quantities: the total car density $\rho_o = N_c/N_s$, the parked car density $\rho_p = N_p/N_s$, and the on-the-road density $\rho_r = \rho_o - \rho_p$. Only ρ_p and ρ_r fluctuate.

The parking garage is the new aspect to this otherwise well-studied ASEP. The latter is exactly soluble by the Bethe ansatz for periodic boundary conditions (a closed loop road without garage) [71], and the stationary state properties are exactly known for an open road with reservoirs on both sides [82, 107]. We will use and comment on these different setups and exact results in the following sections.

3.3 Phase diagram

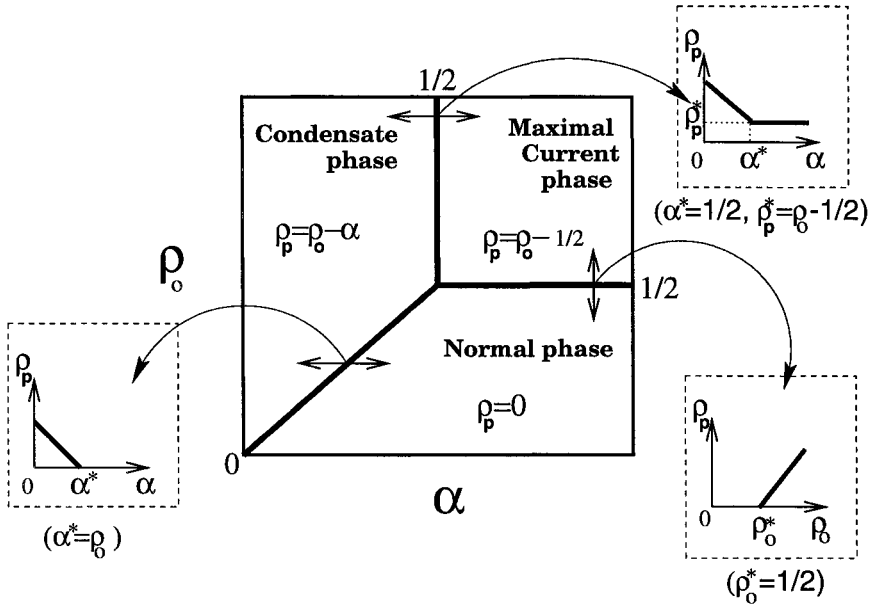

Figure 3.1: Phase diagram with the total car density ρ_o and the exit probability α from the garage. At the phase transition lines into the normal phase, the parked car density ρ_p vanishes, and the garage seizes to be macroscopically occupied (shown schematically in the insets).

Figure 3.1 shows our phase diagram. It contains three phases. In two of them the garage is macroscopically occupied: the condensate (C) phase (where the garage controls the density of cars on the road), and the maximal current (MC) phase (where the road

capacity controls the flow). In the normal (N) phase, the garage contains a finite number of parked cars (typically only a few). This structure can be deduced almost completely from earlier results for ASEPs without the garage, such as the ASEP with closed periodic boundary conditions (no garage), i.e., KPZ growth [35, 71], and the ASEP with open boundary conditions hooked-up to reservoirs on both ends [80, 82, 107].

In the two condensate phases, C and MC, the garage acts like a reservoir, and the model reduces to the open road version studied by Krug [80] and Derrida *et al.* [82, 107]. In their version, the road is in contact with car reservoirs at both ends, $x = 1$ and $x = N_s - 1$, such that a car jumps onto $x = 1$ with probability α (if empty) and leaves from $x = N_s - 1$ with probability β (if occupied). In our model β is always equal to one.

A dynamic second-order phase transition takes place between the MC phase (where the road density is at a constant value, $\rho_r = \frac{1}{2}$) and the C phase (where the road density $\rho_r = \alpha$ varies with the inlet probability α. The result of $\rho_r = \alpha$ is already correct within mean field theory [80, 107]). The MC phase appears because raising the density any further would reduce the flow efficiency (due to overcrowding). This phenomenon has been canonized recently into a "maximal current principle" [90], which states that the bulk road density takes the value that maximizes the flow.

Reduce the total number of cars inside the C and MC phases, i.e., walk in phase diagram towards the N phase along a line of constant α. This has no effect on the cars on the road and their fluctuations because all removed cars are taken from the parked ones residing inside the garage. These surplus cars are dynamically inert. This continues until the reservoir is depleted, the point at which the transition to the N phase takes place. The road density becomes equal to the total car density $\rho_r = \rho_o$. From the C (input-limited) phase perspective, this happens at $\rho_o = \alpha$, see Fig. 3.1, because $\rho_r = \alpha$ inside the C phase [80, 82, 90, 107]. From the MC (road-limited) phase perspective, it occurs at $\rho_o = \frac{1}{2}$ because $\rho_r = \frac{1}{2}$ inside MC. Therefore, the phase boundaries into the N phase are located at $\rho_o = \alpha$ and $\rho_o = \frac{1}{2}$.

The next issue is how many types of normal phases exist in the lower right side of the phase diagram. In a N phase, the garage acts like a localized impurity (a blocking-type site), and it contains typically only a few cars. Suppose we put a cap N_m on the occupation

garage, $N_p = 0, 1, ..., N_m$. This cannot affect the properties of the model in the N phase, except very close to the transition into the condensate phases (where the number of parked cars N_p and the fluctuations in N_p diverge). Janowsky and Lebowitz [8] (JL) studied such a capped version of the ASEP model, a closed loop road with periodic boundary conditions, without a garage, but with one special bond where the hopping probability is reduced from 1 to α. This is equivalent to setting the occupation limit of the garage to $N_m = 1$. Their phase diagram has the same control parameters as ours. It has particle-hole symmetry with respect to $\rho_o = \frac{1}{2}$, see Fig. 3.2. The normal phase in the lower right hand corner is similar to our model. The second normal phase in the upper right corner is equivalent to it by particle-hole symmetry, and the intermediate area is a coexistence region, the jammed phase. In the low-density N phase, the cars are uniformly distributed, but at $\rho_o = \alpha/(1+\alpha)$ a traffic-jam-type shock wave develops between low- and high-density N-type phase regions.

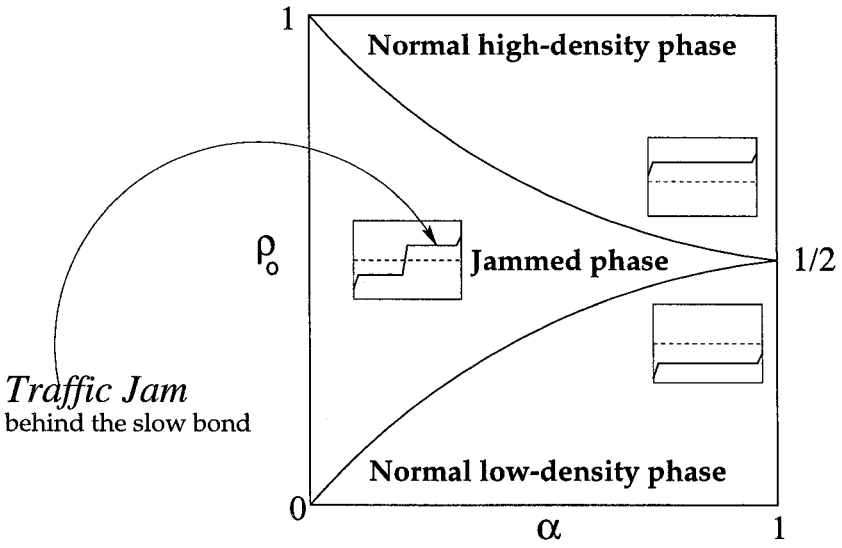

Figure 3.2: Phase diagram of the Janowsky-Lebowitz model. The corresponding density profiles are schematically shown in the insets.

This jammed phase is reminiscent of the condensate phase (macroscopic occupation of the parking garage) in our model. A shock wave does not appear in our model because the garage absorbs the queue. It is also clear that if we would interpolate between the JL model

and would be shifting smoothly, with our N-C phase boundary as the limiting case. JL focused on the finite-size-scaling (FSS) properties of the fluctuations in the position of the tail of the shock wave, $\Delta l \sim L^{\gamma}$, and found $\gamma = \frac{1}{2}$ (except for $\rho_o = \frac{1}{2}$ where a cancellation of the leading time of flight-type fluctuations gives rise to $\gamma = \frac{1}{3}$) [8]. Monitoring the location of the shock wave is analogous to observing the parked car density fluctuations in our model inside the C and MC phases. JL did not address the scaling properties at the queuing transition itself, but their transition is definitely second order (the location of the shock wave moves continuously with the total density away from the blockage point).

3.4 KPZ Growth

The ASEP can be interpreted as a lattice representation of the Burgers equation with a discretized velocity field, both in location and in its values, $n(x) = 0, 1$. The latter is equivalent to the so-called body-centered solid-on-solid growth model [47, 48, 49, 52, 150, 159], a lattice realization of KPZ-type surface growth. Each occupied site represents a down step along the one-dimentional (1D) surface and every empty site an up step. The surface heights, $h(x + \frac{1}{2})$, are limited to even/odd values at even/odd lattice sites, $h(x + \frac{1}{2}) - h(x - \frac{1}{2}) = 1 - 2n(x)$. The surface looks like the alternatively stacked bricks of a masonary wall, but rotated over 90 deg. Each car jump to the right represents the deposition of a new vertical 1x2 brick. The average car density on the road represents the average slope of the surface. At half density the surface is not tilted.

Periodic boundary conditions are the most common in theoretical studies of surface growth, and this brick deposition version of KPZ growth is exactly soluble by the Bethe ansatz [71]. It is a special line in the general phase diagram of the 1D well-known XXZ spin-$\frac{1}{2}$ quantum spin chain Hamiltonian, and also in the so-called six-vertex model of 2D equilibrium critical phenomena [50, 51].

From the surface growth perspective, the open road setup with reservoirs represents an open ended 1D interface with modified particle deposition probabilities α and β at its end points. In the MC phase, where the car density is locked to $\rho_o = \frac{1}{2}$, the crystal surface maintains a net zero tilt. For $\alpha < \frac{1}{2}$ and/or $\beta < \frac{1}{2}$, the reduced growth probabilities at

maintains a net zero tilt. For $\alpha < \frac{1}{2}$ and/or $\beta < \frac{1}{2}$, the reduced growth probabilities at the edge create a nonzero globally tilted surface. Moreover, along the line $\alpha = \beta < \frac{1}{2}$, two tilts coexist. Crossing that line amounts to undergoing a first-order phase transition with different tilt angles. The lock-in transition from the C phase into the MC phase represents a second-order dynamic facetting transition.

Our parking garage setup translates into a surface growth dynamics realization with periodic boundary conditions and a localized defect. The garage could represent something like a stacking defect, where the step height is unlimited (and somehow energetically cost free). The cliff height at the stacking fault can be microscopic (the N phase) or macroscopic (the C and MC phases). This depends on the modified growth probability α near the defect (on top of the cliff, somewhat similar to a Schwoebel energy barrier) and also depends on the global net tilt angle (the total car density). In the MC (C) phase, the average slope of the surface, excluding the cliff, is zero (nonzero).

3.5 Correlations and group velocity

It is well known and easy to show that the stationary state of KPZ growth with periodic boundary conditions, the closed loop road without obstacles where $\alpha = 1$ and $n(N_s) = 0, 1$, is completely random without any correlations whatsoever between finding a car at sites i and j for any $i \neq j$ including nearest neighbor sites. In the surface representation, this means that up and down steps are placed at random [49, 52] and that the width of the interface $W \sim N_s^{\chi}$ scales with the random walk exponent $\chi = \frac{1}{2}$.

The stationary state remains uncorrelated in our model as well (as shown below) except near the garage. Those correlations are governed by the dynamic scaling exponent and the group velocity with which fluctuations travel along the road.

In 1D KPZ-type surface growth, all characteristic times scale as $t \sim N_s^z$ with $z = \frac{3}{2}$. In car language, this means that local car density fluctuations with spatial width l broaden in time as $l \sim t^{1/z}$. The value of the dynamic exponent z follows from the identity $z + \chi = 2$ implied by Galilean invariance of the Burgers equation [35, 71] together with the disordered $\chi = \frac{1}{2}$ nature of the stationary state. The exact (Bethe ansatz) solution of this specific

model confirms this general result.

Fluctuations travel with a group velocity $v_g = 1 - 2\rho_r$ to the right (towards the garage) along the road. From the KPZ surface growth perspective, the group velocity represents the average slope of the KPZ growing surface, and its fluctuations grow perpendicular to the surface orientation. From the ASEP formulation perspective, the value of v_g is set by the average stationary state current $j = \rho_r(1-\rho_r)$ (easy to derive since the stationary state is Gaussian) and the definition of the group velocity is

$$v_g = \frac{\partial}{\partial \rho_r} j(\rho_r) = (1 - 2\rho_r). \tag{3.3}$$

This v_g played an important role, e.g., in the ASEP study by Majumdar and Barma [104] of tagged-particle diffusion, and in describing phase transitions between steady states in the open road setup [89].

3.6 Density profiles in the various phases

The on-the-road car density profiles in the C and MC phases are known exactly from the open boundary model studies, in particular the one by Derrida *et al.* [82, 107]. These profiles play an important role in our later discussions and it is useful to review how the group velocity enters in qualitative explanations of these exact results.

In the road-limited MC phase at $\alpha > \frac{1}{2}$, the density tail has a power-law shape,

$$\rho(x) \simeq \rho_r + A_e x^{-\nu}, \tag{3.4}$$

at both edges e=L(left), R(right), with x the distance from the edge of the road (garage entrance in our model) and $\rho_r = \frac{1}{2}$ the on-the-road car density. In contrast, in the input-limited C phase at $\alpha < \frac{1}{2}$, the car density is constant, $\rho(x) = \rho_r$, at the beginning of the road (garage exit), and has an exponential tail at the end of road (garage entrance),

$$\rho(N_s - x) \simeq \rho_r + A x^{-3/2} e^{-x/\xi}, \tag{3.5}$$

with the on-the-road car density $\rho_r = \alpha$ and the correlation length $\xi = -1/\ln[4\alpha(1-\alpha)]$.

Power laws with exponent $\nu = \frac{1}{2}$ arise naturally in this problem because of its critical fluctuations. The bulk properties of the KPZ stationary state are invariant under a rescaling

of all lengths as $x' = bx$, all times as $t' = b^z t$, and the surface heights as $h' = b^\chi h$. The car density scales, therefore, naively as $\rho = \partial h/\partial x \sim b^{\chi-1}$. This means that power-law tails in the density distribution near the edge of the road, with exponent $\chi - 1 = -\frac{1}{2}$, like in Eq. (3.4), are to be expected.

On the other hand, the disordered nature of the stationary state suggests exponential profiles, like in Eq. (3.5). Indeed, in the bulk, the stationary state density-density correlation function

$$g(r) = \langle \rho(x+r)\rho(x) \rangle - \langle \rho(x+r) \rangle \langle \rho(x) \rangle \tag{3.6}$$

does not decay as a r^{-1} power law as may be suggested by the above scaling argument, but instead decays exponentially with a very short correlation length, that is zero in this specific model since the cars on the road are totally uncorrelated in the stationary state.

To make sense of Eqs. (3.4) and (3.5), it is important to realize that the density profile near the edge of the road incorporates temporal correlations, and also to appreciate the role of the group velocity.

The power-law profile in the MC phase is the result of correlations with cars that reached the edge of the road and moved into the garage at earlier times. Such correlations spread in time over a spatial distance $l \sim t^{1/z}$. The group velocity is zero in the MC phase and therefore the cars at a distance l from the edge of the road are (power-law) correlated with those that entered the garage at times earlier than $\Delta t = l^z$. They have no knowledge about cars arriving at the garage more recently. This explains the power-law tail in the density distribution.

In the C phase, the same correlation spreading takes place within a moving frame of reference with nonzero group velocity. Information reaches the edge of the road (garage entrance) at a rate v_g (linear in time) faster than it can spread backwards as $l \sim t^{1/z}$ (since $1/z = \frac{2}{3} < 1$). Memory has no opportunity to develop near the edge of the road, and the density profile adjusts itself at the road end as if the cars on the road are completely uncorrelated. The exponential tail reflects a suction-type effect; the excluded volume limitation on the car mobility does not act on the cars departing from the road.

Similarly, in the MC phase, power-law correlations with earlier cars that escaped from

the garage and entered the road give rise to a power-law tail in the density profile at the beginning of the road (near the exit of the garage), while in the C phase, this information travels faster away from the road start than it can spread backwards. So, new cars entering the road do so completely uncorrelated, resulting in no road-start tail in the profile whatsoever. This confirms why the MC phase is road limited and the C phase is input limited. In the latter, the car supply at the garage controls the density near the edge of the road and also everywhere else on the road.

In the N phase, we find numerically, from Monte Carlo simulations, an exponential tail at the road end and an $1/x$ tail at the road start as shown in Fig. 3.3. The group velocity is also nonzero in the N phase, which explains the exponential exit tail as follows. Just like in the C phase, the garage is invisible to the incoming of cars from the road; fluctuations arrive at the garage faster (at constant velocity) than they can spread backwards (with $\Delta l \sim t^{1/z}$). The fact that in the N phase only a few cars reside inside the garage is invisible to the cars entering the garage.

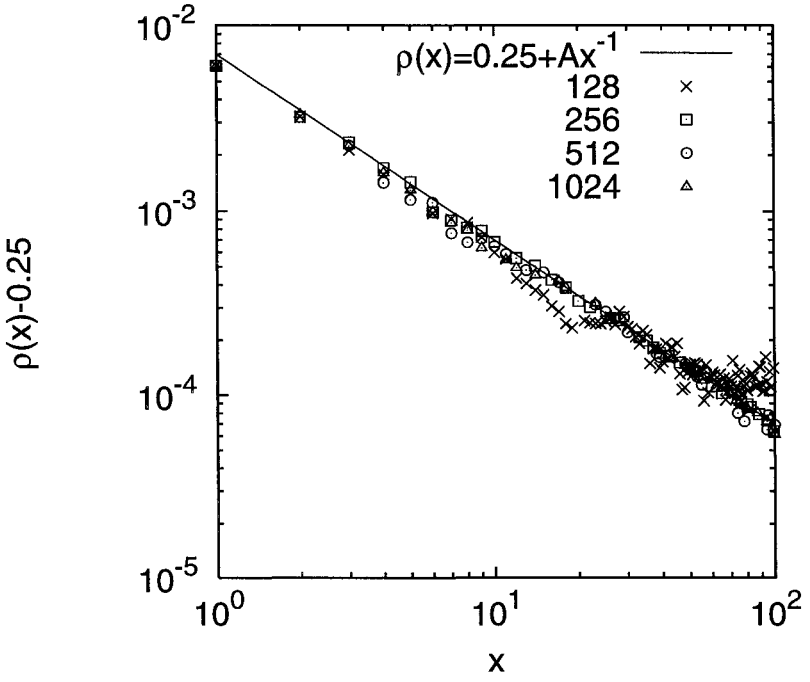

Figure 3.3: Double logarithmic plots of the density profiles in the N phase ($\rho_o = 0.25$ and $\alpha = 1$), showing a $1/x$ tail at the beginning of the road (garage exit).

An $1/x$ tail at the beginning of the road is what one expects from the deterministic part of the Burgers equation. The solution of the deterministic Burgers equation,

$$\frac{\partial v}{\partial t} + \lambda v \frac{\partial v}{\partial x} = \nu \frac{\partial^2 v}{\partial x^2} \tag{3.7}$$

with the velocity v pinned at a specific nonzero value at site $x = 0$, is readily seen (e.g., in the Hopf transformed formulation) to be of the generic form $v(x) \sim 1/(1 + ax)$, i.e., having the $1/x$ power-law shape.

In the C phase, the system selects the value $a = 0$ for the constant, and in the N phase, $a \neq 0$. In both cases, the group velocity $v_g > 0$ carries away KPZ fluctuations faster than they can spread, such that the KPZ noise term can be ignored at the road start (stationary frame of reference). The only noise that remains is that from the random process by which cars are being taken out of the garage and put on the road. In the C phase, the supply of cars is bottomless ($\rho_p > 0$), such that $a = 0$ (the entire on the on-the-road bulk car density is ruled by the garage), while, in the N phase, the supply of cars is limited and the garage does not overwhelm the road, such that $a \neq 0$.

3.7 Density-density correlations

It is useful to discuss how the group velocity affects the car-car correlation function,

$$g(r, \tau) = \langle \rho(x + r)_{t+\tau} \rho(x)_t \rangle - \langle \rho(x + r)_{t+\tau} \rangle \langle \rho(x)_t \rangle . \tag{3.8}$$

According to scaling theory, it obeys the form

$$\begin{aligned} g(r, \tau) &= b^{2(\chi-1)} g(b^{-1} r, b^{-z} \tau) \\ &= \tau^{\frac{2(\chi-1)}{z}} F(\frac{r}{\tau^{1/z}}). \end{aligned} \tag{3.9}$$

In the limit $\phi = r/\tau^{1/z} \to 0$, the scaling function $F(\phi)$ must approach a constant since the autocorrelation decays as a power law,

$$g(0, \tau) \sim \tau^{\frac{2(\chi-1)}{z}} \sim \tau^{-2/3}, \tag{3.10}$$

with $\chi = \frac{1}{2}$. In the opposite limit, of large ϕ, the scaling function must decay exponentially because $g(r, 0) = 0$ due to the random nature of the stationary state (or, more generically,

it decays exponentially with some correlation range ϕ_o of the same order as the interaction range between cars). The above scaling relation suggests the form

$$F(\phi) \sim \phi^{2(\chi-1)} e^{-\phi/\phi_o} \tag{3.11}$$

in the limit $\phi = r/\tau^{1/z} \to \infty$, such that

$$g(r,\tau) \sim r^{2(\chi-1)} e^{-r/\phi_o \tau^{1/z}} \sim \frac{1}{r} e^{-r/l} \tag{3.12}$$

with $\chi = 1/2$ and $l = \phi_o \tau^{1/z}$. The length l in the exponential defines the "correlation cone" that we already mentioned above. Within the cone the correlations decay as a power law, and outside it the cars are uncorrelated (as in the stationary state). The above discussion ignores finite-size effects. For open road or garage type boundary conditions, the correlator explicitly depends on the initial position x_0 of the car at time t_0 and also on the road length N_s,

$$g(r,\tau;x_0,N_s) = b^{2(\chi-1)} g(b^{-1}r, b^{-z}\tau; b^{-1}x_0, b^{-1}N_s). \tag{3.13}$$

Finite-size effects set in at times when the correlation cones hit the road edges, $\tau \sim (x_0)^z$ or $\tau \sim (N_s - x_0)^z$. At times longer than $t_0 \sim N_s^z$, we therefore expect that the car-car correlator decays exponentially, e.g., as

$$g\left(0,\tau;\frac{1}{2}N_s,N_s\right) \sim N_s^{2(\chi-1)} e^{-a(\tau/N_s^{1/z})}. \tag{3.14}$$

The above analysis applies to the MC phase, where the drift (group) velocity is zero. In the C phase (and also the N phase), we need to switch to the moving frame of reference by replacing $r \to r + v_g\tau$. This has some peculiar consequences. For example, the autocorrelation function $g(0,\tau)$ decays exponentially in time (even at short times). The correlation cone l is slanted in the direction of the flow (the correlations move with the flow) and l widens slower than linear in time, such that the $r = 0$ line in the world sheet lies outside the correlation cone. The KPZ-type correlations are somewhat hidden. In order to expose them, one needs to plot them in some special manner, e.g., $g(v_g\tau,\tau)$ (the autocorrelator in the moving frame of reference), as illustrated in Fig. 3.4.

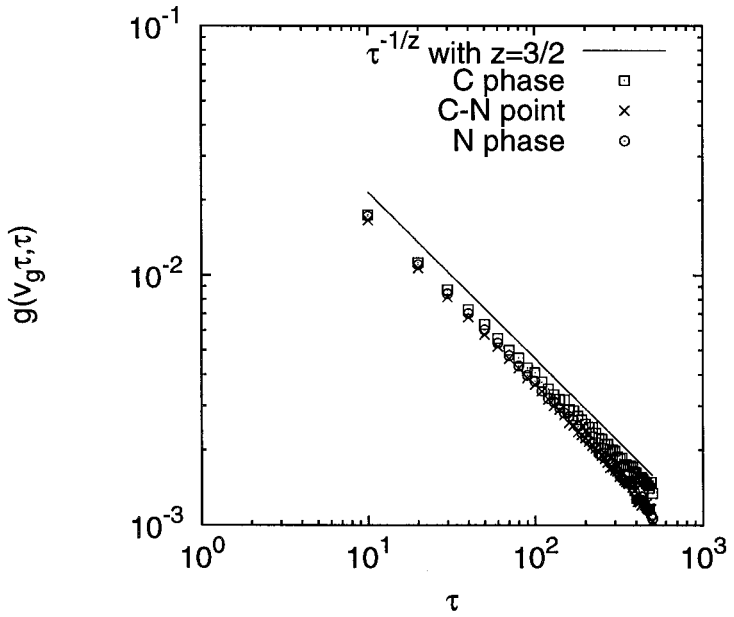

Figure 3.4: Double logarithmic plots of the density-density correlation function $g(r,\tau)$ in the moving frame of reference, i.e., with $r = v_g\tau$ and $v_g = (1-2\rho_r)$. The C phase data are obtained at $\rho_o = 0.75$ and $\alpha = 0.25$, the C-N point data at ρ_o=α=0.25, and the N phase data at $\rho_o = 0.25$ and $\alpha = 1$.

3.8 Scaling at and near condensation transitions

Let us turn now to the scaling properties of the two condensate phase transitions from the C and MC phases into the N phase. The stationary state value of the parked car density $\rho_p = N_p/N_s$ acts as the order parameter. We expect it to obey the FSS relation

$$\rho_p(\epsilon, N_s^{-1}) = b^{-x_p}\rho_p(b^{y_\epsilon}\epsilon, bN_s^{-1}) \tag{3.15}$$

near the two condensation transition lines with a scaling factor b, and $\epsilon = (\alpha - \alpha^*)$ or $\epsilon = (\rho_o^* - \rho_o)$, a measure of the distance from the transition.

In the N phase, the density of parked cars is zero, $\rho_p = 0$. When approached from the C and MC sides, ρ_p goes to zero as $\rho_p \sim |\epsilon|^\beta$, where $\beta = x_p/y_\epsilon$. The removal of cars from the road is accommodated by taking them from the passive inert ones residing inside the garage. This implies that ρ_p must vanishes linearly at the transition, and that $x_p = y_\epsilon$. Our numerical simulations confirm that $\rho_p \sim |\epsilon|$, as $\beta = 1$ in Figs. 3.5 and 3.6.

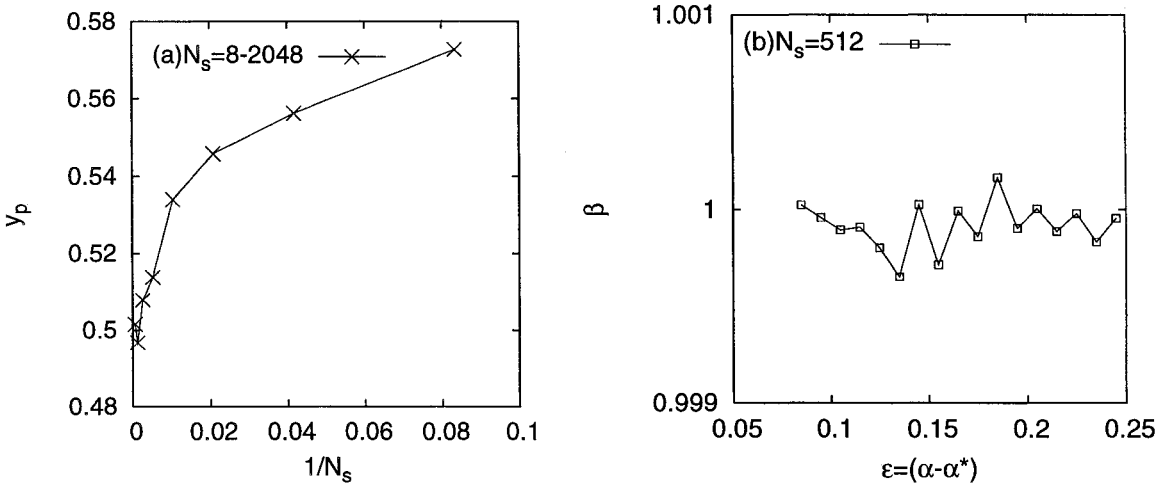

Figure 3.5: The parked car (order parameter) exponents (a) $y_p = 0.505(5)$ and (b) $\beta = 1.000(1)$, defined as $N_p \sim N_s^{y_p}$ and $\rho_p \sim (\alpha - \alpha^*)^\beta$, at ρ_o=α=0.25 of the C-N phase boundary.

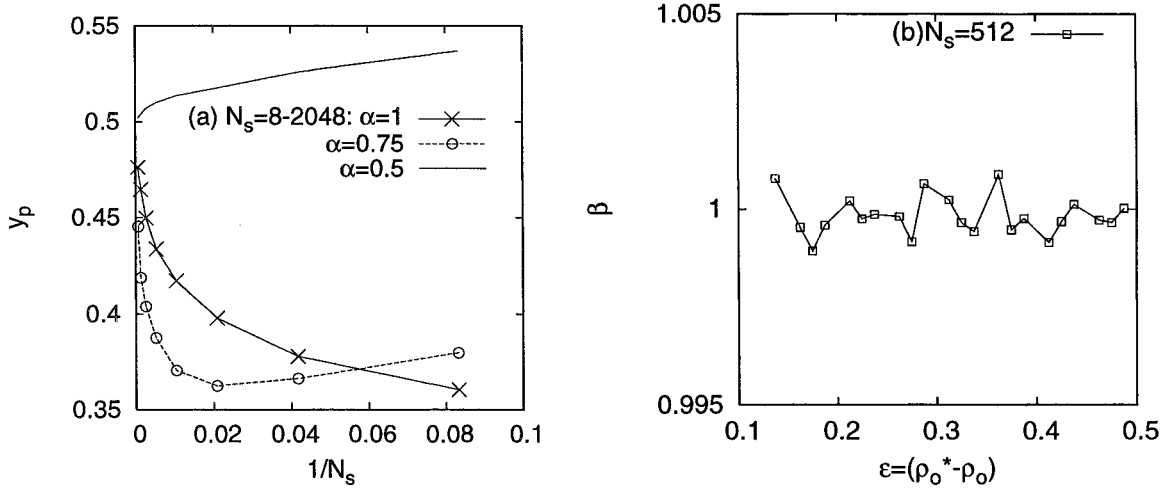

Figure 3.6: The parked car (order parameter) exponents (a) $y_p = 0.495(5)$ and (b) $\beta = 0.997(3)$, at $\rho_o = 1/2$ and $\alpha = 1$ of the N-MC phase boundary. For other two curves in (a), taken along the MC-N phase boundary at $\alpha \geq 1/2$, the exponent y_p retains the same value, but is subject to large/small corrections to finite-size scaling originating from 2/3 power-law density profile at the beginning of the road (garage exit).

The total number of parked cars (N_p) scales as

$$N_p(\epsilon, N_s^{-1}) = b^{y_p} N_p(b^{y_\epsilon}\epsilon, bN_s^{-1}) \tag{3.16}$$

with exponent $y_p = 1 - x_p$ according to Eq. (3.16) and $N_p = \rho_p N_s$. In the N phase, the density ρ_p remains zero, while the total number of parked cars (N_p) diverges towards the transition as $N_p \sim |\epsilon|^{(1-x_p)/y_\epsilon}$. We find numerically that this power law is linear as well, $N_p \sim |\epsilon|$. Combined with the linear scaling of the car density from the C or MC side (implying $y_p = x_p$), this yields $y_p = y_\epsilon = \frac{1}{2}$. The exponent y_p determines the FSS behavior of the total number of parked cars at the transition point itself, $N_p \sim N_s^{y_p}$ (and also that the density of parked cars vanishes as $\rho_p \sim N_s^{y_p - 1}$).

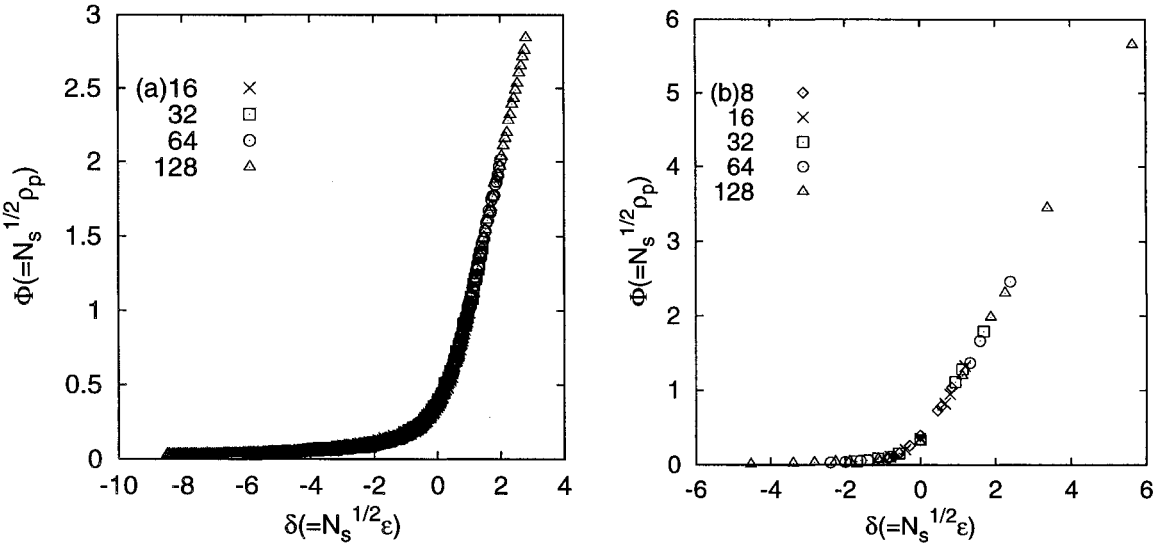

Figure 3.7: Scaling function $\Phi(\xi)$ defined in Eq. (3.17) at the same transition points as in the previous two figures; (a) $\rho_o = \alpha = 0.25$ (C-N) and (b) $\rho_o = 1/2$, $\alpha = 1$ (MC-N). The numerical data collapse very well for $x_p = y_\epsilon = 1/2$, as suggested in Eq. (3.17). The scaling function $\Phi(\xi) \to 0$ for $\xi \ll 0$ and $\Phi(\xi) \to \xi$ for $\xi \gg 0$.

Figure 3.5 shows the numerical results of y_p and β at point $\alpha = 0.25$ of the C-N phase boundary and Figure 3.6 at $\alpha = 1$ (and 0.75) of the MC-N phase boundary. Notice that the FSS corrections in the exponent y_p are much stronger at the MC-N transition than at the C-N transition.

The validity of the scaling relations is further illustrated by plotting the scaling function $\Phi(\xi)$ in the following form

$$\rho_p(\epsilon, N_s^{-1}) = N_s^{-x_p}\Phi(N_s^{y_\epsilon}\epsilon), \tag{3.17}$$

and the associated data collapse while moving through the transition points at constant ρ_o and constant α, respectively. The curves in Fig. 3.7 collapse very well.

The fluctuations and the FSS corrections to the number of parked cars are a mirror of the density-density correlations and the density profile of cars on the road. They also reflect how the latter builds up as a function of the length of the road. At the transition points, the bulk value of the on-the-road density $\rho_r = N_r/N_s$ is exactly equal to the total number of cars in the system divided by the road length, $\rho_r = N_c/N_s$, such that there would be no need for any car to remain inside the garage.

We find numerically that at the C-N transition point, the density profile retains the same structure as inside the C phase; with no tail at the beginning of the road (garage exit) and an exponential tail at the end of the road (garage entrance). Such profiles cannot account for the $y_p = \frac{1}{2}$ FSS divergence in the number of parked cars. The scaling behavior $N_p \sim N_s^{y_p}$ must, therefore, reflect directly the corrections to FSS in the bulk density of cars on the road. The value $x_p = \frac{1}{2}$ naturally arises because at the transition point, $\rho_p \sim \rho_r$, and $\rho_r = \partial h/\partial x$ scales as $L^{\chi-1} \sim L^{-x_p}$, where L corresponds to a given length of the road N_s.

A more intuitive explanation follows again from the nonzero group velocity at the C-N phase boundary. As mentioned above in the discussion of the density distribution tail in the C phase, the events by which cars enter the road from the garage are completely uncorrelated due to the slanting of the correlation cones (the correlations move with the flow towards the garage and spread slower than linearly, only as $l \sim t^{1/z}$, such that communications with later events at the beginning of the road are impossible). So the entry events to the road from the garage behave like uncorrelated random noise, and the fluctuations in the number of cars scale, therefore, as the square root of time. The time in question is proportional to N_s because the fluctuations (created at the garage exit) move along the road with velocity v_g, and are wiped out after they return to the garage. From this, it follows that the fluctuations in the number of parked cars scales as $\sqrt{N_s}$. Moreover, N_p cannot be negative, which means

that the fluctuations sample the bottom of the garage and that the transition from the C to N phase, therefore, takes place when the garage contains $N_p \sim \sqrt{N}_s$ cars.

In summary, the scaling at the C-N phase boundary is governed by the bulk fluctuations in the-on-the-road density, which is ruled by the nonzero group velocity of KPZ fluctuations, and this leads directly to random noise like $N_p \sim \sqrt{N}_s$, corrections to FSS.

The FSS corrections to scaling in exponent x_p (y_p) at the MC-N phase boundary are much more complex. The (bulk) group velocity is zero, and power-law density profiles are realized at both edges of the road. At the end of the road, the density profile follows a critical exponent $\nu = \frac{1}{2}$, the same power as that inside the MC phase discussed in Sec. 3.6. However, at the road start (the exit of the garage), the power-law exponent changes from $\nu = \frac{1}{2}$ inside the MC phase to $\nu = \frac{2}{3}$ at the MC-N transition. This is shown in Fig. 3.8 for $\alpha = 1$ and $\rho_o = \frac{1}{2}$, where the effect is the strongest.

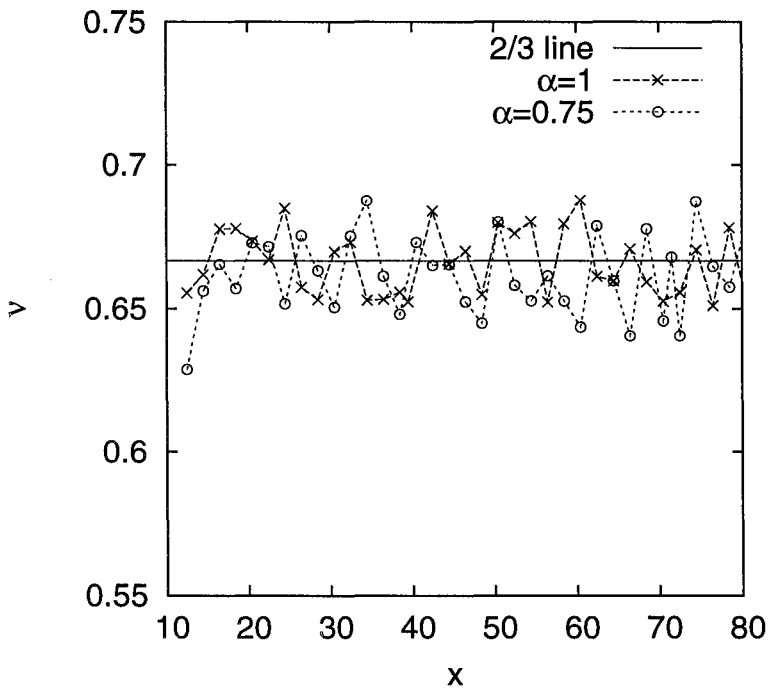

Figure 3.8: Effective (finite-size-scaling type) value for the exponent ν of the density profiles at the beginning of the road: $\nu = 0.66(1)$ at $\rho_o = 1/2$ and $\alpha = 1$ (or 0.75). At the MC-N phase boundary, the density profiles decay as a 2/3 power law, instead of the 1/2 power found inside the MC phase.

The $\frac{2}{3}$ power law does not change the $N_s^{1/2}$ FSS behavior of the number of parked cars. It is responsible, however, for strong corrections to FSS, as clearly visible in Fig. 3.6(a). The $\nu = \frac{2}{3}$ power-law profile contributes only a subdominant term to ρ_p because it decays faster than the two $\nu = \frac{1}{2}$ contributions (from the density profile at the end of the road and from the KPZ-like bulk road density fluctuations). We have not achieved yet a good understanding of this novel value, $\frac{2}{3}$, for the exponent of the density profile at the beginning of the road. It obviously lies correctly in between the MC and N values, $\frac{1}{2}$ and 1, respectively. Moreover, its value, $\nu = \frac{2}{3}$, is likely linked to the KPZ dynamic exponent $z = \frac{3}{2}$. But it remains unclear how to glue the following pieces together.

At the MC-N transition, the group velocity of the fluctuations, $v_g = 1 - 2\rho_r$, is still zero (but only barely) since $\rho_r = \frac{1}{2}$. This means that time of flight aspects, which dominate the C and N phases, do not come into play. Near the garage, the tail in the density profile, $\rho(x) = \frac{1}{2} + \Delta\rho(x)$, creates a local nonzero group velocity $v_g(x) = -2\Delta\rho(x)$ pointing back into the garage (instead of away from it as in the C and N phases).

Recall from Sec. 3.6 that the density profile in the MC phase has the same type of power-law profile $\Delta\rho(x) \sim x^{-\nu}$, but with the "KPZ" (power-counting) exponent value $\nu = \frac{1}{2}$. In that case, fluctuations at the road start do not reach the bulk of the road: the leading edge of the information cone is stationary because the backward movement of its center of mass $x_c \sim -t^{1/(1+\nu)}$ (implied by $dx_c/dt \sim x_c^{-\nu}$) matches exactly the rate of its spreading, $x \sim t^{1/z}$. So the $\nu = \frac{1}{2}$ density profile fully screens the garage from view in the bulk of the road. Exactly the same screening of the information takes place at the end of the road (garage entrance) since also there the MC phase density profile has exponent $\nu = \frac{1}{2}$ (but in an opposite forward moving v_g sense and with a negative density profile amplitude).

The density profile exponent $\nu = \frac{2}{3}$ at the MC-N transition does not fully screen the garage any more from observers located far away on the road. Total screening is not needed because KPZ fluctuations start to tunnel through the garage since it has only a $\sqrt{N_s}$ occupation. It is yet unclear to us, however, how to deduce (in a convincing manner) the exponent $\nu = \frac{2}{3}$ from these considerations.

3.9 *Parked car fluctuations*

In this section, we explore the fluctuations in the parked car density and also car-car correlations on the road. Of particular interest is the onset of transmission of information through the garage at the phase transitions. In the two condensate phases, the garage acts as a car reservoir and as a sink of fluctuations, while in the normal phase it contains only a few cars and transmits fluctuations.

The temporal fluctuations in the total number of parked cars, $G(N_s, \tau)$, measures also the fluctuations in the total number of cars on the road. It is therefore equal to the integrated car-car correlator (defined in Sec. 3.7),

$$\begin{aligned} G(N_s,\tau) &= \sum_{x_1,x_0=1}^{N_s-1} [\langle \rho(x_0,t_0)\rho(x_1,t_1)\rangle - \bar{\rho}(x_0)\bar{\rho}(x_1)] \\ &= \sum_{x_0=1}^{N_s-1} \sum_{r=-x_0+1}^{N_s-x_0-1} g(r,\tau;x_0,N_s) \end{aligned} \tag{3.18}$$

with $\tau = t_1 - t_0$ and $r = x_1 - x_0$. The summations run over all road sites x_0 and distances r that fit on the road. Direct integration of the scaling relation, Eq. (3.13), yields that (in the MC phase) G obeys the scaling form

$$G(N_s,\tau) = b^{2\chi}\, G(b^{-1}N_s, b^{-z}\tau) = N_s^{2\chi}\, \mathcal{F}(\tau/N_s^z). \tag{3.19}$$

In the KPZ representation, G is the global slope-slope autocorrelator, and at $\tau = 0$, reduces to the conventional definition of interface width (second moment of the height distribution). We will now discuss how G behaves in the various phases and at the phase transition points.

3.9.1 Inside the MC phase

The following intuitive discussion tells us how the scaling function $\mathcal{F}$ behaves in the MC phase. Each $g(r,\tau)$ has a correlation cone of size $l \sim \tau^{1/z}$. The cars within this cone are correlated with the one at site x_0 at time t_0 as $\tau^{2(\chi-1)/z}$. The integration over x_0 and r in Eq. (3.18) yields

$$G \sim N_s \times l \times \tau^{2(\chi-1)/z} \sim N_s \tau^{(2\chi-1)/z}, \tag{3.20}$$

where the correlation cones $l \sim \tau^{1/z}$ are assumed to be small with respect to the road size N_s. The exponent is equal to $\chi = \frac{1}{2}$, such that $G \sim N_s$, and that $\mathcal{F}$ approaches a constant in the limit $\tau/N_s^z \to 0$.

This estimate fails to take into account finite-size effects. Correlations are truncated near the two road edges (all information is entering the garage). The loss term is of the order

$$2\int_0^l dx_0\ (l - x_0)\tau^{2(\chi-1)/z} \sim l^2\ l^{2(\chi-1)} \sim \tau^{2\chi/z}. \tag{3.21}$$

This suggests that G is of the form

$$G = N_s\left(a - b\frac{\tau^{1/z}}{N_s} + \cdots\right), \tag{3.22}$$

with constants a and b, and suggests that the scaling function $\mathcal{F}(\phi)$ is analytic at short times in the parameter $\phi = \tau^{1/z}/N_s$ instead of $\phi' = \tau/N_s^z$. Our numerical results shown in Fig. 3.9(a) are consistent with this.

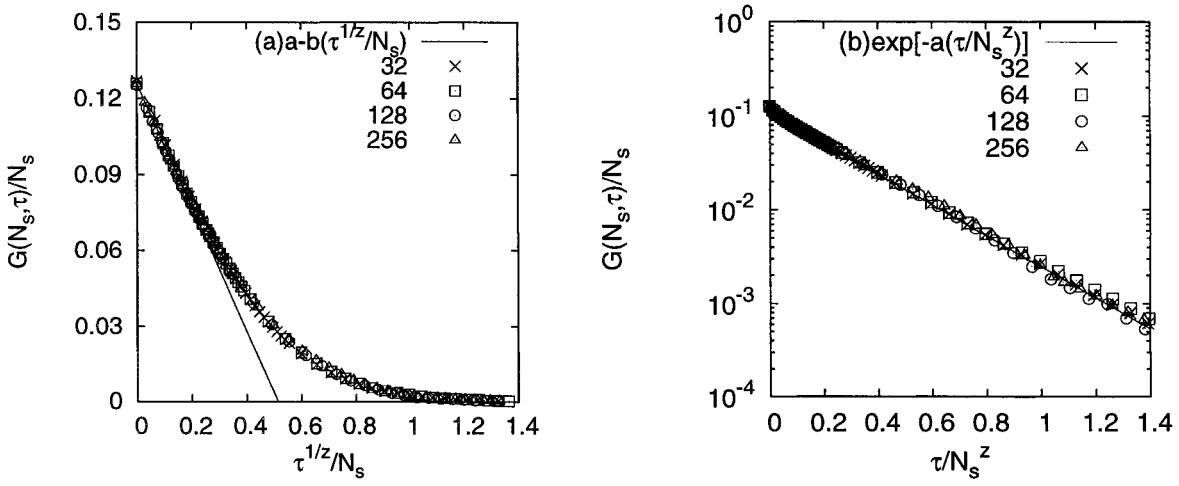

Figure 3.9: The parked car correlator $G(N_s, \tau)$ in the MC phase, for small τ (a), it decays linearly as function of $\tau^{1/z}/N_s$, and for large τ (b), it exponentially as function of τ/N_s^z, where $z = 3/2$. The data are obtained at $\rho_o = 0.75$ and $\alpha = 1$.

In the opposite limit, $\phi, \phi' \to \infty$, where time is large compared to the length of the road, all correlation cones are limited and equal to $l \simeq N_s$, and G behaves as in Eq. (3.14)

$$G \sim N_s \times l \times g(0, \tau; \frac{1}{2}N_s, N_s) \sim N_s\ e^{-a(\tau/N_s^z)}. \tag{3.23}$$

Our numerical results in Fig. 3.9(b) are consistent with this as well.

3.9.2 Inside the C phase

In the C phase, the fluctuations scale with the same exponents as in the MC phase, but the nonzero group velocity $v_g = 1 - 2\rho_r$ changes completely the appearance of correlation functions, like $G(N_s, \tau)$. The density-density correlations spread just like in the MC phase, but only with respect to the moving frame of reference and with r replaced by $\tilde{r} = r + v_g\tau$. The correlation function $g(r,t)$ scales as a power law $g \sim \tau^{2(\chi-1)/z}$ at $\tilde{r} = v_g\tau$ (i.e., $r = 0$) but exponentially at nonzero r. The fluctuation cones, $l \sim t^{1/z}$, are slanted and move with the flow.

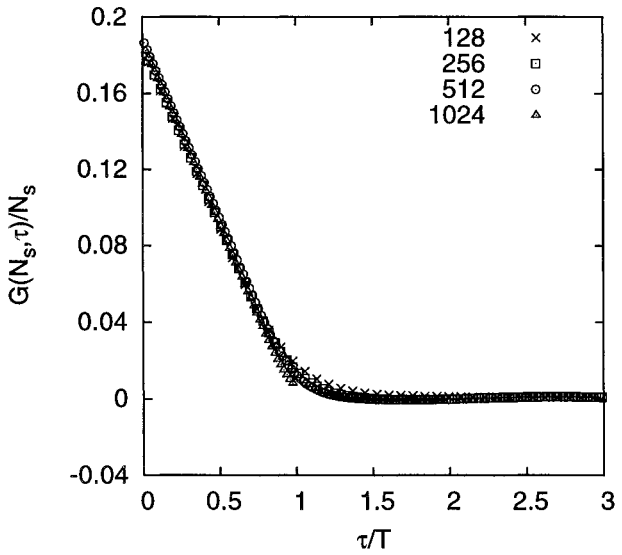

Figure 3.10: The parked car correlator $G(N_s, \tau)$ in the C phase; it decays linearly as function of τ and becomes zero after one time of flight $T = N_s/v_g (= \tau_{\text{flight}})$. Since it grows linearly with system size N_s, we plot G/N_s. The data are obtained at $\rho_o = 0.75$ and $\alpha = 0.25$.

Figure 3.10 shows $G(N_s, \tau)$ inside the C phase as a function of time τ for various road sizes N_s. It decays linearly until hitting zero at $\tau_{\text{flight}} = N_s/v_g (\equiv T)$, and then it remains at zero. All fluctuations move with the group velocity v_g to the right and reach the garage at a constant rate. After one time of flight, T, all correlations with the initial configuration have

disappeared. The rounding in G at T is of order $\Delta t \sim T^{1/z}$, and is due to the broadening of the remaining correlation cones just before they are absorbed by the garage.

3.9.3 Inside the N phase

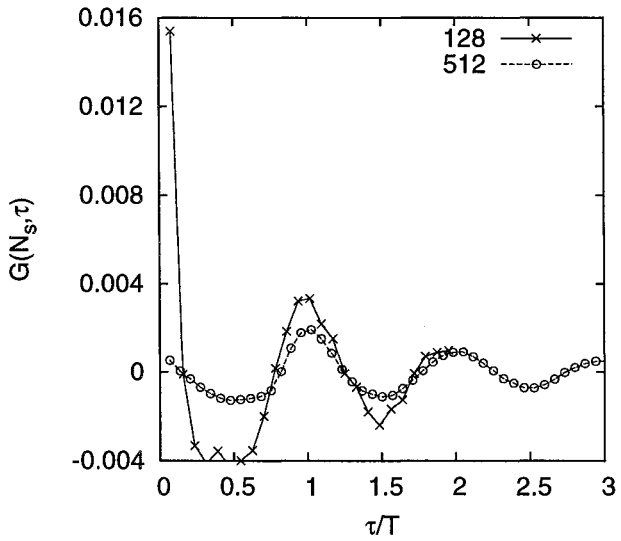

Figure 3.11: The parked car correlator $G(N_s, \tau)$ in the N phase; the garage is no longer macroscopically occupied, such that G does not scale with N_s any more. The correlations light up, like a lighthouse beam, at every time-of-flight interval $\tau_{\text{flight}} = T$. The data are obtained at $\rho_o = 0.25$ and $\alpha = 1$.

In the N phase, the fluctuations in the total number of cars on the road, $G(N_s, 0)$, are not proportional to N_s but are only of order one. The garage is not macroscopically occupied any more and acts very much like an ordinary road site. Figure 3.11 shows the behavior of $G(N_s, \tau)$ inside the N phase. The total number of cars in the system is conserved, such that G reduces to

$$G(N_s, \tau) = \langle N_p(t_0 + \tau) N_p(t_0) \rangle - \overline{N}_p^2, \tag{3.24}$$

and behaves similar to the autocorrelator $g(0, \tau)$. The group velocity is nonzero, and therefore G decays exponentially fast. However, because of periodic boundary conditions, G comes back to life, like a lighthouse light beam, after every time-of-flight interval

$T(= N_s/v_g)$, with an amplitude of order $T^{2(\chi-1)/z}$ and with a temporal width of order $l \sim T^{1/z}$.

3.9.4 At the C-N transition

Figure 3.12 shows how $G(N_s, \tau)$ at the C-N transition decays in time for various system sizes. At small τ, it decays linearly, rather like in the C phase, but then it seems to oscillate with a period determined by the time-of-flight time scale T; $G(N_s, \tau)$ goes through zero at about $t \simeq \frac{1}{2}T$ and shows a strong anticorrelation at $t \simeq T$ (the maximum lies just before it).

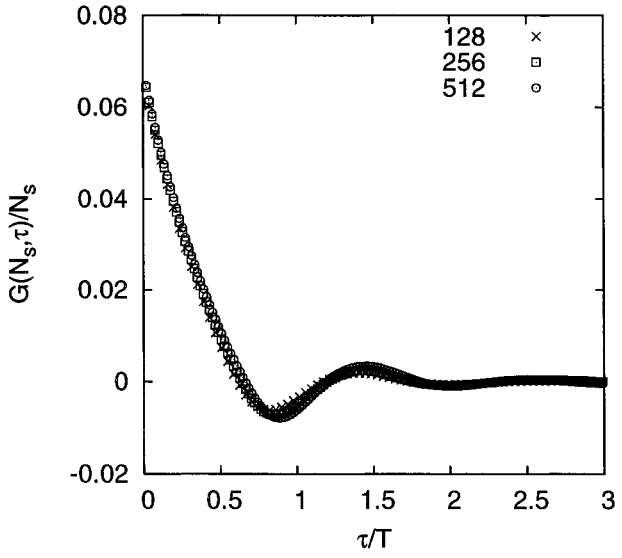

Figure 3.12: The parked car correlator $G(N_s, \tau)$ at the C-N transition; it has a strong anticorrelation after one time-of-flight interval, T, even though for small τ it decays linearly just like in the C phase (and with almost the same group velocity). The data are obtained at $\rho_o = \alpha = 0.25$.

Figure 3.13 illustrates how the transmission of information through the garage commences at the phase transition. Suppose we approach the transition point from the C phase following a line of constant α. In the C phase, these lines coincide with lines of constant group velocity. (In the N phase, v_g is constant along lines of constant ρ_o.) So nothing changes on the road until we hit the transition point, and G decays linearly to zero

and remains zero after one time-of-flight time scale. At the transition point, G transforms abruptly into the oscillatory shape, with an anticorrelation after one time of flight. After that, it reduces inside the N phase to the lighthouse shape, in which $G(N_s, 0)$ oscillates in phase and does not scale with N_s any more.

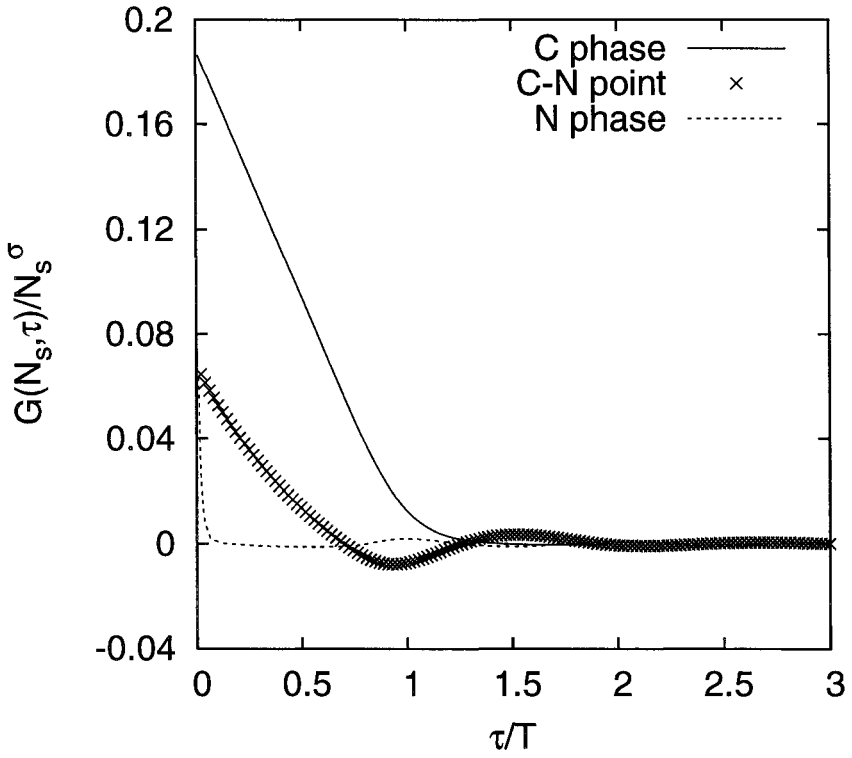

Figure 3.13: Evolution of the parked car correlator $G(N_s, \tau)$ through the phase boundary at fixed system size $N_s = 512$ along a line of constant group velocity: $v_g = 1 - 2\rho_r$ with $\rho_r = 0.25$; $\sigma = 1$ in the C phase and at the C-N transition, while $\sigma = 0$ in the N phase.

The anticorrelations at the C-N transition point are intriguing and need to be explained. Imagine a localized positive density fluctuation at the beginning of the road at time t_0. In the MC phase, it simply sits there while broadening as $l \sim \tau^{1/z} \sim \tau^{2/3}$ and weakening in amplitude as $\tau^{2(\chi-1)/z} \sim \tau^{-2/3}$. In the C phase, it broadens and weakens in the same manner, but travels like a solitary wave to the right with velocity $v_g = 1 - 2\rho_r$ and drops out of the road after one time-of-flight unit T. In the N phase, it behaves very much the same, except that the positive density fluctuation creates a deficit inside the garage since

the number of cars in the garage is finite, such that fewer cars can be put on the road in the immediate wake of the positive fluctuation. Therefore, in the N phase, every positive fluctuation carries a compensating (again localized) negative tail with it. Figure 3.14 illustrates the difference schematically, and our numerical simulations confirm this picture.

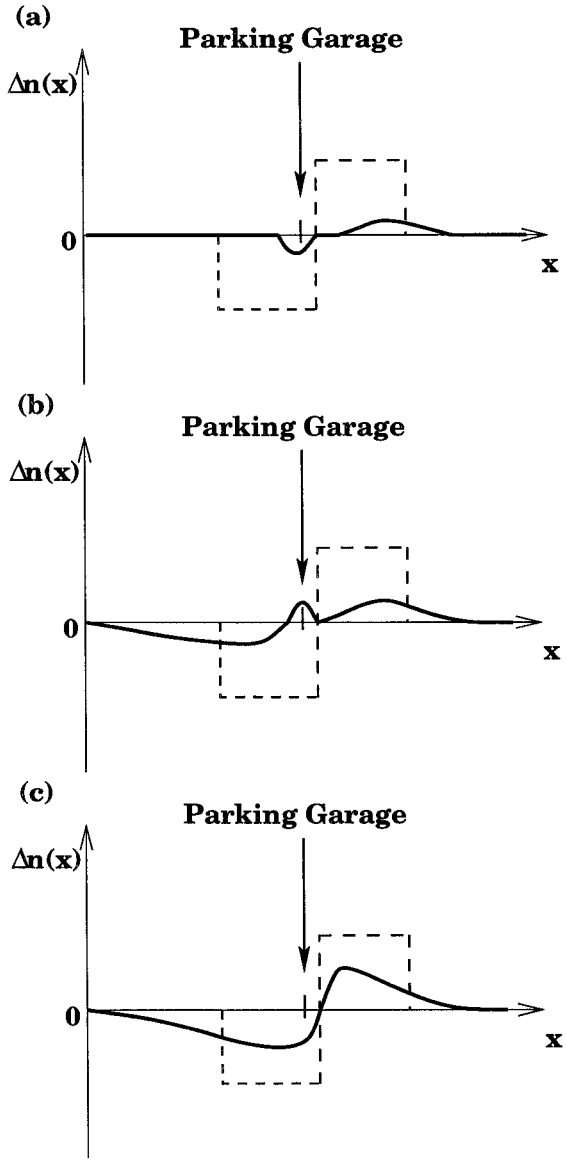

Figure 3.14: Schematics of soliton-type local perturbations diffusively spreading from the initial configurations (dashed lines) to one time-of-flight interval later (solid lines); (a) in the C phase, (b) at the C-N transition, and (c) in the N phase.

One could say that in the N phase positive and negative local excitations are bound in pairs, and that they unbind at the N-C transition. On approach of the transition from the N side, the width of the negative tail grows, but with conserved total area (equal to the area of the positive part of the excitation), because the average number of cars in the garage increases towards the transition (and diverges) and therefore the reduced car output is being spread over more time. At the transition point itself, the negative tail has vanished, except for the finite-size scaling effect of order $(N_s)^{-1/2}$.

Local excitations, thus, behave quite interestingly. However, they do not explain the difference in the behavior of G at the transition point and in the C phase. These solitary waves do not deplete the garage sufficiently to trigger its bottom because at the transition point the number of parked cars still diverges as $\sqrt{N_s}$.

Only nonlocal excitations, which encompass the entire system, are able to empty out the garage. Consider an excitation where the density of cars is globally and uniformly enhanced along the entire road, $\rho_i = \rho_r + \Delta$. This requires that the number of cars to be taken out of the garage should be proportional to the road length N_s. In the C phase, those will not deplete the garage because the number of parked cars is also proportional to N_s. Such a Δ regiment of extra cars marches with group velocity v_g to the right, reaches the end of the road, and thus returns to the garage at a rate uniformly in time, row by row. Throughout this process, the garage is not aware of the existence of the regiment since we did not hit its bottom and because the information cones $l \sim \tau^{1/z}$ on the road do not broaden fast enough compared to the group velocity to maintain its memory at the garage exit. This implies that the exact stationary state rebuilds itself in the wake of the regiment, and also that the enhanced road density decays linearly in time and vanishes completely after one time of flight T, just like our G as a function of time τ.

At the transition point, the garage only contains $N_p \sim \sqrt{N_s}$ cars, so that the same type of global uniform excitation can only have an amplitude of order $(N_s)^{-1/2}$, and always depletes the garage. This regiment of cars travels to the right with velocity v_g, just like in the C phase, but in its wake the garage cannot rebuild the stationary state because it is empty. A depleted road density is established in the wake of the enhanced excitation, and thus anticorrelations build up, and after one time of flight the average density of cars

on the road is below normal (and a surplus of cars resides in the garage). This explains qualitatively the oscillatory behavior of G at the transition point and the anticorrelations at T.

3.9.5 At the MC-N transition

The correlations at the MC-N transition are less spectacular than at the C-N transition. The group velocity is zero inside the MC phase, and still remains zero at the MC-N transition. Only inside the N phase, does it start to shift continuously away from zero. Figure 3.15 shows how G scales at the $MC-N$ transition. These numerical results are almost the same as those inside the MC phase in Fig. 3.9.

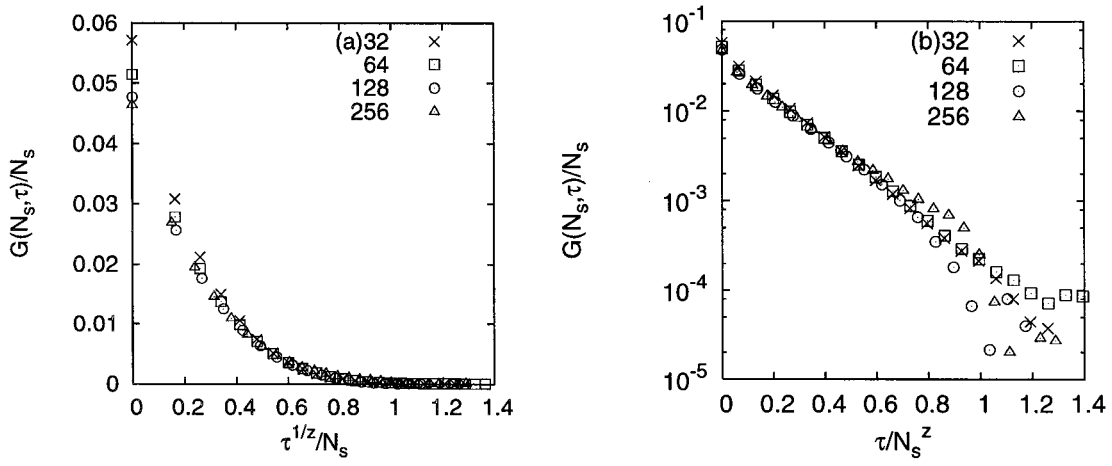

Figure 3.15: The parked car correlator $G(N_s, \tau)$ at the MC-N transition; the shape is very similar to that inside the MC phase, see Fig. 3.9. The data are obtained at $\rho_o = 1/2$ and $\alpha = 1$.

Recall the argument about the behavior of $G(\tau, N_s)$ inside the MC phase (in subsection 3.9.1), and imagine how this was modified at the MC-N transition. The factor N_s in Eq. (3.20) represents the number of cars on the road (the number of sites x_0 that are occupied). This should be modified to $\rho_o N_s - a\sqrt{N_s}$, since the number of parked cars scales as $\sqrt{N_s}$. The other terms, the spreading in time of the correlation cones and the autocorrelations on the road, are likely unchanged. Such differences are subtle and not surprisingly numerically invisible.

3.10 Summary and conclusion

In this chapter, we presented the scaling properties of dynamic condensate phase transitions in terms of an 1D asymmetric exclusion process with a parking garage. There are two types of condensate phases: the maximal current (MC) phase, where the road controls the density of cars on the road, and the condensate (C) phase, where the garage (as a reservoir) controls the number of cars on the road. The existence of a group velocity is crucial for understanding the behaviors of correlations and the density profiles in these two phases and at the phase transitions.

At both condensate transitions, the number of parked cars scales as $N_p \sim N_s^{y_p}$ with $y_p = \frac{1}{2}$, while on approach of the transition, the density of parked cars vanishes linearly with the control parameters (the total density of cars in the system and the exit probability from the garage) $\rho_p \sim |\epsilon|^\beta$, with $\beta = 1$. Also, the transition points represent the onset of communication of information through the garage. This leads to interesting autocorrelations in the number of parked cars, particularly at the C-N transition, due to the nonzero group velocity and associated time-of-flight effects.

Our parking garage model is a bare-bone version of dynamic Bose condensation and queuing phenomena, like traffic jams. The fundamental issue that needs further study is whether the above scaling behavior, in particular the values of the critical exponents, are universal or not. How do more realistic interactions between the cars on the road change this? Do the simplifications in the traffic jams, like a stationary truck versus a moving one and ignoring the spatial structure inside the queue of cars behind it by collapsing them (piling them up) into a "garage," affect the exponents?

There is some evidence suggesting that the exponents are indeed robust, e.g., in the Janowsky and Lebowitz [8] model, the same simple KPZ-type values of the exponents appear in the fluctuations of the queue, although a detailed study of the queuing transition itself needs still to be performed. In addition, introducing short-range car-car interactions [80, 170, 171] do not seem to change the exponents either [172].

Chapter 4

QUEUING TRANSITIONS IN THE ASEP

Stochastic driven flow along a channel can be modeled by the asymmetric simple exclusion process. We numerically confirm the presence of a dynamic queuing phase transition at a non-zero obstruction strength and establish its scaling properties. Below the transition, the traffic jam is macroscopic in the sense that the length of the queue caused by the obstruction scales linearly with system size. Above the transition, only a power-law type queue remains, i.e., a density profile $\delta\rho \sim x^{-\nu}$ with exponent $\nu = \frac{1}{3}$, where x is the distance from the obstacle. Fast bonds never create macroscopic queues, but only a power-law depletion queue with exponent $\nu \simeq \frac{2}{3}$. We construct heuristic arguments for these values of ν in addition to our numerical evidence, indicating these values are universal. In particular, $\nu = \frac{1}{3}$ above the transition appears to be independent of the dynamic exponent of the underlying dynamic process.

This chapter will be separately published in M. Ha and M. den Nijs [173].

4.1 Introduction

Queuing is a common nonequilibrium phenomenon in nature. It appears, e.g., in stochastic type driven transport through narrow channels, where applications can range from electrons flowing along nanowires to traffic flow on highways. Queuing has received a lot of attention from the theoretical side for more than a decade [7, 59]. It is well established that many driven flow processes belong to the same universality class as Kardar-Parisi-Zhang (KPZ) type growth of one-dimensional (1D) interfaces [35, 159]. In particular, the so-called asymmetric simple exclusion process (ASEP) [70, 71, 72] maps exactly onto the so-called body-centered solid-on-solid lattice version of KPZ growth [47, 48, 49]. The ASEP has been used to describe biopolymerization [68, 69, 174], gel electronics [175, 176], directed polymers in a random medium [86], traffic jams [76, 151], and the fluctuations of shock

fronts [8, 111, 121, 177]. Moreover, in the case of periodic boundary conditions, the time development of the ASEP is exactly soluble by the Bethe ansatz [70, 71, 72] while in several other setups the exact stationary state has been constructed as well [7, 81, 82, 111, 177].

The starting point and motivation for the study presented here was actually not queuing in driven flow but faceting in KPZ growth. Slow flameless combustion of paper produces 1D burning fronts that evolve in time according to KPZ type growth. Early experimental results [178] seemed to deviate from KPZ behavior, but more recent and more detailed investigations have demonstrated that random pinning effects do not play a role anymore at length scales larger than approximately 0.8 cm and the interface obeys 1D KPZ scaling [1, 26]. In these experiments, the paper is impregnated with KNO_3 in order to provide a steady oxygen source. The burning speed can thus be controlled by the KNO_3 concentration. In particular, the KNO_3 concentration can be enhanced or reduced in a narrow strip along the burning direction. Such experiments nicely illustrate the presence of nonlinear terms in the equation of motion; the burning front facets for enhanced concentrations but not for reduced concentrations. The detail of these experiments, as well as the matching of the experimental data with our numerical results for the slow and fast bond ASEP will be published separately [126]. In this chapter we only present the ASEP queuing perspective.

One of the fundamental questions in driven flow is whether a static obstruction, such as a slow bond, always results in a traffic jam caused by the slow bond, or whether stochastic fluctuations destroy the queue at weak obstacle strengths. Such a vanishing of the queue as a function of the slow bond strength represents a dynamic phase transition. The size of the queue is the order parameter, i.e., it being finite or infinite in length; or more carefully formulated (in terms of finite size scaling), whether the number of "cars "in the queue scales and diverges with system size or remains finite (in obvious analogy with macroscopic occupation of the ground state in equilibrium Bose condensation). The existence of such a transition, its scaling properties, the shape of the density profile near the obstruction (above, below, and at the transition), and also how and whether information percolates through the weak bond, are the most important issues.

The ASEP is one of simplest nonequilibrium driven dynamic processes displaying queuing phenomena. Particles move stochastically along a chain of sites $1 \leq x \leq N_s$ in a

preferred direction with hopping probability p under the constraint that the particles can not pass each other nor occupy the same site, with the occupation number $n_x = 0, 1$ only. We use random sequential updating of the sites. An obstacle is introduced by selecting one specific bond along the chain and modifying the hopping probability at this bond to rp. $0 \leq r < 1$ represents a slow bond and $r > 1$ a fast one. We choose open boundary conditions with the slow/fast bond in the middle of the chain.

Mean-field theory predicts an infinitely long traffic jam for all $r < 1$ and only a logarithmic depletion density profile near a fast bond [114]. The literature is confusing about what happens in the KPZ-type model study. Kandel and Mukamel [110] presented numerical data for a different but related growth model (namely parallel updating in polynuclear growth), suggesting a critical point at $p_c/p \simeq 1.3$ which corresponds to approximately $r_c \simeq 0.7$ in our model. Above the queuing transition, where the queue becomes finite, they reported evidence of continuously varying exponents in the density profiles. Our study confirms the existence of $r_c < 1$ in the ASEP (with the random sequential updating rule) but the density profile exponents definitely do not vary continuously.

The notion that the queuing transition at $r_c < 1$ seems to have been implicitly presumed in the literature ever since, but to our knowledge, the issue was not unambiguously resolved [125]. For example, in earlier ASEP studies with a blockage (slow bond), Janowsky and Lebowitz presented their phase diagrams with periodic boundary conditions as if $r_c = 1$ (the mean-field location) [8]. In retrospect, however, the result of $r_c \simeq 0.8$ is consistent with their result by series expansions [108]. Their main focus was on the fluctuations in the position of the shock front of the queue, at the far end from the slow bond, and not the precise value of r_c. Based on our detailed analysis in the half-filled system with periodic boundary conditions, the same queuing transition occurs at the same value of r_c as that which we claim in this chapter. See Appendix A.

Schütz [111] also addressed the slow bond issue in the ASEP. He applied the so-called matrix method and the Bethe ansatz to derive exact forms of the stationary state, but this method typically works only for very specific boundary conditions and/or specific update rules. His phase diagram for periodic boundary conditions and parallel updating does not have an $r_c < 1$. However, that is to be expected because for parallel updating the stochastic

noise is intrinsically weaker than that for random sequential updating [1].

Faced with the realization of this process in terms of experimental slow combustion of paper, our first goal of this study is to settle the location of r_c for the sequential updating rule, numerically as accurately as possible. We demonstrate the presence of a dynamic phase transition at $r_c \simeq 0.80(2)$. The queue remains infinite in length all the way up to r_c, but its density $\rho_b = \frac{1}{2}(1 + \Delta_b)$ decreases as $\Delta_b \sim |r_c - r|^\beta$ with $\beta \simeq 1.46(4)$. These results are presented in Sec. 4.3 after a detailed discussion of the boundary condition setup in Sec. 4.2.

Having settled the existence of a critical point $r_c < 1$, we turn our attention to two more issues. In Sec. 4.4, we establish numerically that the density profile near the slow/fast bond always follows a power law, $\Delta(\tilde{x}) \simeq \Delta_b + A\tilde{x}^{-\nu}$, with $\rho(\tilde{x}) = \frac{1}{2}[1+\Delta(\tilde{x})]$ and $\rho_b = \frac{1}{2}(1+\Delta_b)$ in the bulk, where $\tilde{x}$ is the distance from the slow/fast bond. The numerical results for ν as a function of r are as follows: Below the transition, $r < r_c$, the density profile in the traffic jam has a power-law tail near the slow bond with the exponent $\nu = \frac{1}{2}$. Above the transition, $r_c < r < 1$, where $\Delta_b = 0$, the density profile has a power-law shape with the exponent $\nu \simeq \frac{1}{3}$. In the fast bond scenario, the queue remains finite (i.e., $\Delta_b = 0$) for all $r > 1$ and the density profile again follows as a power law, but with the exponent $\nu \simeq \frac{2}{3}$. Such power-law density profiles and these values of their exponents ν are quite intriguing.

Recall that the bulk stationary state in ASEP is uncorrelated (far from boundaries and the slow/fast bond), yielding a random walk type interface with a width diverging with system size N_s as $W \sim N_s^\chi$. This means that the density operator in the ASEP scales as $\hat{n}_x \sim \partial h/\partial x \sim N_s^{\chi-1}$ with $\chi = \frac{1}{2}$. Fluctuations in the stationary-state density profile broaden with the KPZ dynamic exponent value $z = \frac{3}{2}$ as $\xi \sim t^{1/z}$. For example, The KPZ surface width scales in time as $W \sim t^\beta$ with $\beta = \chi/z = \frac{1}{3}$.

The density profiles near reservoirs are well understood. Consider, e.g., the exact results of Derrida *et al.* [82] for the open boundary ASEP setup. The density profile tails near the two reservoirs have exponential tails in the reservoir dominated phases, and $\frac{1}{2}$ power-law tails in the maximal-current phase. It is well known how to explain these profiles with

[1] It is known that the ASEP with other update procedures show only minor differences without changing major features, see [180] in detail.

the help of simple scaling arguments involving the values of z and ξ given above, and the absence or presence of a non-zero group velocity for fluctuations (see Ref. [151]). In Sec. 4.6, we generalize these types of arguments to the density profiles for the slow/fast bond.

Another unexpected result of our study is that the passage of particles through the slow bond sets itself up to be an uncorrelated stationary state process both below and above r_c. All fluctuations travel away from the slow bond on both sides. This expresses itself in a simple correlation relation, as discussed in Sec. 4.5, between the density operators $\hat{n}_L$ and $\hat{n}_R$ at the sites immediately before and after the slow/fast bond. The road acts as a particle reservoir as far as the passage process is concerned. Finally, in Sec. 4.7, we summarize our results.

4.2 Boundary conditions

The choice of boundary conditions is crucial for the accuracy of our numerical analysis. The slow/fast bond creates a power-law density profile and therefore we need to minimize and fully control the way the boundary conditions affect this [2].

We have chosen open boundary conditions with the slow/fast bond in the middle of the road, and particle reservoirs on both ends of site $x = 1$ and site $x = N_s$. Particles can only hop to the right, $x \to x + 1$. The hopping probability for a bulk site is equal to p. The probability to hop through the slow/fast bond is equal to $p' = rp$. The probability to enter (leave) the road from (into) the reservoir at site $x = 1$ ($x = N_s$) is equal to αp (βp). It is often advantageous to set $p = 1$, to speed up the Monte Carlo (MC) simulations, but that would exclude us from addressing the fast bond scenario $r > 1$. We set $p = \frac{1}{2}$ throughout this study.

Our choice to employ open boundary conditions may seem surprising. In critical phenomena, open boundary conditions introduce the edge effect (surface critical phenomena) that is typically more difficult to interpret and control than periodic boundary conditions.

[2] To get rid of boundary effects clearly in the maximal-current phase of the ASEP with open boundary conditions, $\alpha = \beta = a = 1/2$ is the correct choice, unlike $a = 1$ chosen in the earlier work [108]. If $a > 1/2$, the edge density profiles from boundaries decay as a power law, so that there are very strong boundary effects (see exact solutions in Ref. [82]).

In the ASEP, however, periodic boundary conditions introduce a shock wave in the density profile at half way around the chain, opposite from the slow bond (see Appendix A). Janowsky and Lebowitz [8] studied the fluctuations of the shock wave positions and found it to scale as system size, implying power-law tails and the absence of a characteristic length scale. We decouple the slow bond from those fluctuations and can do so by using open boundary conditions. The trade-off is that density profiles near the edges of the road are induced by the particle reservoirs. But those are under full control with help of the exact solution of the $r = 1$ ASEP with open boundary conditions [82]. The density profiles near the edges have only exponential tails, provided that we choose suitable values for α and β. At $r = 1$ for $\alpha = \beta = \frac{1}{2}$, the density profile is completely flat without any features; $\rho_x = \frac{1}{2}$ exactly for all x [82]. Thus, we select $\alpha = \beta = \frac{1}{2}$ throughout this study.

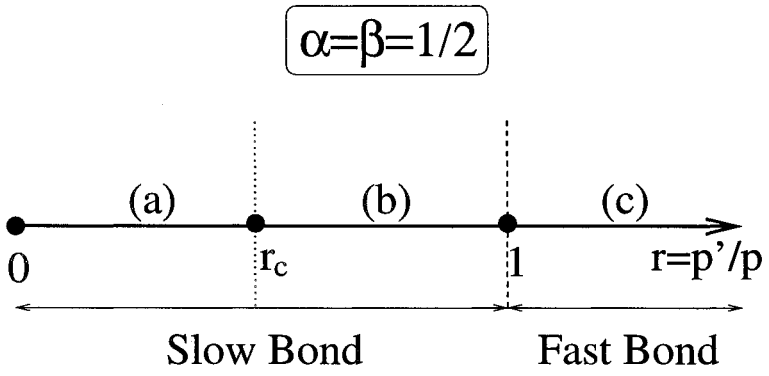

Figure 4.1: Three phases of the ASEP in the presence of a blockage, where the boundary-free setup ($\alpha = \beta = \frac{1}{2}$) is chosen: (a) queued slow bond phase, (b) non-queued slow bond phase, and (c) non-queued fast bond phase.

Assume that the slow bond creates an infinite queue. In the bulk of that queue, far from both the slow bond and the road edge, the stationary state is uncorrelated because locally it is indistinguishable from a setup with periodic boundary conditions without the slow bond. Moreover, from the perspective of the sites near the $x = 1$ edge, this situation is indistinguishable from the setup with $r = 1$ (no slow bond) where an exit probability β at the opposite edge of the road could be responsible for this enhanced bulk density Δ_b. From the exact solution of that setup, we know that the density profile near the entry edge is

exponential, $\rho(x) \simeq \frac{1}{2} + B \exp^{-x/\xi}$ with a constant B and a finite correlation length $\xi \sim \Delta_b^2$. Our simulations completely confirm this [3].

Other important features of the density profile are predetermined as well. For all $\alpha = \beta$, the density profile has particle-hole symmetry with respect to the slow/fast bond, $\rho(x) = 1 - \rho(N_s + 1 - x)$. Define $\Delta(x)$ as the deviation of the density from $\frac{1}{2}$, $\rho(x) = \frac{1}{2}[1 + \Delta(x)]$, such that $\Delta(x) = -\Delta(N_s + 1 - x)$. Then, Δ_b is the order parameter of our process and represents the spontaneous faceting angle of the slow combustion interface profile in the KPZ interpretation.

The current along the chain must be uniform in the stationary state. From the fact that the bulk stationary state is uncorrelated, it follows immediately that its value through such a bulk bond is equal to

$$J = p\langle \hat{n}_x(1 - \hat{n}_{x+1})\rangle = \frac{p}{4}(1 - {\Delta_b}^2). \tag{4.1}$$

This means that we have the option to determine Δ_b by measuring J. The current from the reservoir to the first site

$$J = \alpha p\langle (1 - \hat{n}_1)\rangle = \frac{\alpha p}{2}(1 - \Delta_1) \tag{4.2}$$

must be equal to the bulk current in the stationary state. This yields, for $\alpha = \frac{1}{2}$, that the density at site $x = 1$ is equal to $\Delta_1 = \Delta_b^2$.

The density profile in front of and beyond the slow/fast bond obey particle-hole symmetry, $\langle \hat{n}_L\rangle = 1 - \langle \hat{n}_R\rangle$, with x_L and x_R the sites immediately in front of and beyond the slow/fast bond. Moreover, we will demonstrate, in Sec. 4.5, that the ratio $\mathcal{R} = \langle \hat{n}_L\hat{n}_R\rangle / \langle \hat{n}_R\rangle$ is very close to $\mathcal{R} = \frac{1}{2}$ for all values of r. The current through the slow/fast bond

$$J = rp\langle \hat{n}_L(1 - \hat{n}_R)\rangle = rp[(1 + \mathcal{R})\langle \hat{n}_L\rangle - \mathcal{R}] \tag{4.3}$$

must again be equal to the stationary bulk current, thus anchoring the value of the density immediately in front of the slow/fast bond to the order parameter of our process as $\Delta_L = \frac{1}{3}[(1 - \Delta_b^2)/r - 1]$ if $\mathcal{R}$ is exactly equal to $\frac{1}{2}$.

[3] Recently, Kolomeisky [181] studied the same setup as ours for various α and β. He limited his study to the exponential density profile near the reservoir edge, comparing numerical results with mean-field theory.

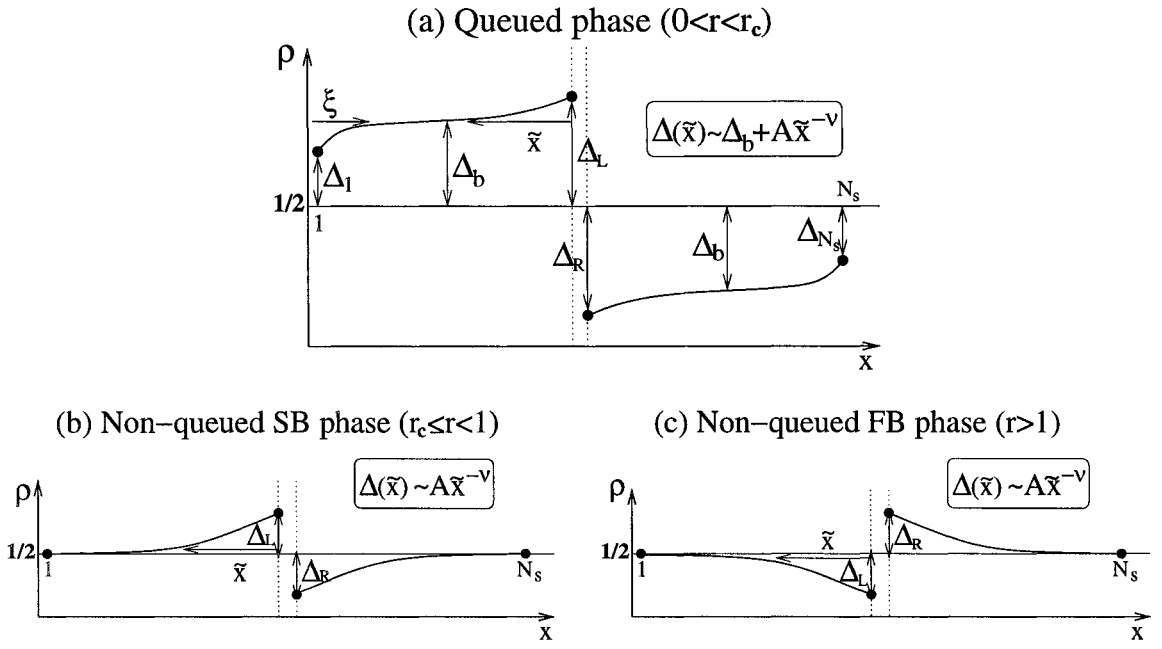

Figure 4.2: Schematic density profiles are shown: for the slow bond (SB), (a) $0 < r < r_c$ (queued phase) and (b) $r \leq r_c < 1$ (non-queued SB phase), and for the fast bond (FB), (c) $r > 1$ (non-queued FB phase).

Figure 4.2 summarizes the above discussion. The current, the densities at the first and last sites, the characteristic exponential length scale of the density profile near the edge (in the faceted phase), and the bulk density are all linked to one another. This leaves only the spontaneous creation of a non-zero Δ_b and the density profile near the slow/fast bond as independent issues.

4.3 Queuing Phase Transition

The first issue at hand is to settle by numerical means the question whether there exists a queuing transition at $r_c < 1$. As mentioned already, this is the general consensus, but none of the previous numerical studies was definitive. We performed MC simulations for system sizes up to $N_s = 4096$ and analyzed them by finite size scaling (FSS) techniques.

The order parameter of the queuing transition is the offset of the density in the bulk, Δ_b (far from both the slow/fast bond and the edge). There are several ways to measure Δ_b:

One can directly measure the density at site $x = \frac{1}{4}N_s$, and perform a FSS analysis to determine the asymptotic value. This works, but neither $x = \frac{1}{4}N_s$ nor any other fixed site is optimal for such an analysis, because the density profile has a power-law tail at the slow/fast bond side, and only an exponential one near the edge. Therefore, the values for Δ_b shown in Fig. 4.3 are those of the power-law density profile fit

$$\Delta(\tilde{x}) \simeq \Delta_b + A\ \tilde{x}^{-\nu} \tag{4.4}$$

(with $\tilde{x} = x_L - x$ the distance from the slow/fast bond) at our maximum system size $N_s = 4096$.

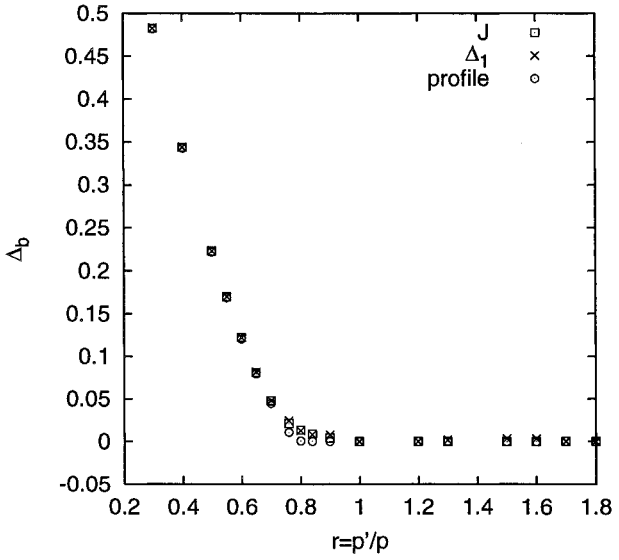

Figure 4.3: The order parameter Δ_b versus the strength r of the slow/fast bond at $N_s = 4096$, determined from three different data sets: the average current J (squares), the density Δ_1 at the first site near the reservoir edge (crosses), and the power fits to the density profiles near the slow/fast bond (circles).

As pointed out in the previous section, Δ_b is directly linked to various other quantities, like the average current J, the density at the first site near the edge Δ_1, and the characteristic length ξ of the exponential tail in the density near the edge. We measured these quantities as well, and translate the first two into their prediction for Δ_b. The results, shown in Fig. 4.3, are almost indistinguishable from those of the power-law density profile fits. This confirms our analysis of the previous section.

Figure 4.3 suggests very strongly the existence of a critical point at about $r_c \simeq 0.8$. However, as usual, this becomes visually less convincing in Fig. 4.4 when we zoom in to this point. This reflects usual FSS effects.

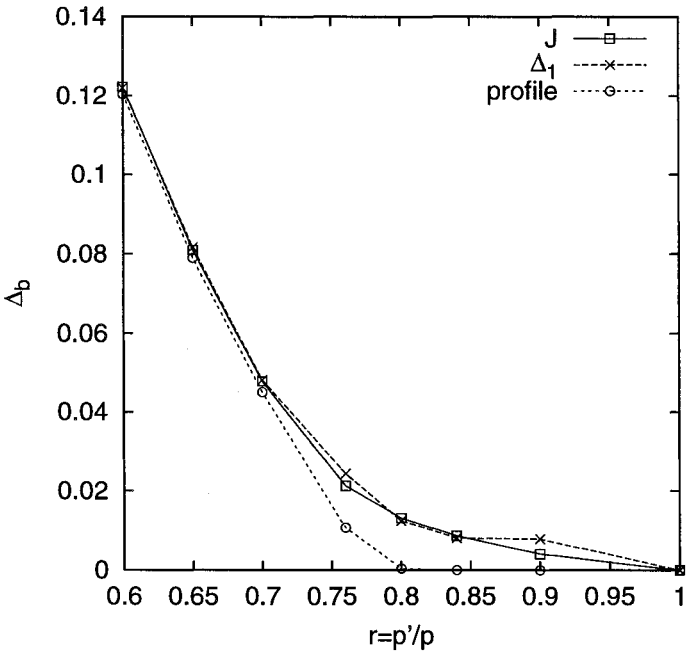

Figure 4.4: The order parameter Δ_b versus the slow bond strength r in the vicinity of the critical point r_c.

Assume that the order parameter obeys the conventional FSS form

$$\Delta_b(N_s, \epsilon) = b^{-x_\Delta} \Delta_b(b^{-1} N_s, b^y \epsilon), \tag{4.5}$$

where $\epsilon = r_c - r$. We test how well our numerical data obey this scaling relation, and what the best values of r_c, x_Δ, and $\beta = x_\Delta / y$ are. The order parameter should scale as a function of ϵ as $\Delta_b \sim \epsilon^\beta$. In Fig. 4.5, we show a log-log plot of Δ_b versus ϵ for various choices of r_c at $N_s = 4096$. The best straight line is obtained for $r_c = 0.80(2)$ and with a slope $\beta = 1.46(4)$. At the same choice for r_c, the order parameter also scales perfectly as a power law $\Delta_b \sim N_s^{-x_\Delta}$ with a critical dimension $x_\Delta = 0.370(5)$.

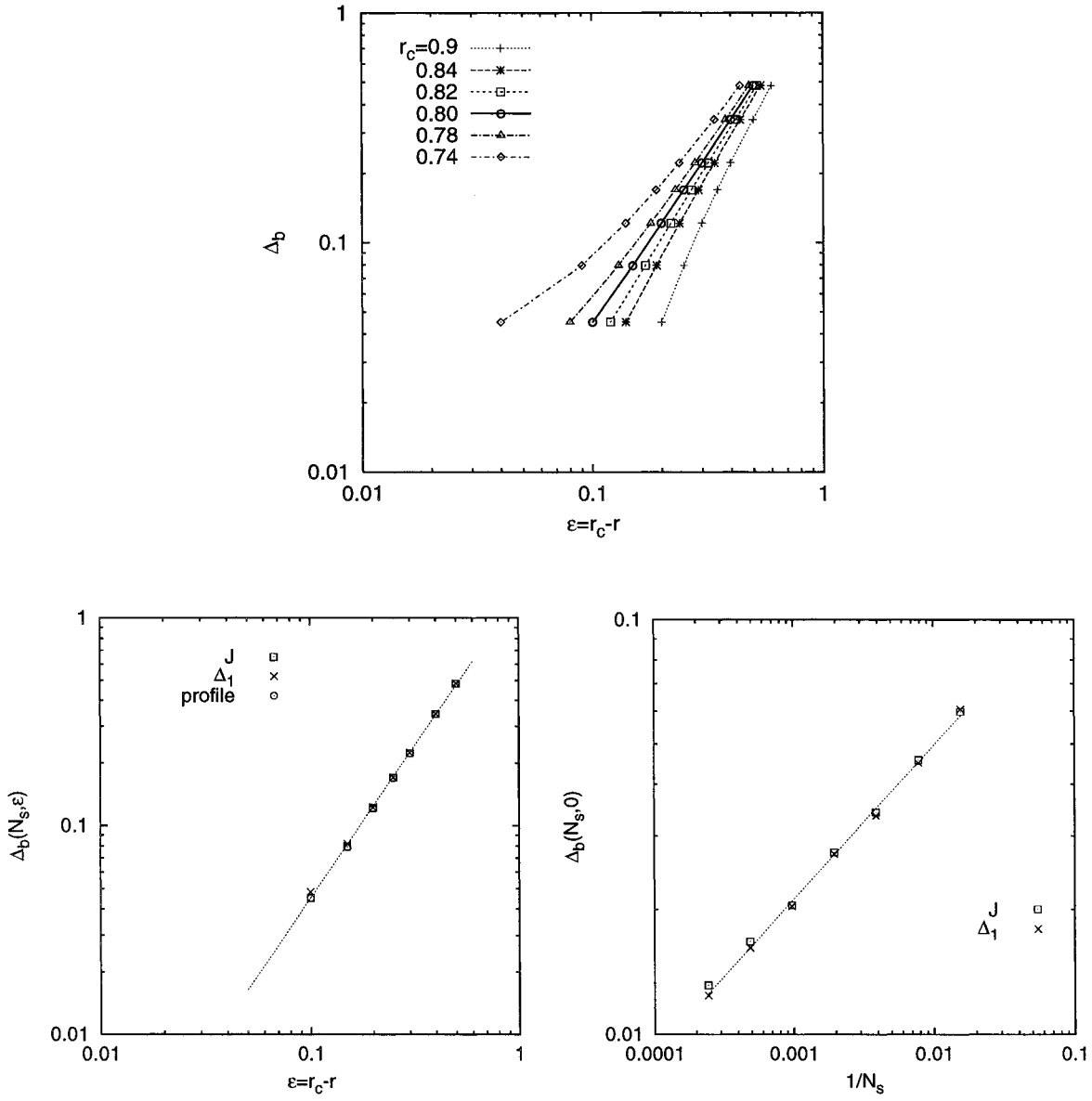

Figure 4.5: Determination of the critical point and critical exponents: (a) Double logarithmic $\Delta_b \sim |\epsilon|^\beta$ type plots of the order parameter with $\epsilon = r_c - r$ at $N_s = 4096$. The best straight line is found at $r_c = 0.80(2)$ and with slope $\beta = 1.46(4)$. Only the values of Δ_b obtained from the average current J are shown. (b) All three values of Δ_b are shown at $r_c = 0.8$. (c) Double logarithmic plots of $\Delta_b \sim N_s^{-x_\Delta}$ as a function of system size N_s at $r_c = 0.8$. The slope (dashed line) yields $x_\Delta = 0.370(5)$. For clarity, we show only the data for Δ_b obtained from J (squares) and Δ_1 (crosses).

The power-law scaling relation is thus very well satisfied and points to a critical point at $r_c = 0.80(2)$. One should always be on guard for FSS corrections and even for exponential type scaling behaviors (as in infinite-order type equilibrium phase transitions). Fig. 4.6 rules these out. We plot here the scaling function $\mathcal{S}$ defined as

$$\Delta_b(N_s, \epsilon) = N_s^{-x_\Delta}\ \mathcal{S}(N_s^y \epsilon) \tag{4.6}$$

for $r_c = 0.80$, $x_\Delta = 0.370$, and $\beta = x_\Delta / y = 1.46$. The data collapse quite well, suggesting only minor corrections to scaling.

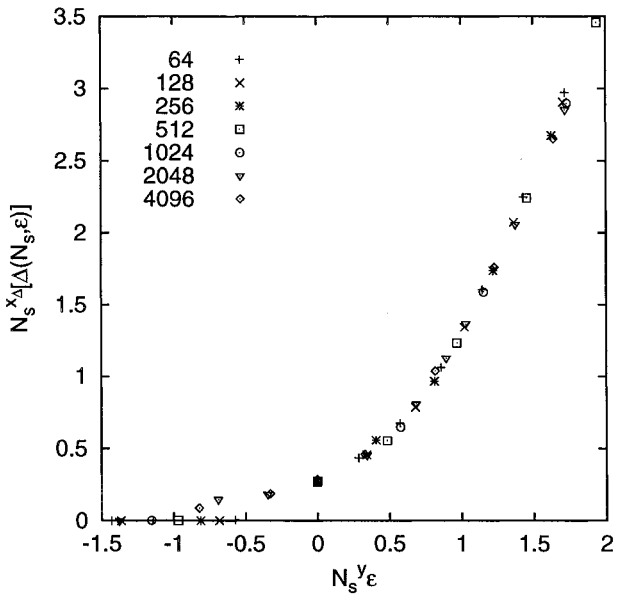

Figure 4.6: Data collapse by Eq. (4.6), i.e., the scaling function of the order parameter is obtained by using the values $r_c = 0.80$, $x_\Delta = 0.370$, and $\beta = 1.46$ as found in Fig. 4.5.

4.4 Density profiles

The density profiles near the slow/fast bond have a power-law shape for all values of r. The various types of data points reflect that we performed not only straight forward three-parameter fits to the density profile but also used two-point fits using the numerical values of the current and the density at site $x = 1$ for the value of the bulk density, Δ_b. The results are insensitive to these choices. Numerical MC noise is the main limiting factor.

Figures 4.7, 4.8, and 4.9 illustrate numerical data of the density profile for various r at $N_s = 4096$ and show three different power-law decay behaviors.

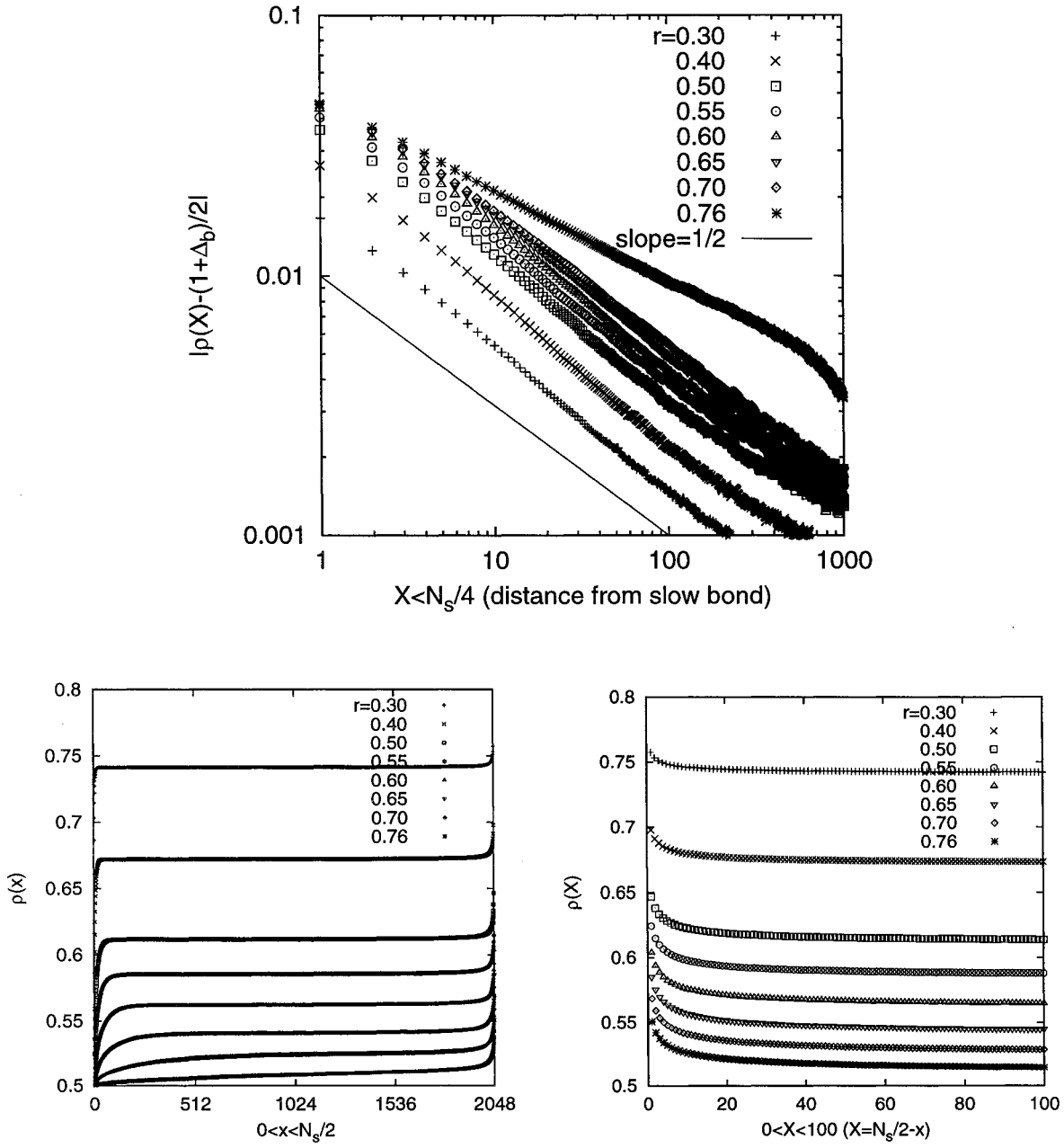

Figure 4.7: Numerical data of density profiles at $N_s = 4096$ near $r < r_c$. Double-logarithmic plots are obtained after the detailed evaluation of Δ_b.

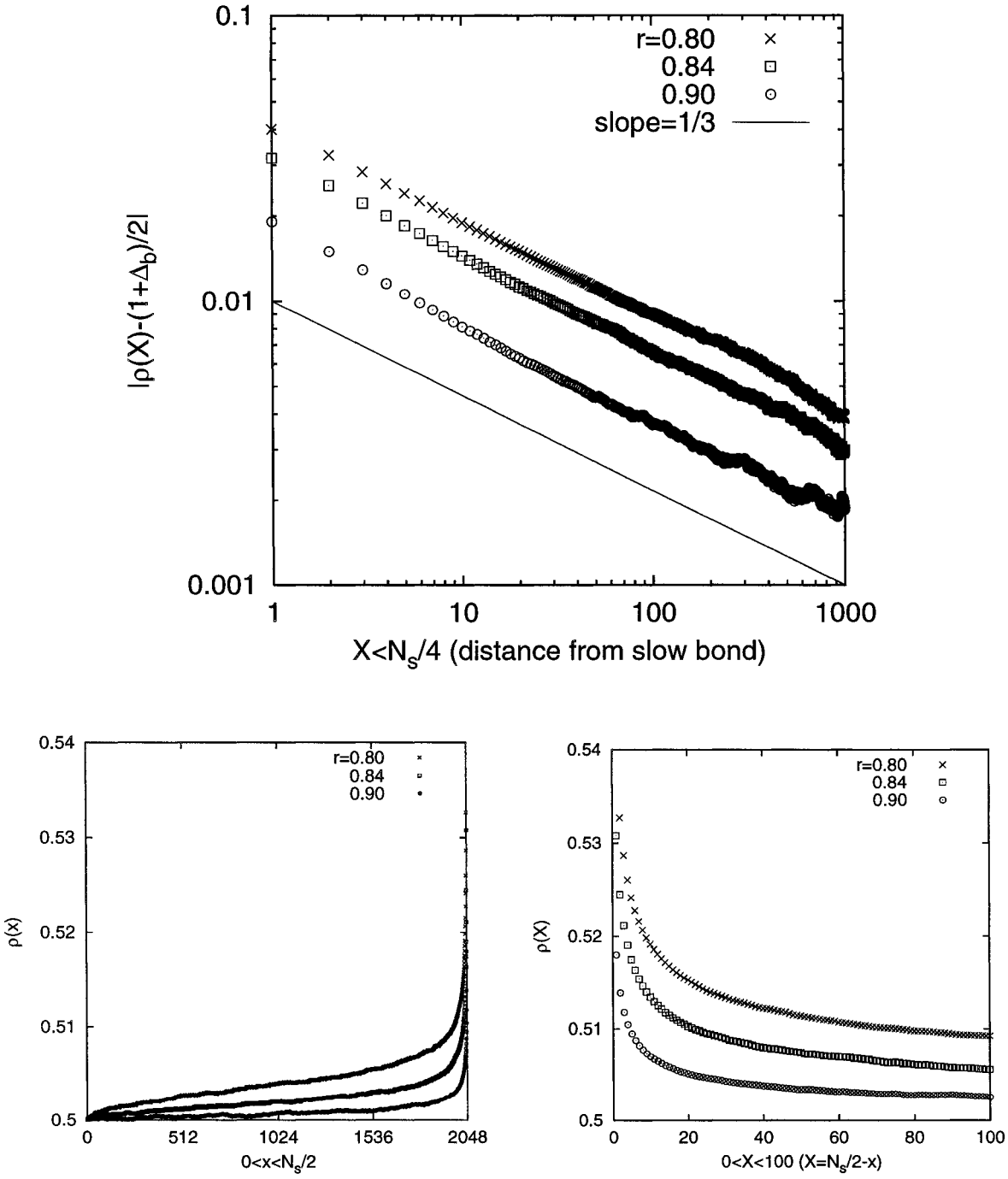

Figure 4.8: Numerical data of density profiles at $N_s = 4096$ for $r > r_c$. Double-logarithmic plots are obtained after the detailed evaluation of Δ_b.

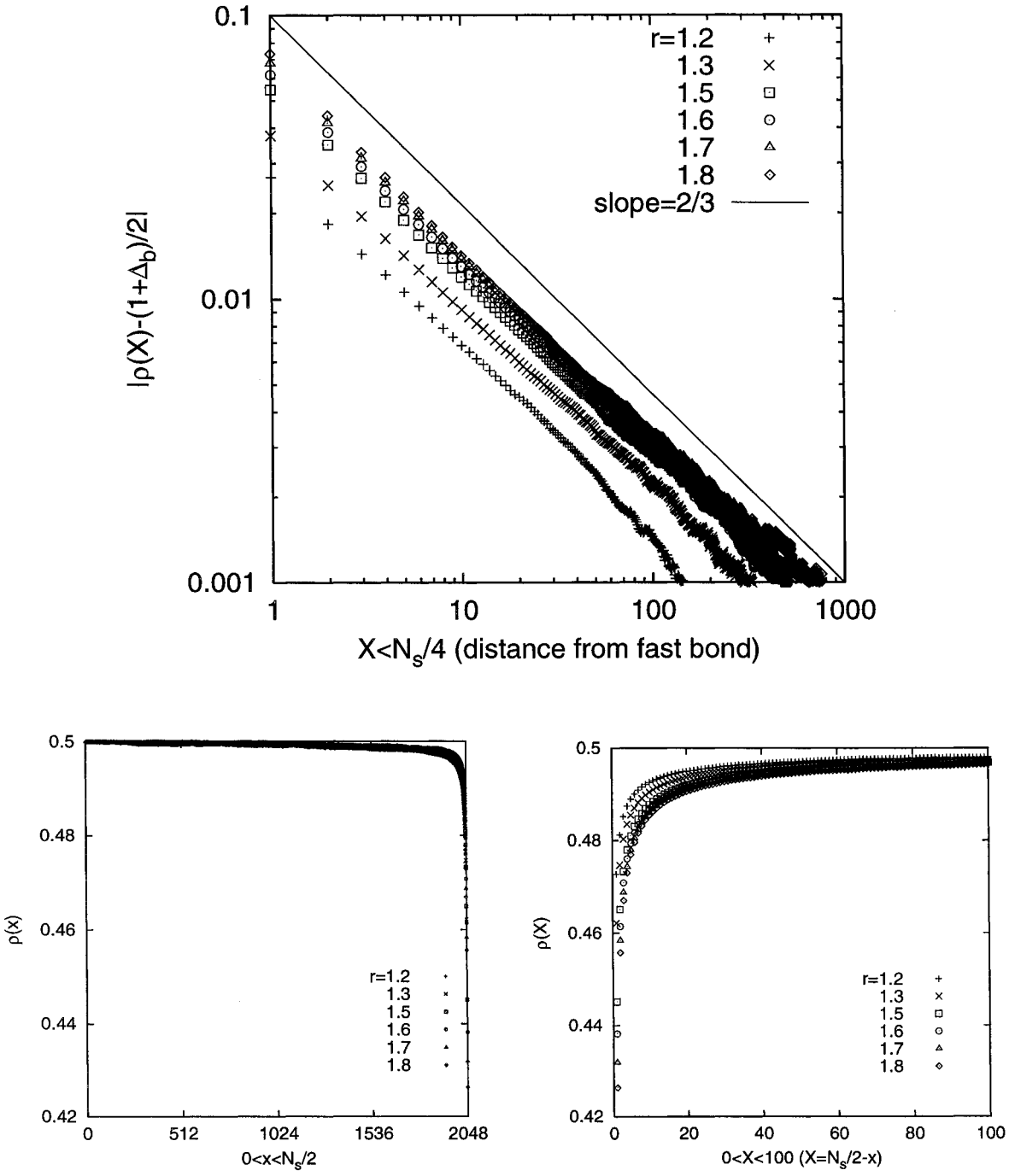

Figure 4.9: Numerical data of density profiles at $N_s = 4096$ for $r < r_c$. Double-logarithmic plots are obtained after the detailed evaluation of Δ_b.

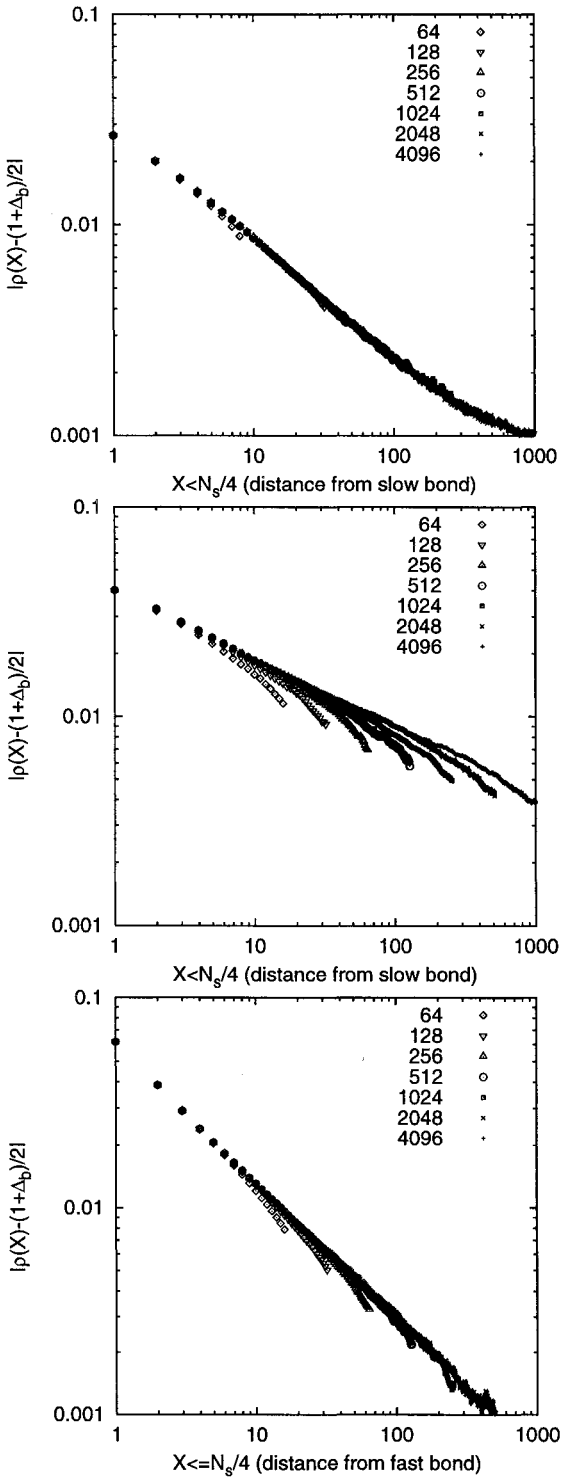

Figure 4.10: The size-dependent behavior of the power-law density profile for three different regime, $r = 0.2$ (top), $r = r_c = 0.8$ (middle), and $r = 1.6$ (bottom).

Figure 4.11 shows the numerical results for the exponent ν and the amplitude A of the density profile according to Eq. (4.4).

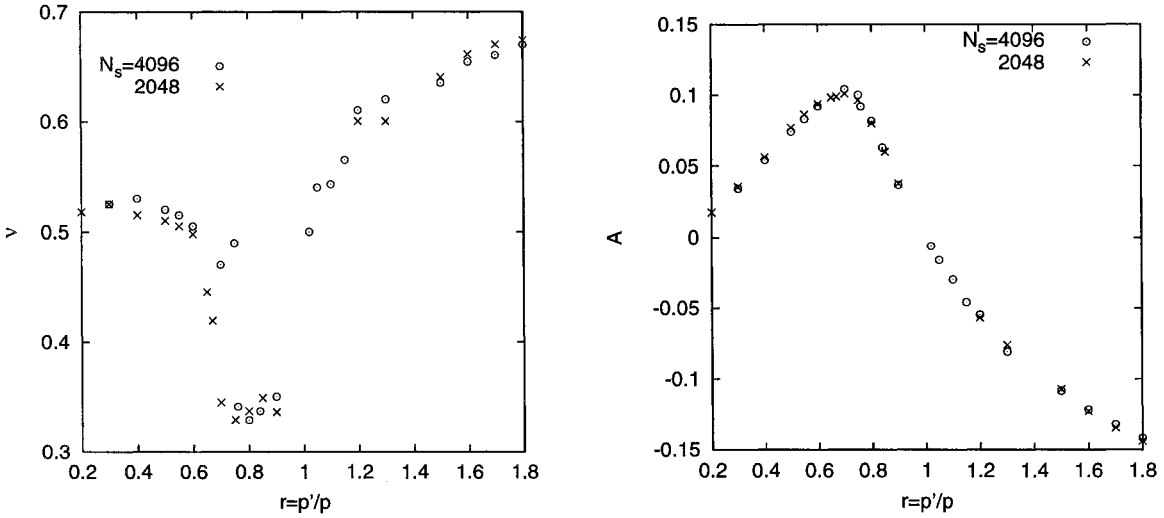

Figure 4.11: The exponent ν, (a), and the amplitude A, (b), of the power-law density profile, defined in Eq. (4.4), for various r at for $N_s = 2048$ and $N_s = 4096$.

The jumps in ν at r_c and $r = 1$ are pronounced. For $r > 1$, we see some evidence of a continuously varying exponent as originally suggested by Kandel and Mukamel [110] but this likely only represents crossover scaling. It seems safe to conclude, and surely as a starting assumption in the following discussions, that in the queued phase the exponent takes the value $\nu = \frac{1}{2}$, in the non-queued slow bond phase $\nu = \frac{1}{3}$, and in the fast bond (always non-queued) phase $\nu \simeq \frac{2}{3}$.

4.5 Uncorrelated passage

The passage through the slow bond is an uncorrelated process. Passage fluctuations are uncorrelated in time, and density fluctuations originating on the road do not affect it either. The following ratio embodies this

$$\mathcal{R} = \frac{\langle \hat{n}_L \hat{n}_R \rangle}{\langle \hat{n}_R \rangle} = \frac{1}{2}, \tag{4.7}$$

where $\hat{n}_L$ and $\hat{n}_R$ are the density operators at the site immediately in front of and beyond the slow/fast bond.

Figures 4.12 shows that this ratio is almost equal to $\mathcal{R} = \frac{1}{2}$ for all values of r, irrespective of whether the bond is slow or fast, or the density profile is queued or not. The deviations are only about 3%.

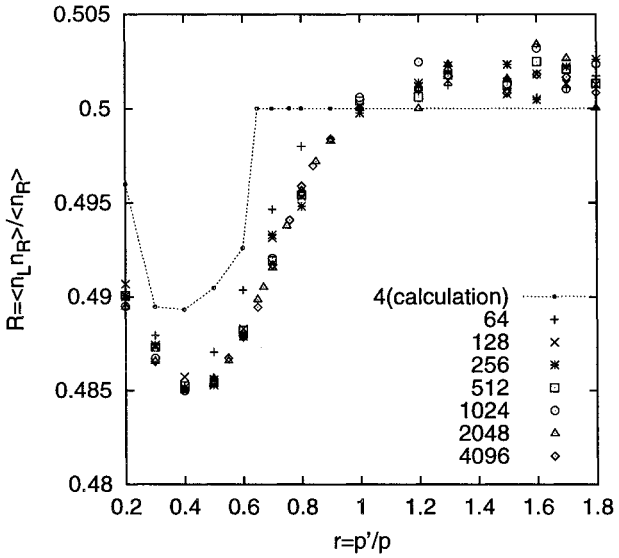

Figure 4.12: The ratio $\mathcal{R}$ defined in Eq. (4.7). R remains close to the uncorrelated passage value $\frac{1}{2}$ for all r. The small deviations, about 3%, do not scale with system size, and are well described by a 4-site type mean-field approximation (dashed line).

Below we show that all fluctuations travel away from the slow bond on both sides. The road acts as a particle reservoir as far as the passage process is concerned. $\mathcal{R}$ is exactly equal to $\mathcal{R} = \frac{1}{2}$, in a mean-field type approach where we treat the road in front of and beyond the slow bond as reservoirs (meaning as being devoid of fluctuations as far as the slow bond is concerned).

We simply solve the following 2-site problem: Introduce only sites x_L and x_R on either side of the slow bond. Let particles hop onto site x_L with an effective probability $\alpha_{\text{eff}}p$ from the road treating it as a reservoir, and let them hop away from x_R onto the road beyond the slow bond with probability $\alpha_{\text{eff}}p$ treating it as a reservoir as well. Finally, we tune $\alpha_{\text{eff}}p$ to a value for which the actual current J of the true system is established. This yields trivially

that $\mathcal{R} = \frac{1}{2}$ for all r and all $\alpha_{\text{eff}}p$. The dashed line in Fig. 4.12 shows the result for $\mathcal{R}$ in the next level of the mean-field theory, with 4 sites instead of 2. This already reproduces most of the small deviations. We conclude therefore that these minor deviations from $R = \frac{1}{2}$ reflect only short distance correlations.

The current-current auto correlation function at the slow bond would be a more direct quantity to illustrate the uncorrelated nature of the passage process. We measure it and find that it decays over two orders of magnitude within 10 MC time steps. This is not conclusive nor meaningful, however, because it decays similarly fast anywhere else along the road, reflecting that in KPZ growth $\delta J \sim N_s^{-y}$ scales with the exponent $y \simeq 2$.

In the queued phase, the absence of passage correlations is easily explained. Fluctuations travel away from the slow bond, both in front of and beyond it. The group velocity of fluctuations v_g points away from the slow bond in both directions. $v_g = \delta J/\delta\rho(x)$ represents the local response of the current to a density fluctuation. The stationary state is uncorrelated inside the bulk, such that the current is equal to $J = p\rho_b(1-\rho_b)$ and $v_g = p(1-2\rho_b) = -p\Delta_b$. Fluctuation type wave packets travel with this velocity along the road, while they broaden in space as $\xi \sim t^{1/z}$, with the 1D KPZ dynamic exponent $z = \frac{3}{2}$. In the KPZ growth context, Δ_b represents the average slope of the growing surface, and the traveling wave packet reflects that the surface grows perpendicular to the surface.

The precise form of v_g in the case of spatially varying densities $\rho(x)$ is more complex, but for slowly varying densities we can assume that v_g can be approximated as

$$v_g(x) = p[1 - 2\rho(x)] = -p\Delta(x). \tag{4.8}$$

In the queued phase, $\Delta(x)$ is positive (with $\Delta_b > 0$), such that the center of mass of a wave packet moves away from the slow bond linearly in time, $x_{\text{CM}} \sim t$. During this process, it spreads over a width $\xi \sim t^{3/2}$. The latter scales slower in time. This means the wave packet detaches itself from the slow bond, and that therefore the density fluctuations at the slow bond must be uncorrelated in time. No memory remains at the slow bond of what happened there before.

Above the queuing phase transition, $r_c < r < 1$, the weak strength of the slow bond creates only a power-law density tail, $\Delta(\tilde{x}) = A\tilde{x}^{-\nu}$. The center of mass of a wave packet

still moves away from the slow bond as $x_{\mathrm{CM}} \sim t^{1/(1+\nu)}$, following Eq. (4.8). For all $\nu < \frac{1}{2}$, it moves away faster from the slow bond than it spreads, such that the wave packet still detaches itself from the slow bond. Numerically, we find that $\nu = \frac{1}{3}$, see Fig. 4.11(a). Therefore, the passage through the slow bond remains an uncorrelated memoryless process also in the non-queued slow bond phase.

In the fast bond case, $r > 1$, $\mathcal{R}$ remains exactly equal to $\frac{1}{2}$. How do fluctuations travel there? The group velocity has changed direction because the amplitude A of the density tail, $\Delta(\tilde{x}) = A\tilde{x}^{-\nu}$, changed sign. Fluctuations travel now towards the fast bond from both sides. Consider a fluctuation created at a distance x from the fast bond. The center of mass of this fluctuation moves towards the fast bond, and arrives there after a time of flight $t \sim x_{\mathrm{CM}}^{\nu+1}$. During this time, it has broadened over a width $\xi \sim t^{2/3}$. In the fast bond case, we find that $\nu \simeq \frac{2}{3} > \frac{1}{2}$ (see Fig. 4.11 (a)). This means that the leading edge of fluctuations actually arrives much earlier at the fast bond than its center of mass, and that the center of mass movement is a secondary effect. Those fluctuations treat the fast bond site (either x_L or x_R) just like an ordinary bulk site. Recall that in the bulk the stationary state is uncorrelated, $\langle \hat{n}_x \hat{n}_{x+1} \rangle = \langle \hat{n}_x \rangle \langle \hat{n}_{x+1} \rangle$. This explains $\mathcal{R} = \frac{1}{2}$ in the fast bond case.

4.6 Intuitive Explanations

Our observation that the density profile near the slow/fast bond always follows a power law, $\delta\rho \sim \tilde{x}^{-\nu}$, in all three phases, is far from obvious. After all, near the reservoir edge, it has an exponential edge. Moreover, we just demonstrated that the passage process is uncorrelated for both slow and fast bond cases. The actual values for the exponents ν are quite intriguing as well. In this section, we will present intuitive heuristic explanations.

First, consider the $\nu = \frac{1}{2}$ power-law density profile in the queued phase. The total number of excess particles in this power-law tail scales with system size N_s as $\delta N \sim N_s^{1/2}$. This has a familiar ring to it. In the open system setup with reservoirs on both sides but without any special bonds, the fluctuations in the total number of particles on the road scales also as $\delta N \sim N_s^{1/2}$. However, that does not imply that there is a power-law tail in the density profile near reservoirs at the edge of the road, i.e., not in the phases where

the group velocity of fluctuations is non-zero (the phases where one of the two reservoirs controls the density on the road), similar to the queued phase we have here.

In Chapter 3, we studied an ASEP setup consisting of a closed loop starting and ending at the same site, i.e., a parking garage (P) type reservoir [151]. The number of cars in the system is conserved, leading to phase transitions between condensate type phases where the garage is macroscopically occupied and a normal phase where it is not. That process has two parameters, the total number of cars in the system, and a modified hopping probability αp to jump from the garage onto the first site of the road. In that setup, the above FSS correction to the number of cars on the road shows up a correction to the total number of parked cars, $\delta N_P \sim N_s^{1/2}$ at the normal to condensate phase transition point.

The explanation of this power is straight forward. The group velocity of fluctuations v_g is non-zero in both phases and also at the transition point. The latter implies that the departure of cars from P is an uncorrelated process. Fluctuations detach from P because they travel away faster (linear in time) than they are spreading backwards (as $\xi \sim t^{1/z}$ with $z = \frac{3}{2}$). Moreover, after a time of flight $t_{\text{flight}} = N_s/v_g$, they move around the loop, return to P, and are completely erased. So we can deal with t_{flight} random uncorrelated deposition events. The fluctuations in the number of cars on the road should therefore scale as $t_{\text{flight}}^{1/2}$. In the condensate phase, P is macroscopically occupied, and these fluctuations are unbiased, but not so at the transition point. At the transition point, each of these uncorrelated fluctuations is biased towards increased occupation at P, thus implying that the number of parked cars scales as $\delta N_P \sim N_s^{1/2}$.

We face a similar situation near the slow bond in the queued phase. Passage through the slow bond is a stochastic uncorrelated event (similar to the departures from P in the above discussion). Moreover, fluctuation wave packets move away from it faster than they spread; v_g points away from the slow bond (as discussed in the previous section). The fluctuations in the number of cars passing through the slow bond therefore scales also as $t_{\text{flight}}^{1/2}$. These fluctuations are biased because the site in front of the slow bond is not a parking garage, i.e., the excess cars waiting to pass are spread out and the cars available for immediate passage through the slow bond is limited. Low density fluctuations pass quicker. So the total number of excess cars near the slow bond scales as $\delta N_P \sim N_s^{1/2}$. These extra

particles must be accommodated over a stretch of road $x < x_L$ in front of the slow bond. We can imagine two ways to realize this: an exponential density profile with a correlation length diverging as $\xi \sim N_s^{1/2}$, or a power-law profile with the exponent $\nu = \frac{1}{2}$ as we actually observe. The power law is indeed more likely, given the intrinsic critical nature of ASEP.

Next, consider the $\nu = \frac{1}{3}$ power-law density profile above the queuing transition, $r_c < r < 1$. Here fluctuations also travel faster across the system than they broaden. The time of flight for a fluctuation to move from the slow bond all the way back to site $x = 1$ scales as, $t_{\text{flight}} \sim N_s^{\nu+1}$ since $v_g = -p\Delta(\tilde{x}) \sim \tilde{x}^{-\nu}$. Assume that $\nu < \frac{1}{2}$, in which case the passage through the slow bond remains uncorrelated; fluctuations detach from the slow bond because they travel faster across the system than they broaden. Just as in the queued phase, the FSS correction to the total number of cars in the bulk must scale as t_{flight} uncorrelated events. This yields that the FSS correction to the total number of cars in the bulk part of the road scales as

$$\delta N \sim t_{\text{flight}}^{\frac{1}{2}} \sim N_s^{\frac{\nu+1}{2}} \tag{4.9}$$

This bulk deficit heaps up in front of the slow bond, and again arranges itself in the form of a power-law shaped density profile, $\delta\rho \sim \tilde{x}^{-\nu}$. Self consistency implies that $(\nu+1)/2 = -\nu+1$. This yields $\nu = \frac{1}{3}$, in accordance with the value we observed.

Finally, consider the $\nu \simeq \frac{2}{3}$ power-law density profile in the fast bond case, $r > 1$. This is a fundamentally different phenomenon. Again fluctuations travel across the system, but now into the fast bond instead of away from it. More importantly, the time of flight of the center of mass of a fluctuation $t_{\text{flight}} \sim N_s^{\nu+1}$ is now longer than the time it takes that same fluctuation to spread over the entire system $t \sim N_s^z$ with $z = \frac{3}{2}$. This is true for all $\nu > (z-1) = \frac{1}{2}$. For the slow bond case, $r < 1$, we are allowed to ignore the spreading of the fluctuations, and only consider their center of mass motion (the time of flight). For the fast bond case, $r > 1$, this is reversed. For $r < 1$ (slow bond), the exponent ν was insensitive to the actual value of the dynamic exponent z of the dynamic process. For $r > 1$ (fast bond), it must depend on on the value of z.

As a start one might look for signs of $\nu \simeq \frac{2}{3}$ power-law tails in the so-called maximal-current phase of the exactly soluble open system with reservoirs on both sides [82], where

the group velocity is zero. In that setup, the stationary state shows no hint whatsoever of a $\nu \simeq \frac{2}{3}$ power. To the contrary, the density profile has $\frac{1}{2}$ power-law tails, in accordance with the fact the the density operator $\rho(x)$ scales with the exponent $-\frac{1}{2}$ and fluctuations in the total number of particles on the road therefore scale as $\delta N \sim N_s^{1/2}$.

Interestingly, however, a $\nu \simeq \frac{2}{3}$ power in the density profile appeared earlier in our previous ASEP study with a parking garage [151], see also Chapter3. That process has a "normal" to "maximal-current" phase transition. In the condensate phases, the garage acts as an information sink, while in the normal phase, fluctuations travel freely through the garage (P). The maximal-current to normal transition is the onset point where information starts to percolate through P. At the transition point, we found numerically a $\nu \simeq \frac{2}{3}$ power-law density profile at the beginning of the road. The similarities with the fast bond density profile are striking; e.g., also there is no group velocity, except near P where it pushes fluctuations into P. At this time, we could not explain this profile, but it is clear we are looking at the same phenomenon.

An obvious guess is that the value of the exponent might be equal to $\nu = 1/z$; but how to argue for that? One of the crucial aspects must be again that fluctuations are being biased at the fast bond, leading to a total deficit of cars in front of the fast bond that scales as $\delta N \sim \int_0^{N_s/2} d\tilde{x}\ \tilde{x}^{-\nu} \sim N_s^{1-\nu} \sim N_s^{1/3}$. Density fluctuations are being created everywhere along the road, all the time, and with roughly the same amplitude A. Each spreads in time over a region $\xi \sim t^{1/z}$. A fluctuation created at a distance $\tilde{x}$ from the fast bond arrives at the fast bond after a time $t \sim \tilde{x}^z$ and with a reduced amplitude (by spreading) of order $A\tilde{x}^{-1/z}$. The fast bond processes high and low density fluctuations differently (it processes high densities better than a normal bond, and negative densities do not exist). This gives rise to a density deficit of order $A\tilde{x}^{-1/z}$. Next, adopting superposition principle ideas, one would guess that the total density deficit in front of the fast bond scales as $\delta N \sim \int_0^{N_s/2} d\tilde{x}\ A\tilde{x}^{-1/z} \sim N_s^{1-1/z}$ in agreement with what we observed numerically.

4.7 Summary

In this study, we numerically reconfirmed, beyond doubt, the presence of a queuing phase transition in the ASEP at a slow bond strength $r_c \simeq 0.80(2)$. This confirms general expectations based mainly on the earlier less accurate work . We established two scaling exponents of this transition: The order parameter, the excess density in the queue, vanishes as $\Delta_b \sim |r_c - r|^\beta$ with $\beta = 1.46(4)$. At the transition point, this excess density scales with system size $\Delta_b \sim N_s^{-x_\Delta}$ with $x_\Delta = 0.370(5)$.

From a more general perspective, the transition illustrates that weak obstructions do not give rise to macroscopic traffic jams (queues with lengths that scale linearly with the system size). The stochastic fluctuations overwhelm the blockage above r_c.

The second and truly novel result of our study is that above such a transition a power-law shaped traffic jam queue remains, $\delta\rho \simeq A\tilde{x}^{-\nu}$, with $\tilde{x}$ the distance from the obstruction and opposite signs for A in front and behind the obstruction. The exponent is equal to $\nu = \frac{1}{3}$ in this ASEP model. This value is most likely universal because our heuristic derivation for it depends only on very general aspects. It does not involve the KPZ value of the dynamic exponent z. The same argument applies for any process with a $z > (1 + \nu) = \frac{4}{3}$.

In the fast bond case (a local widening of the road), a macroscopic depletion queue (with a length proportional to the road length) never appears. Instead, a power-law shaped depletion queue is always present with the exponent $\nu \simeq \frac{2}{3}$. This value probably reflects directly the KPZ dynamic exponent of the process since in our heuristic explanation it is equal to $\nu = 1/z$.

It will be interesting to confirm our results in other models for driven flow along one-dimensional channels, in particular non-KPZ type dynamics. If the results prove universal, as we expect, they might apply even to highway traffic flow.

BIBLIOGRAPHY

[1] M. Myllys, J. Maunukesela, M.J. Alava, T. Ala-Nissila, J. Merikoski, and J. Timonen. Kinetic roughening in slow combustion of paper. *Phys. Rev. E*, 64:036101, 2001.

[2] R. Surdeanu, R.J. Wijngaarden, E. Visser, J.M. Huijbregtse, J.H. Rector, B. Dam, and R. Griessen. Kinetic roughening of penetrating flux fronts in high-T_c thin flim superconductors. *Phys. Rev. Lett.*, 83:2054, 1999.

[3] E.A. Eklund, R. Bruinsma, J. Rudnick, and R.S. Williams. Submicro-scale surface roughening induced by ion bombardment. *Phys. Rev. Lett.*, 67:1759, 1991.

[4] T.M. Mayer, E. Chason, and A.J. Howard. Roughening instability and ion-induced viscous relaxation of SiO_2 surfaces. *J. Appl. Phys.*, 76:1633, 1994.

[5] H.E. Stanely. Fractal landscapes in physics and biology. *Physica A*, 186:1, 1992.

[6] A.-L. Barabási and H.E. Stanley. *Fractal Concepts in Surface Growth.* Cambridge University Press, Cambridge, 1995.

[7] G.M. Schütz. Exactly solvable models for many-body systems far from equilibrium. In C. Domb and J. Lebowitz, editors, *Phase Transitions and Critical Phenomena*, volume 19. Academic Press, London, 2001.

[8] S.A. Janowsky and J. L. Lebowitz. Finite-size effects and shock fluctuations in the asymmetric simple-exclusion process. *Phys. Rev. A*, 45:618, 1992.

[9] S. Katz, J.L. Lebowitz, and H. Spohn. Phase transitions in stationary nonequilibrium stats of model lattice systems. *Phys. Rev. B*, 28:1655, 1983.

[10] S. Katz, J.L. Lebowitz, and H. Spohn. Nonequilibrium steady states of stichastic lattice gas models of fast ionic conductors. *J. Stat. Phys.*, 34:497, 1984.

[11] K. Huang. *Statistical Mechanics.* Wiley, New York, 2nd edition, 1987.

[12] D.J. Amit. *Field Theory, the Renormalization Group and Critical Phenomena.* World Scientific, Singapore, 2nd revised edition, 1984.

[13] R. Kubo. The fluctuation-dissipation theorem. *Rep. Progr. Phys.*, 29:255, 1966.

[14] H.E. Stanley. *Introduction to Phase Transitions and Critical Phenomena.* Oxford University Press, New York, 1971.

[15] S.-K. Ma. *Modern Theory of Critical Phenomena.* Addison-Wesley, New York, 1976.

[16] J. Zinn-Justin. *Quantum Field Theory and Critical Phenomena.* Clarendon Press, Oxford, 1990.

[17] G. Nicolis and I. Prigogine. *Self-Organization in Non-equilibrim Systems.* Wiley, New York, 1977.

[18] H. Haken. *Synergetics.* Springer-Verlag, Berlin, 2nd edition, 1978.

[19] H. Haken. *Advanced Synergetics.* Springer-Verlag, Berlin, 1983.

[20] R. Graham. In G. Nicolis. G. Dewel and J.W. Turner, editors, *Order and Fluctuations in Equilibrium and Nonequilibrium Statistical Mechanics.* John Wiley & Sons, New York, 1981.

[21] M.C. Cross and P.C. Hohenberg. Pattern formation outside of equilibrium. *Rev. Mod. Phys.*, 65:851, 1993.

[22] D. Sornett and Y.-C. Zhang. Nonlinear Langevin model of geomorhic erosion processes. *Geophys. J. Int.*, 113:382, 1993.

[23] M.A. Rubio, C.A. Edwards, A. Dougherty, and J.P. Gollub. Self-affine fractal interfaces from immiscible displacement in porous media. *Phys. Rev. Lett.*, 63:1685, 1989.

[24] A.-L. Barabási, S.V. Buldyrev, S. Havlin, G. Huber H.E. Stanley, and T. Vicsek. Imbibition in poros media: Experiment and theory. In R. Jullien, J. Kertész, P. Meakin, and D.E. Wolf, editors, *Surface Disordering: Growth, Roughening and Phase Transitions*. Nova Science, New York, 1992.

[25] D.G. Green, A.M. Gill, and I.R. Noble. Fire shapes and the adequacy of fire-spread models. *Ecological Modeling*, 20:33, 1983.

[26] M. Myllys, J. Maunukesela, M.J. Alava, T. Ala-Nissila, and J. Timonen. Scaling and noise in slow combustion of paper. *Phys. Rev. Lett.*, 84:1946, 2000.

[27] S. Das Sarma and P. Tamborenea. A new universality class for kinetic growth: One-dimensional molecular-beam epitaxy. *Phys. Rev. Lett.*, 66:325, 1991.

[28] J.A. Shapiro. Organization of developing escherichia-coli colonies viewed by scanning electron-microscopy. *J. Bacteriology*, 169:142, 1987.

[29] E. Ben-Jacob, O. Shochet, A. Tenenbaum, A. Czirók I. Cohen, and T. Vicsek. Communication, regulation and control during complex patterning of bacterial colonies. *Nature*, 368:46, 1994.

[30] Z. Csahók and T. Vicsek. Kinetic roughening in a model of sedimentation of granular materials. *Phys. Rev. A*, 46:4577, 1992.

[31] M. Eden. In H.P. Yockey, editor, *Symposium of Information Theory in Biology*. Pergamon, New York, 1958.

[32] F. Family and T. Vicsek. Scaling of the active zone in the eden process on percolation networks and the ballistic deposition model. *J. Phys. A*, 18:L75, 1985.

[33] S.T. Chui and J.D. Weeks. Dynamics of the roughening transition. *Phys. Rev. Lett.*, 40:773, 1978.

[34] S.F. Edwards and D.R. Wilkinson. The surface statistics of a granular aggregate. *Proc. R. Soc. London A*, 381:17, 1982.

[35] M. Kardar, G. Parisi, and Y.C. Zhang. Dynamic scaling of growing interfaces. *Phys. Rev. Lett.*, 56:889, 1986.

[36] J.M. Burgers. *The Nonlinear Diffusion Equation.* Riedel, Boston, 1974.

[37] N.G. van Kampen. *Stochastic Processes in Physics and Chemistry.* North-Holland, Amsterdam, 1981.

[38] C.W. Gardiner. *Handbook of Stochastic Methods.* Springer-Verlag, Berlin, 1985.

[39] T. Halpin-Healy and Y.-C. Zhang. Kinetic roughening phenomena, stochastic growth, directed polymers and all that. Aspects of multidisciplinary statistical mechanics. *Phys. Rep.*, 254:215, 1995.

[40] L.M. Sander and H. Yan. Temporal characteristics in nonequilibrium surface-growth models. *Phys. Rev. A*, 44:4885, 1991.

[41] D. Forster, D.R. Nelson, and M.J. Stephen. Large-distance and long-time properties of a randomly stirred fluid. *Phys. Rev. A*, 16:732, 1977.

[42] E. Medina, T. Hwa, M. Kardar, and Y.C. Zhang. Burgers equation with correlated noise: Renormalization-group analysis and applications to directed polymers and interface growth. *Phys. Rev. A*, 39:3053, 1989.

[43] E. Marinari, A. Pagnani, and Z. Rácz. Width distributions and the upper critical dimension of kardar-parisi-zhang interfaces. *Phys. Rev. E*, 65:026136, 2002.

[44] J.M. Kim and J.M. Kosterlitz. Growth in a restricted solid-on-solid model. *Phys. Rev. Lett.*, 62:2289, 1989.

[45] C.-S. Chin and M. den Nijs. Stationary state skewness in two dimensional KPZ type growth. *Phys. Rev. E*, 59:2633, 1999.

[46] C.-S. Chin and M. den Nijs. Reconstructed rough phases during surface growth, ridgeline trapping of domain walls. *Phys. Rev. E*, 64:031606, 2001.

[47] P. Meakin, P. Ramanlal, L.M. Sander, and R. C. Ball. Ballistic deposition on surfaces. *Phys. Rev. A*, 34:5091, 1986.

[48] M. Plischke, Z. Rácz, and D. Liu. Time-reversal invariance and universality of two-dimensional growth models. *Phys. Rev. B*, 35:3485, 1987.

[49] J. Neergaard and M. den Nijs. Crossover scaling functions in one dimensional dynamic growth models. *Phys. Rev. Lett.*, 74:730, 1995.

[50] M. den Nijs. In C. Domb and J. Lebowitz, editors, *Phase Transitions and Critical Phenomena*, volume 12. Academic Press, London, 1988.

[51] H. van Beijeren and I. Nolden. In W. Schommers and P. von Blanckenhagen, editors, *Structures and Dynamics of Surfaces*, volume 2. Springer-Verlag, Berlin, 1987.

[52] D. Davidson and M. den Nijs. Temperature dependence of facet ridges in crystal surfaces. *Phys. Rev. E*, 59:5029, 1999.

[53] E. Hopf. *Comm. Pure Appl. Math.*, 3:201, 1950.

[54] J.D. Cole. *Quart. Appl. Math.*, 9:225, 1951.

[55] R.P. Feynman and A.R. Hibbs. *Quantum Mechanics and Path Integrals.* McGraw-Hill, New York, 1965.

[56] M. Kardar and Y.C. Zhang. Scaling of directed polymers in random media. *Phys. Rev. Lett.*, 58:2087, 1987.

[57] G. Forgacs, R. Lipowsky, and Th.M. Nieuwenhuizen. In C. Domb and J.L. Lebowitz, editors, *Phase Transitions and Critical Phenomena*, volume 14. Academic Press, New York, 1991.

[58] H. Spohn. *Large Scale Dynamics of Interacting Particles.* Springer-Verlag, Berlin, 1991.

[59] B. Schmittmann and R.K.P. Zia. Statistical mechanics of driven diffusive systems. In C. Domb and J.L. Lebowitz, editors, *Phase Transitions and Critical Phenomena*, volume 17. Academic Press, London, 1995.

[60] V. Privman, editor. *Nonequilibrium Statistical Mechanics in One Dimension*, Cambridge, 1997. Cambridge University Press.

[61] D.C. Mattis and M.L. Glasser. The uses of quantum field theory in diffusion-limited reactions. *Rev. Mod. Phys.*, 70:979, 1998.

[62] S.F. Edwards. The statistical mechanics of polymerized material. *Proc. Roy. Soc. London*, 92:9, 1967.

[63] P.G. de Gennes. *J. Chem. Phys.*, 55:572, 1971.

[64] F. Spitzer. Interaction of Markov processes. *Adv. Math.*, 5:246, 1970.

[65] S. Alexander and T. Holstein. Lattice diffusion and the Heisenberg ferromagnet. *Phys. Rev. B*, 18:301, 1978.

[66] J. Käs, H. Strey, and E. Sackmann. Direct image of reptation for semiflexible actin filaments. *Nature*, 368:226, 1994.

[67] T.T. Perkins, D.E. Simth, and S. Chu. Direct observation of tube-like motion of a single polymer chain. *Science*, 264:819, 1994.

[68] J.T. MacDonald, J.H. Gibbs, and A.C. Pipkin. *Biopolymers*, 6:1, 1968.

[69] J.T. MacDonald and J.H. Gibbs. *Biopolymers*, 7:707, 1969.

[70] D. Dhar. An exactly solved model for interfacial growth. *Phase Transitions*, 9:51, 1987.

[71] L.-H. Gwa and H. Spohn. Six-vertex model, roughened surfaces, and an asymmetric spin hamiltononian. *Phys. Rev. Lett.*, 68:725, 1992.

[72] L.-H. Gwa and H. Spohn. Bethe solution for the dynamic-scaling exponent of the noisy Burgers equation. *Phys. Rev. A*, 46:844, 1992.

[73] V. Kukla, J. Kornatowski, D. Demuth, I. Girnus, H. Pfeifer, L. Ree, S. Schunk, K. Unger, and J. Kärger. NMR studies of single-file diffusion in unidimensional channel zeolites. *Science*, 272:702, 1996.

[74] K. Kawasaki. Diffusion constants near the critical point for time-dependent Ising models. I. *Phys. Rev.*, 145:224, 1966.

[75] F.L. Hall, L.A. Brian, and M.A. Gunter. *Transpn. Res. A*, 20:197, 1986.

[76] M. Schreckenberg, A. Schadschneider, K. Nagel, and N. Ito. Discrete stochastic models for traffic flow. *Phys. Rev. E*, 51:2939, 1995.

[77] K. Nagel. Particle hopping models and traffic flow theory. *Phys. Rev. E*, 53:4655, 1996.

[78] R. Kroon and R. Sprik. Diffusion-limited exciton kinetics in one-dimensional systems. In V. Privman, editor, *Nonequilibrium Statistical Mechanics in One Dimension*. Cambridge University Press, Cambridge, 1997.

[79] R. Kopelman and A.L. Lin. Experimental investigations of molecular and excitonic elementary reaction kinetic in one-dimensional systems. In V. Privman, editor, *Nonequilibrium Statistical Mechanics in One Dimension.* Cambridge University Press, Cambridge, 1997.

[80] J. Krug. Boundary-induced phase transitions in driven diffusive systems. *Phys. Rev. Lett.*, 67:1882, 1991.

[81] G. Schütz and E. Domany. Phase transitions in a exactly soluble one-dimensional exclusion process. *J. Stat. Phys.*, 72:277, 1993.

[82] B. Derrida, M.R. Evans, V. Hakim, and V. Pasquier. Exact solution of a 1D asymmetric exclusion model using a matrix formulation. *J. Phys. A*, 26:1493, 1993.

[83] G. Schütz. Time-dependent correlation functions in a one-dimensional asymmetric exclusion process. *Phys. Rev. E*, 47:4265, 1993.

[84] H.C. Fogedby, A.B. Eriksson, and L.V. Mikheev. Continuum limit, Galilean invariance, and solitons in the quantum equivalent of the noisy Burgers equation. *Phys. Rev. Lett.*, 75:1883, 1995.

[85] H.K. Jassen and B. Schmittmann. Field theory of long time behavior in driven diffusive systems. *Z. Phys. B*, 63:517, 1986.

[86] J. Krug and L.-H. Tang. Disorder-induced unbinding in confined geometries. *Phys. Rev. E*, 50:104, 1994.

[87] H.K. Janssen and K. Oerding. Renormalized field theory and particle density profile in driven diffusive systems with open boundaries. *Phys. Rev. E*, 53:4544, 1996.

[88] K. Oerding and H.K. Janssen. Surface critical behavior of driven diffusive systems with open boundaries. *Phys. Rev. E*, 58:1446, 1998.

[89] A.B. Kolomeisky, G.M. Schütz, E.B. Kolomeisky, and J.P. Straley. Phase diagram of one-dimensional driven lattice gases with open boundaries. *J. Phys. A*, 31:6911, 1998.

[90] V. Popkov and G.M. Schütz. Steady-state selection in driven diffusive systems with open boundaries. *Europhys. Lett.*, 48:257, 1999.

[91] R.J. Baxter. *Exactly Solved Models in Statistical Mechanics.* Academic Press, New York, 1982.

[92] E.H. Lieb and F.Y. Wu. In C. Domb and M.S. Green, editors, *Phase Transitions and Critical Phenomena*, volume 2. Academic Press, New York, 1972.

[93] P.W. Kasteleyn. In E.D.G. Cohen, editor, *Fundamental Problems in Statistical Mechanics III.* North-Holland, Amsterdam, 1975.

[94] J. Quastel. PhD thesis, Courant Institute, New York, 1990.

[95] D. Kandel and E. Domany. Rigorous derivation of domain growth kinetics without conservation laws. *J. Stat. Phys.*, 58:685, 1990.

[96] D. Kandel, E. Domany, and B. Nienhuis. A six-vertex model as a diffusion problem: derivation of correlation functions. *J. Phys. A*, 23:Ł755, 1990.

[97] D. Kim. Bethe ansatz solution for crossover scaling functions of the asymmetric XXZ chain and the Kardar-Parisi-Zhang-type growth model. *Phys. Rev. E*, 52:3512, 1995.

[98] M. Henkel and G. Schütz. Boundary-induced phase transitions in equilibrium and non-equilibrium systems. *Physica A*, 206:187, 1994.

[99] A. DeMais and P.A. Ferrari. Self-diffusion in one-dimensional lattice gases in the presence of an external field. *J. Stat. Phys.*, 38:603, 1985.

[100] R. Kutner and H. van Beijeren. Influence of a uniform driving force on tracer diffusion in one-dimensional hard-core lattice gas. *J. Stat. Phys.*, 39:317, 1985.

[101] H. van Beijeren, K.W. Kehr, and R. Kutner. Diffusion in concentrated lattice gases. III. tracer diffusion on a one-dimensional lattice. *Phys. Rev. B*, 28:5711, 1983.

[102] J. Gärtner and E. Presutti. Shock fluctuations in a particle system. *Ann. Inst. Henri Poincaré.* Section *A*, 53:1, 1990.

[103] H. van Beijeren. Fluctuations in the motions of mass and patterns in one-dimensional driven diffusive system. *J. Stat. Phys.*, 63:47, 1991.

[104] S.N. Majumdar and M. Barma. Tag diffusion in driven systems, growing interfaces, anomalous fluctuations. *Phys. Rev. B*, 44:5306, 1991.

[105] S.N. Majumdar and M. Barma. Two-tag correlation functions in one-dimensional lattice gases. *Physica A*, 177:366, 1991.

[106] B. Derrida, M.R. Evans, and D. Mukamel. Exact diffusion constant for one-dimensional asymmetric exclusion models. *J. Phys. A*, 26:4911, 1993.

[107] B. Derrida, E. Domany, and D. Mukamel. An exact solution of a one-dimensional asymmetric exclusion model with open boundaries. *J. Stat. Phys.*, 69:667, 1992.

[108] S.A. Janowsky and J.L. Lebowitz. Exact results for the asymmetric simple exclusion process with a blockage. *J. Stat. Phys.*, 77:35, 1994.

[109] F.J. Alexander, Z. Cheng, S.A. Janowsky, and J.L. Lebowitz. Shock fluctuations in the two-dimensional asymmetric simple exclusion process. *J. Stat. Phys.*, 68:761, 1992.

[110] D. Kandel and D. Mukamel. Defects, interface profile and phase transitions in growth models. *Europhys. Lett.*, 20:325, 1992.

[111] G. Schütz. Generalized Bethe ansatz solution of a one-dimensional asymmetric exclusion process on a ring with blockage. *J. Stat. Phys.*, 71:471, 1993.

[112] B. Derrida, S.A. Janowsky, J.L. Lebowitz, and E.R. Speer. Microscopic shock profiles: Exact solution of a nonequilibrium system. *Europhys. Lett.*, 22:651, 1993.

[113] B. Derrida and M.R. Evans. Exact correlation functions in an asymmetric exclusion model with open boundaries. *J. Physique I*, 3:311, 1993.

[114] D.E. Wolf and L.-H. Tang. Inhomogeneous growth processes. *Phys. Rev. Lett.*, 65:1591, 1990.

[115] J. Cook and D.E. Wolf. Wetting dynamics: two simple model. *J. Phys. A*, 24:L351, 1991.

[116] D. Wick. A dynamical phase transition in an infinite particle system. *J. Stat. Phys.*, 38:1015, 1985.

[117] P.A. Ferrai. The simple exclusion process as seen from a tagged particle. *Ann. Prob.*, 14:1277, 1986.

[118] A. DeMasi, C. Kipnis, E. Presutti, and E. Saada. Microscopic structure at the shock in the asymmetric simple exclusion. *Stochastics*, 27:151, 1988.

[119] P.A. Ferrai, C. Kipnis, and E. Saada. Microscopic structure of travelling waves for asymmetric simple exclusion process. *Ann. Prob.*, 19:226, 1991.

[120] P.A. Ferrai. Shock fluctuations in asymmetric simple exclusion. *Prob. Th. Rel. Fields*, 91:81, 1992.

[121] B. Derrida, S.A. Janowsky, J.L. Lebowitz, and E.R. Speer. Exact solution of the totally asymmetric simple exclusion process: Shock profiles. *J. Stat. Phys.*, 73:813, 1993.

[122] C. Boldrighi, G. Cosimi, S. Frigio, and M. Grasso Nunes. Computer simulation of shock waves in the completely asymmetric simple exclusion process. *J. Stat. Phys.*, 55:611, 1989.

[123] Z. Cheng, J.L. Lebowitz, and E.R. Speer. *Comm. Appl. Pure Math.*, 44:971, 1991.

[124] F.J. Alexander, S.A. Janowsky, J.L. Lebowitz, and H. van Beijeren. Shock fluctuations in one-dimensional lattice fluids. *Phys. Rev. E*, 47:403, 1993.

[125] G.M. Schütz. Exact solution of the master equation for the asymmetric exclusion process. *J. Stat. Phys.*, 88:427, 1997.

[126] J. Timonen *et al.* (in preparation).

[127] M. Ha, H. Park, and M. den Nijs. Particle dynamics in a mass-conserving coalescence process. *J. Phys. A*, 32:L495, 1999.

[128] M. Bramson and D. Griffeath. *Ann. Prob.*, 8:183, 1980.

[129] M. Bramson and D. Griffeath. *Z. Wahrsch. Geb.*, 53:183, 1980.

[130] D.C. Torney and H.M. McConnell. Diffusion-limited reaction rate theory for two-dimensional systems. *Proc. Roy. Soc. Lond. A*, 387:147, 1983.

[131] L. Peliti. Renormalisation of fluctuation effects in the $a + a \to a$ reaction. *J. Phys. A*, 19:L365, 1985.

[132] Z. Rácz. Diffusion-controlled annhilation in the presence of particle sources: Exact results in one dimension. *Phys. Rev. Lett.*, 55:1707, 1985.

[133] A.A. Lushnikov. Binary reaction $1 + 1 \to 0$ in one dimesion. *Phys. Lett. A*, 120:135, 1987.

[134] J.L. Spouge. Exact solutions for a diffusion-reaction process in one dimension. *Phys. Rev. Lett.*, 60:871, 1988.

[135] V. Privman. Model of cluster growth and phase separation: Exact results in one dimension. *J. Stat. Phys.*, 69:629, 1992.

[136] V. Privman. Discrete to continuous time crossover due to anisotropy in diffusion-limited two-particle annhilation reactions. *J. Stat. Phys.*, 72:845, 1993.

[137] E. Clément, R. Kopelman, and L. Sander. *Chem. Phys.*, 180:337, 1994.

[138] M.A. Burschka, C.R. Doering, and D. ben Avraham. Transition in the relaxation dynamics of a reversible diffusion-limited reaction. *Phys. Rev. Lett.*, 63:700, 1989.

[139] D. ben Avraham, M.A. Burschka, and C.R. Doering. Statics and dynamics of a diffusion-limited reaction: Anomalous kinetics, nonequilibrium self-ordering and a dynamic transition. *J. Stat. Phys.*, 60:695, 1990.

[140] C.R. Doering, M.A. Burschka, and W. Horsthemke. Fluctuations and correlations in a diffusion-reaction system: Exact hydrodynamics. *J. Stat. Phys.*, 65:953, 1991.

[141] C.R. Doering. Microscopic spatial correlations induced by external noise in a reaction-diffusion system. *Physica A*, 188:386, 1992.

[142] D. ben Avraham. The method of inter-particle distribution functions for diffusion-reaction systems in one dimension. *Mod. Phys. Lett. B*, 9:895, 1995.

[143] C.R. Doering and D. ben Avraham. Interparticle distribution functions and rate equations for diffusion-limited reactions. *Phys. Rev. A*, 38:3035, 1988.

[144] C.R. Doering and M.A. Burschka. Long crossover times in a finite system. *Phys. Rev. Lett.*, 64:245, 1990.

[145] Z. Cheng, S. Redner, and F. Leyvraz. Coagulation with a steady point monomer source. *Phys. Rev. Lett.*, 62:2321, 1989.

[146] H. Hinrichsen, V. Rittenberg, and H. Simon. Universality properties of the stationary states in one-dimensional coagulation-diffusion model with external particle input. *J. Stat. Phys.*, 86:1203, 1997.

[147] G.B. Field and W.C. Saslaw. A statistical model of the formation of stars and interstella clouds. *Astrophys. J.*, 142:568, 1965.

[148] G.J. Madelaine, M.L. Perrin, and M. Itoh. *J. Aerosol. Sci.*, 12:202, 1979.

[149] P.H. McMurry. *J. Colloid Interface Sci.*, 78:513, 1980.

[150] H. Park, M. Ha, and I.-M. Kim. Exact solutions of a restricted ballistic deposition model on a one-dimensional staircase. *Phys. Rev. E*, 51:1047, 1995.

[151] M. HA and M. den Nijs. Macroscopic car condensation in a parking garage. *Phys. Rev. E*, 66:036118, 2002.

[152] T.M. Liggett. *Interacting Particle Systems.* Springer-Verlag, New York, 1985.

[153] J. Marro and R. Dickman. *Nonequilibrium Phase Transitions in Lattice Models.* Cambridge University Press, Cambridge, 1999.

[154] L. Frachebourg, P.L. Krapivsky, and S. Redner. Heterogeneous catalysis on a disordered surface. *Phys. Rev. Lett.*, 75:2891, 1995.

[155] I.M. Campbell. *Catalysis as Surfaces.* Chapman and Hall, New York, 1988.

[156] G C. Bond. *Heterogeneous Catalysis: Principles and Applications.* Clarendon Press, Oxford, 1987.

[157] V. Méndez and J. Camacho. Dynamics and themodynamics of delayed poplulation growth. *Phys. Rev. E*, 55:6476, 1997.

[158] J.D. Murray. *Mathematical Biology.* Springer-Verlag, Berlin, 1989.

[159] J. Krug and H. Spohn. Kinetic roughening of growing surfaces far from equilibrium. In C. Godrèche, editor, *Solids Far From Equilibrium.* Cambridge University Press, Cambridge, 1991.

[160] R. Parthasarathy, X.-M. Lin, and H.M. Jaeger. Electronic transport in metal nanoscrystal arrays: The effect if structural disorder on scaling behavior. *Phys. Rev. Lett.*, 87:186807, 2001.

[161] C. Papadopoulos, A. Rakitin, J. Li, A.S. Vedeneev, and J.M. Xu. Electronic transport in y-junction carbon nanotubes. *Phys. Rev. Lett.*, 85:3476, 2000.

[162] E. Emberly and G. Kirczenow. State orthogonalization by building a hilbert space: A new approach to electronic quantum transport in molecular wires. *Phys. Rev. Lett.*, 81:5205, 1998.

[163] F. Capasso, K. Mohammed, and A.Y. Cho. Electronic transport and depletion of quantum wells by tunneling through deep levels in semiconductor superlattices. *Phys. Rev. Lett.*, 57:2303, 1986.

[164] M.R. Evans, N. Rajewsky, and E.R. Speer. Exact solution of a celluar automaton for traffic. *J. Stat. Phys.*, 95:45, 1999.

[165] M. Schrenckenberg and D.E. Wolf, editors. *Traffic and Granular Flow '97*, Singapore, 1998. Springer-Verlag.

[166] H.-W. Lee, V. Popkov, and D. Kim. Two-way traffic flow: Exactly solvable model of traffic jam. *J. Phys. A*, 30:8497, 1997.

[167] M. Bretz, J.B. Cunningham, P.L. Kurczynski, and F. Nori. Imaging of avalanches in granular materials. *Phys. Rev. Lett.*, 69:2431, 1992.

[168] G.A. Held, D.H. Solina, H. Solina, D.T. Keane, W.J. Hagg, P.M. Horn, and G. Grinstein. Experimental study of critical-mass fluctuations in an evolving sandpile. *Phys. Rev. Lett.*, 65:1120, 1990.

[169] P. Bak, C. Tang, and K. Wiesenfeld. Self-organized criticality: An explanation of the $1/f$ noise. *Phys. Rev. Lett.*, 59:381, 1987.

[170] J.S. Hager, J. Krug, V. Popkov, and G.M. Schütz. Minimal current phase and universal boundary layers in driven diffusive systems. *Phys. Rev. E*, 63:056110, 2001.

[171] T. Antal and G.M. Schütz. Asymmetric exclusion process with next-nearest-neighbor interaction: Some comments on traffic flow and a nonequilibrium reentrance transition. *Phys. Rev. E*, 62:83, 2000.

[172] M. Ha and M. den Nijs (unpublished).

[173] M. Ha and M. den Nijs (in preparation).

[174] G.M. Schütz. The heisenberg chain as a dynamical model for protein synthesis - some theoretical and experimental results. *Int. J. Mod. Phys. B*, 11:197, 1997.

[175] B. Widom, J.L. Viovy, and A.D. Defontanies. Repton model of gel electrophoresis and diffusion. *J. Physique I*, 1:1759, 1991.

[176] G.T. Barkema, J.F. Marko, and B. Widom. Electrophoresis of charged polymers: Simulation and scaling in a lattice model of reptation. *Phys. Rev. E*, 49:5303, 1994.

[177] K. Mallick. Shocks in the asymmetry exclusion model with an impurity. *J. Phys. A*, 29:5375, 1996.

[178] J. Zhang, Y.-C. Zhang, P. Alstrøm, and M.T. Levinsen. Modeling forest fire by a paper-burning experiment, a realization of the interface growth mechanism. *Physica A*, 189:383, 1992.

[179] N. Rajewsky, L. Santen, A. Schadschneidr, and M. Schreckenberg. The asymmetric exclusion process: Comparison for update procedures. *J. Stat. Phys.*, 92:151, 1998.

[180] A.B. Kolomeisky. Asymmetric simple exclusion model with local inhomogeneity. *J. Phys. A*, 31:1153, 1998.

Appendix A

DETAILED DISCUSSION OF THE ASEP WITH A BLOCKAGE

In Chapter 4, we find that a queuing transition occurs in the ASEP with open boundary conditions (OBC)and it is related to the power-law decay of the excess density from the blockage. This must be true with the periodic boundary conditions (PBC) if there is also such a transition. As revisiting the earlier work of the ASEP with a blockage at the middle of the periodic system [8] through the detailed numerical analysis, we show that the periodic case also undergoes the same queuing transition at the same blockage strength as what we showed in Chapter 4. Here we focus only on the half-filled system, i.e., $\rho_o = \frac{1}{2}$, which is equivalent to our boundary-free setup $\alpha = \beta = \frac{1}{2}$.

By using the power-law best-fit method for various r, we can find the critical value of r_c in terms of the decay exponent ν. If the strength of the slow bond is smaller than r_c, the system yields a queued phase with $J = J(r) < J_{\max}$ with a shock wave. For $r_c < r < 1$ $(r > 1)$, there is a non-queued slow bond (fast bond) phase. For all r, the density profile from the blockage decays as a power law:

$$\rho(X) \simeq \frac{1}{2}(1 + \Delta_b + AX^{-\nu}), \tag{A.1}$$

where $X = \frac{N_s}{2} + 1 - x$ is the distance from the blockage. Recall that the order parameter is Δ_b, but the exponent ν also indicates the value of r_c.

As a starting point of a detailed numerical analysis, we address that excess density profiles from the blockage decays as a the same power law as that found in Chapter 4. The earlier result claimed by Janowsky and Lebowitz was $1/|X|$ without any further investigation [8]. However, their result looks only valid for small X. By using two different fitting function forms, $|X|^{-1}$ and $|X|^{-\nu}$ with $\nu < 1$, we compare ours to their earlier result. Figure A.1 confirms that the density profile indeed decays as a power law with $\nu \simeq \frac{1}{2}$ rather than $1/|X|$ when including a larger X region.

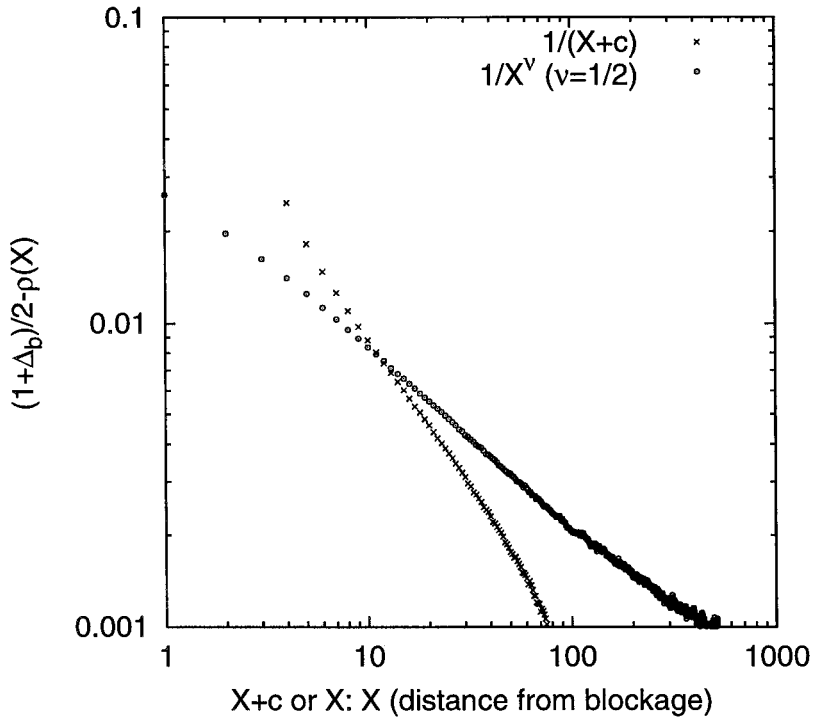

Figure A.1: The decay of the density profile from the slow bond is fitted by two different ways, namely JL-fit (see Fig. 2 in Ref. [8] for the details) versus our power-law fit ($\nu \simeq \frac{1}{2}$). The data are obtained at $r = 0.4$ for $N_s = 1200$ with PBC.

Figures A.2 and A.3 confirm our scenario and phase digram, which show how density profiles changes as increasing r at $N_s = 2048$. Since there is particle-hole symmetry, we plot them up to $\frac{N_s}{2}$ (just in front of the slow/fast bond). As expected, the decay of density profiles from the slow/fast bond with PBC is exactly the same as that with OBC, even including the average value of the density just in front of the slow/fast bond, see Fig. A.2(b).

Through three-parameter fits for each density profile in terms of Eq. (A.1), we get the order parameter Δ_b, the amplitude A, and the exponent ν. In Fig. A.4, we show the power-law decay of the density profile from the slow/fast bond. The best-fit values of A and ν for various r are shown in Fig. A.3 and the plot of the order parameter versus r in Fig. A.5(a). For comparison, our OBC data (from Chapter 4) are also plotted. Figure A.5(b) indicates that $r_c \simeq 0.8$ and $\Delta_b \sim \epsilon^\beta$ with $\beta \simeq 1.5$, where $\epsilon = r_c - r$. This is almost the same results as what we obtained with OBC.

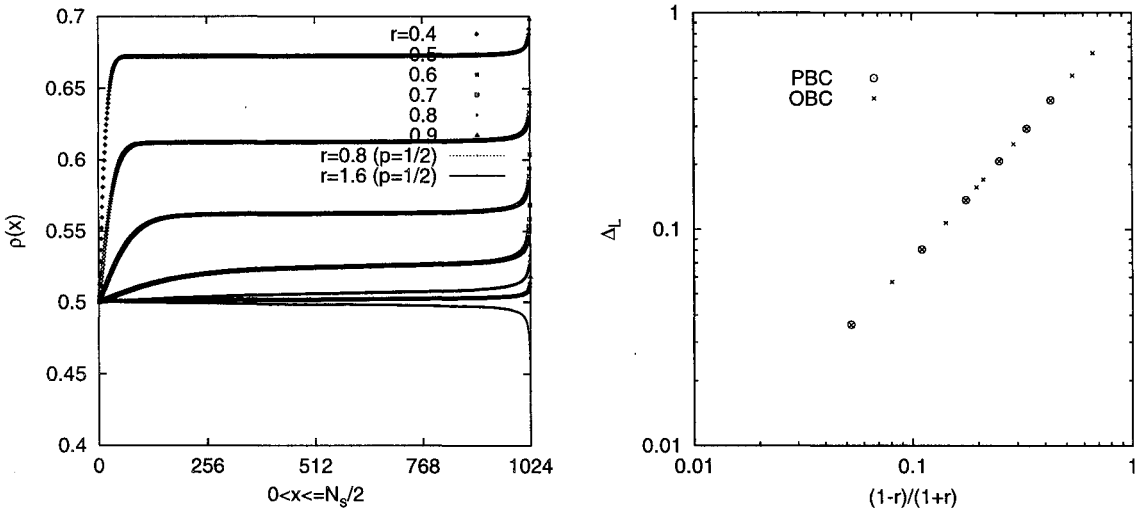

Figure A.2: (a) MC simulation data of density profiles for various r are obtained at $N_s = 2048$. Note that the location of the slow/fast bond is changed to the middle of the system. (b)$\Delta_L = 2(\langle \hat{n}_L \rangle - 1)$ versus $(1-r)/(1+r)$.

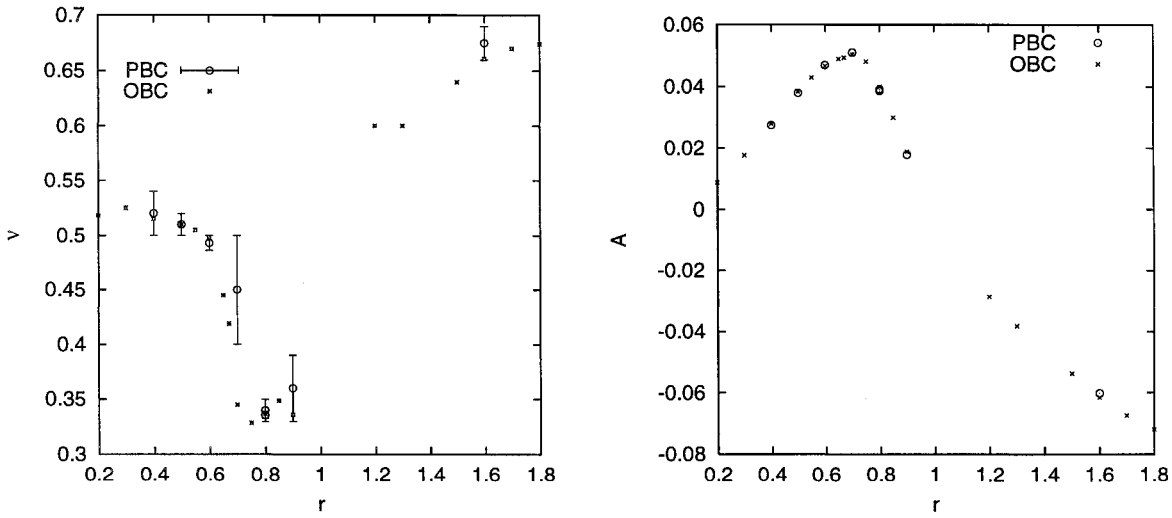

Figure A.3: The best-fit values of (a) the exponent ν and (b) the amplitude A for various r in Eq. (A.1). Again, we also plot the OBC results for comparison.

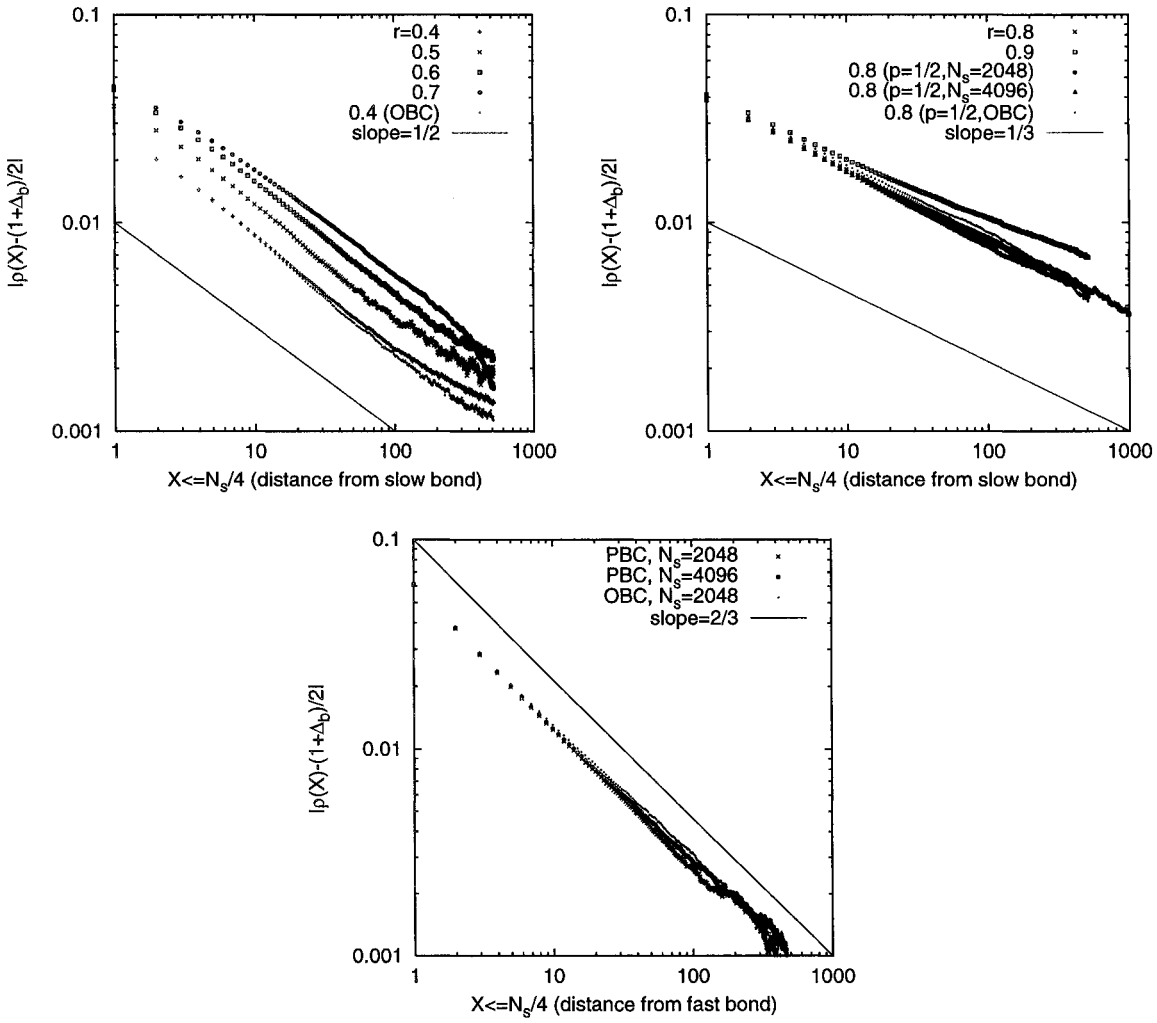

Figure A.4: Double logarithmic plots for the power-law decay of density profiles from the SB/FB with $N_s = 2048$: (a) $r = 0.4 - 0.7$ (queued phase), (b) $r = 0.8, 0.9$ (non-queued slow bond phase), and (c) $r = 1.6$ (non-queued fast bond phase). The data of $N_s = 4096$ are only shown for $r = 0.8$ and $r = 1.6$ where $p = \frac{1}{2}$. For comparison, we also plot the OBC data.

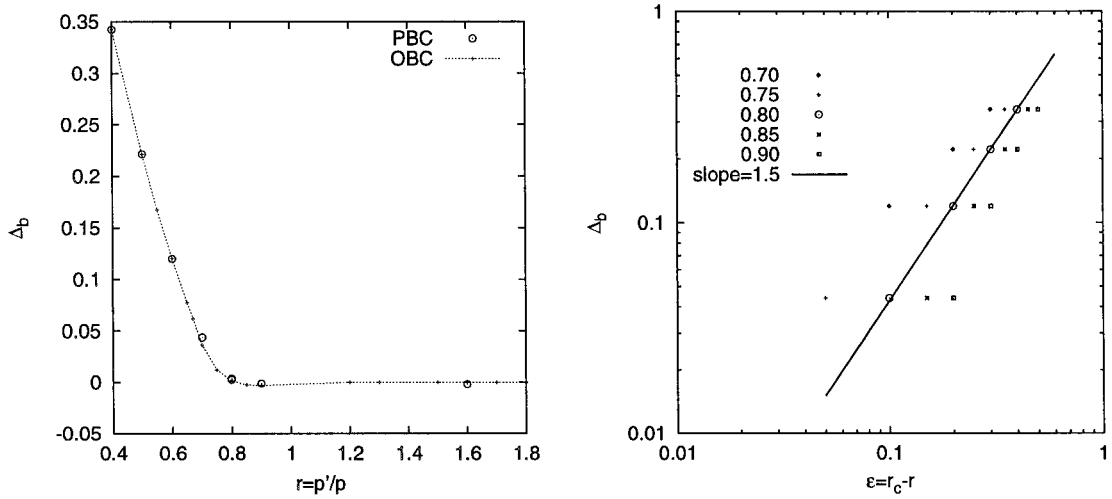

Figure A.5: (a)The order parameter Δ_b versus the strength r is compared to that in OBC. (b) Double logarithmic plots indicate the value of r_c and the critical exponent β in $\Delta_b \sim \epsilon^\beta$, where $\epsilon = r_c - r$.

On the other hand, the edge density profile are quite different from each other, since PBC generate a shock wave for $r < 1$, see [8] for a detailed discussion. We find that it is well-fitted by the form:

$$\rho(x) \simeq \frac{1}{2} + a \tanh(bx). \tag{A.2}$$

Here the amplitude a is related to the order parameter Δ_b, i.e., $a \simeq \Delta_b/2$ since $\rho(x) \simeq \frac{1}{2}(1 + \Delta_b)$ for $0 \ll x \ll \frac{N_s}{2}$.

Through two-parameter fit, we get the best-fit values of a and b for various r and for various system sizes. Due to less statistical averages for large system sizes, we cannot get such a good FSS results. However, we can show data collapse by using the best values of a and b at the largest system size, $N_s = 2048$, for various r, and at $r_c = 0.8$ for various N_s.

Figure A.6 confirms the validity of Eq. (A.2) for the shock profile in the presence of the blockage. In particular, we reconfirm the FSS at $r_c = 0.8$ in Fig. A.6(b), where we used $b \sim N_s^{-y_b}$ and $a \sim N_s^{-x_a}$ with $y_b \simeq 1$ and $x_a \simeq 0.32(4)$. Recall that $\Delta_b \sim N_s^{-x_\Delta}$ with $x_\Delta = 0.360(5)$. The detailed analysis is shown in Fig. A.7.

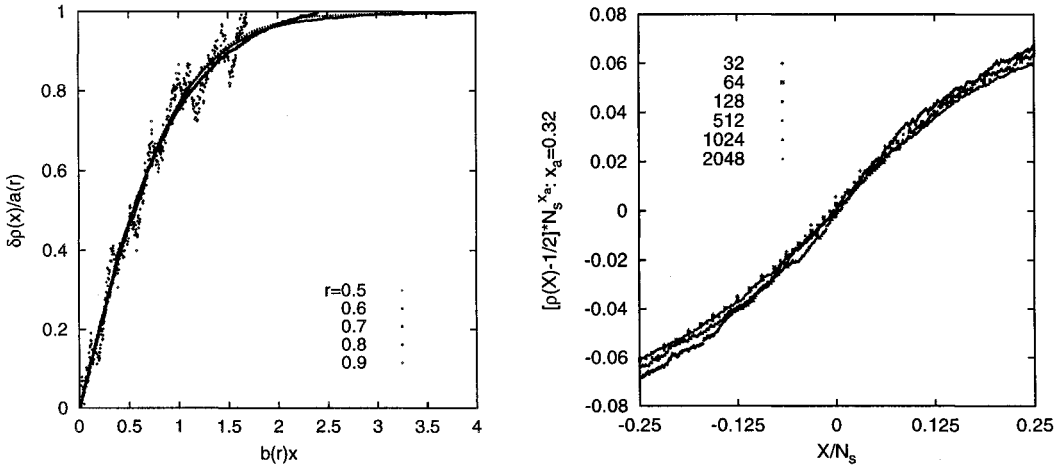

Figure A.6: Data collapse with the best-fit values of a and b for the shock profile by Eq. (A.2).

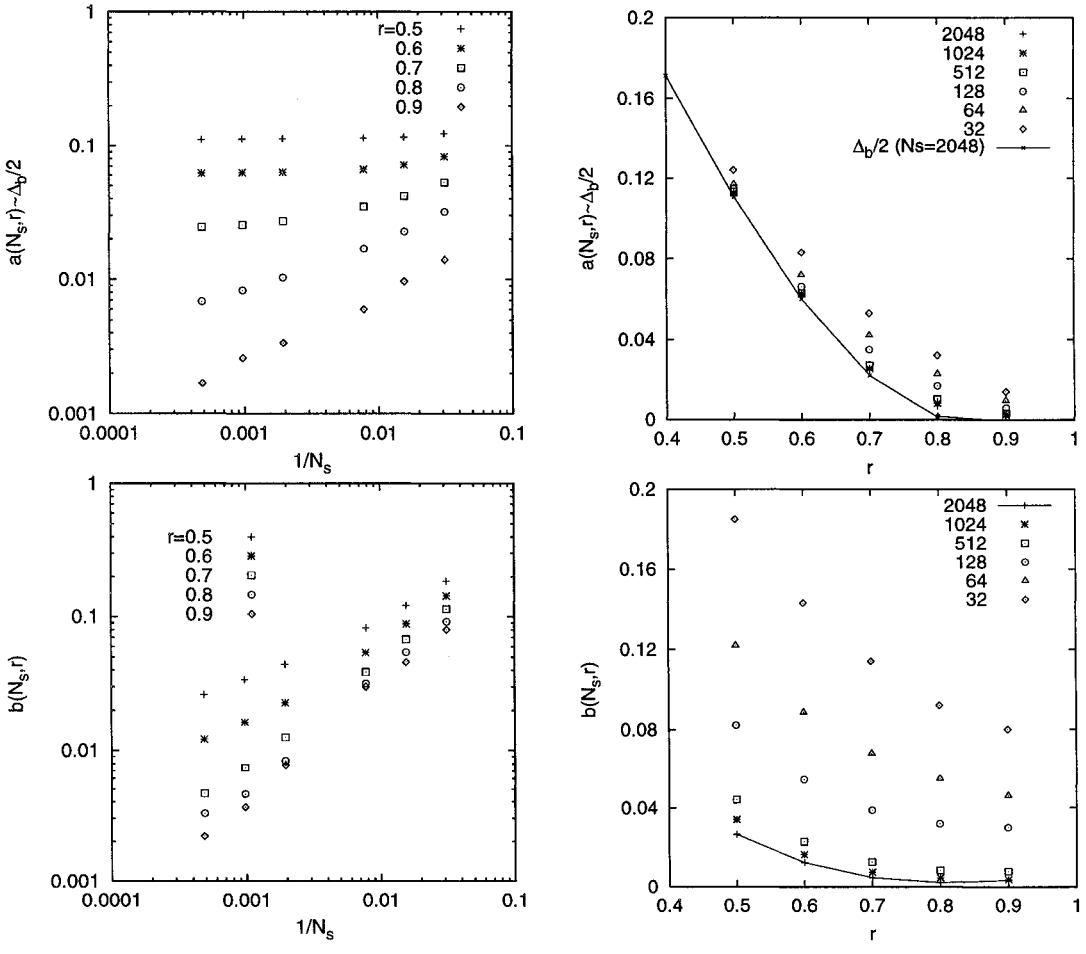

Figure A.7: Shock profiles are fitted by Eq. (A.2) for various r and various system sizes N_s.

VITA

Meesoon Ha was born on December 7, 1970 in Seoul, Korea as the youngest daughter of Junghee Kim and Sangkeun Ha. She has been interested in Physics since her elementary school. After graduating from Baewha Woman High school in February, 1989, she went to Inha University in Inchon, Korea for her Bachelor of Science in Physics and received it in February, 1993. Her Master of Science in Physics was finished at Korea University in Seoul, Korea in February, 1995. Since June, 1997, she has continued her Doctor of Philosophy study in Physics at the University of Washington. She married Youngkyun Jung in Seoul on June 25, 2000. She is the co-author of "Exact solutions of a restricted ballistic deposition model in a one-dimensional staircase", *Physical Review E*, **51**, 1047 (1995); "Particle Dynamics in a mass-conserving coalescence process", *Journal of Physics A*, **32**, L495 (1999); "Macroscopic car condensation in a parking garage", *Physical Review E*, **66**, 036118 (2002); "A queuing phase transition in the asymmetric simple exclusion process" (in preparation).